universität wien

DISSERTATION

Titel der Dissertation

Soft Metal Sulfide Nanoparticles and Nanocomposite Based Sensors for Thiol and Alcohol Detection

angestrebter akademischer Grad

Doktor/in der Naturwissenschaften (Dr. rer. nat.)

Verfasserin / Verfasser:	Mag. Ghulam Mustafa
Matrikel-Nummer:	0719170
Dissertationsgebiet	Doktoratsstudium der Naturwissenschaften (Chemie)
Betreuerin / Betreuer:	Ao. Univ.-Prof. Mag. Dr. Peter A. Lieberzeit

Wien, am 8. Juni 2011

Preface

This work is done in the work-group of Chemical Sensors and Optical Molecular Spectroscopy from September 2008 till June 2011, under the supervision of Ao. Univ.-Prof. Dr. Peter A. Lieberzeit and Prof. Dr. Franz L. Dickert at the Department of Analytical Chemistry, University of Vienna, Waehringer Straße 38, 1090-Vienna, Austria.

To

My Parents

Acknowledgements

I am grateful to God the Almighty for giving me this magnificent life and utmost courage to follow the path of knowledge discovery and to achieve the milestone of my Doctoral Thesis.

I am most thankful to my research supervisor, Professor Dr. Peter A. Lieberzeit, who has been my inspiration and the role model for both independent and collaborative research. I am incredibly fortune to have him as my supervisor. I wish I could have spent more time in his group of self motivated researchers and excellently managed working environment. I am also incredibly fortune to have Professor Franz L. Dickert as my advisor. I owe my thanks to him for his guidance and encouragement. Without his inspiration, guidelines and continuous support, this thesis would not have been possible. I feel myself lucky to work closer to both of my supervisors.

I would like to thank my colleagues at institute, especially the members of my laboratory that I had the privilege to work with for the fruitful discussions and for creating such a nice working environment. I owe a special thanks to institute secretary and all administrative staff, who made everything at the institute run smoothly.

It was not easy to start this big endeavor at the beginning. I am obliged to all my teachers and friends who gave me stimulation for going ahead with my Doctorate and for moral and technical support during the course of my studies.

I thank to my family, especially my parents for their prayers. I am also thankful to my brothers and sisters, who cooperated with me during my stay in Austria.

I have to say thanks to the Higher Education Commission (HEC) of Pakistan, the Austrian Exchange Service (ÖAD) for providing me a marvelous opportunity to study in Austria. I am especially thankful to the HEC for the funding for my Doctoral studies.

Table of Contents

1. Chemical Sensors

1.1 Introduction

The origin of sensor is from the Latin word ‘sentire’, which means ‘to perceive or to become aware of through the senses’. There are two main classes of sensors: physical sensors which measure physical parameters such as pressure, electric charges, light intensity, temperature etc., and chemical sensors that measure chemical phenomena, however often in combination with physical sensor to transform the chemical informations into an analytically useful signal. The definition of a sensor according to IUPAC is a device able to convert chemical information ranging from the concentration of a specific sample component to total composition analysis, into an analytically useful signal [1]. More general and specific definitions to particular type of sensor are also available in literature [2,3]. So, in short words the purpose of a chemical sensor is to change the chemical informations into measureable quantities, preferably electronic quantities such as voltage.

Chemical sensors usually require a recognition layer that is sensitive to chemical changes taking place in the surrounding environment and transmits theses signals to the transducer, which converts them into useful analytical informations. The layer plays a crucial role in the effectiveness of a chemical sensor because it is fundamentally responsible for selectivity, response time and lifetime of a chemical sensor, sometimes also for sensitivity. This sensor layer may be composed of polymer thin films, nanoparticles, selective membranes, bio-macromolecules or composite materials. Chemical sensor fabrication involves knowledge from a broad range of fields including chemistry, physics, mathematics, biology, material sciences and electronics. The main task of

chemistry is, of course fabrication of sensor layer which is capable of binding reversibly and selectively with an analyte of interest present in a complex mixture. Additionally, electronics and physics play a crucial role in the development of suitable electronic circuits and signals conversion. So, chemical sensing is a multidisciplinary field. The combined efforts of all these fields make it possible to detect a chemical change in the surrounding atmosphere to improve our environmental and living conditions.

1.2 Need and Importance of Chemical Sensors

In the last century, due to a great revolution in the field of industry and technology development, precise and accurate analytical measurement tools got crucial importance in the field of analytical chemistry. There was a substantial demand for online, real-time and continuous process measuring devices, especially for industrial and environmental applications. The ability of a chemical sensor to detect and quantify different chemical and biological species in liquids and gases has proven it to be an ideal and promising candidate for this purpose. As compared to conventional analytical instruments and methods, chemical sensors offer non-destructive and rapid detection of the analyte of interest in complex media. In contrast to this, analytical instrumental techniques in analysis are capable of dealing with wide variety of different analytes up to a very low detection limits but usually at high cost [4,5]. Chemical sensors have many desirable advantages over conventional instruments [6] due to their small size, low cost, ease of operation and their manufacturing by established technical methods.

Chemical sensors have small size as compared to other analytical instruments and because of their small sizes and ruggedness; these can be used

for remote measurements. These devices do not require too much maintenance because of their simplicity in design and can be easily operated by nonprofessional. Chemical sensors are promising candidate for on-line and real-time monitoring of specified analytes and are highly suitable for all kinds of applications. As these are miniaturized instruments, so it is possible to fabricate several sensors on one device for multi-analyte measurements. The problem of cross sensitivity arising from these devices can be overcome using modern data analysis tools.

1.3 History and Development of Chemical Sensor Technology

In 1922 [7] glass pH electrode was invented to measure pH and have limitation to use only in solution and calibration problems. Until 1950's, only glass pH electrode was considered a chemical sensor and then in 1950's oxidation-reduction reaction based sensors were developed for the detection of metals and organic compounds [8,9,10]. Clark developed first chemical sensor for the detection of oxygen in biological fluid and tissues by using semi-permeable membrane between analyte fluid and electrodes [11]. There was a dramatic development in this field in last two decades. The main reason behind this development is low cost, portability and capability of these devices to make accurate continuous and online chemical detection of analyte of interest in the field of biomedicinal, environmental and industrial chemistry. The table given below shows the history of chemical sensors development.

Table 1.1 Chemical sensors invention history along with their inventors.

Year	***Inventor***	***Invention***
1906	Cremer	Dependence of EMF on pH

1909	Haber, Klemendiewicz	Development of glass electrode
1936	Beckman	Commercial production of pH-meter
1937	Nikolsky	Nikolski equation and theory of glass electrode
1937	Kolthoff	Crystalline electrode
1937	Nikolsky	Crystalline membrane
1961	Pungor	Heterogeneous solid ISE
1962	Seiyama	Semiconductor gas sensor
1966	Frant, Ross	LaF3-electrode
1966	Simon	Liquid ISE with neutral carrier
1967	Rose	Ion-exchange membrane
1969	Guibault, Montalvo	Biosensor
1969	Baker, Trachtenberg	Chalcogenides glass membrane for ISE
1970	Bergveld	ISFET
1972	Shone	Piezoelectric biosensor
1975	Lundstorm	Gas FET
1976	Lundstorm	Immuno FET
1978	Lubbers, Optiz	Opt(r)ode
1982	Persaud, Dodd	Electronic nose
1986	Thorn	EMI Microsensor-first commercial ISFET
1995	Valasov,Legin, D'Amigo	Electronic tongue

1.4 Basic Components of Chemical Sensor

A chemical sensor has three basic components: sensitive layer, transducer and electronics as shown in figure 1.1. The sensitive layer interacts with analyte

and is selective to specific chemical species. When a sensitive layer is exposed to analyte of interest, it interacts with analyte molecules and shows a change in some physical properties like mass, optical absorbance, reflectance, polarity, impedance, voltage or florescence [12,13].

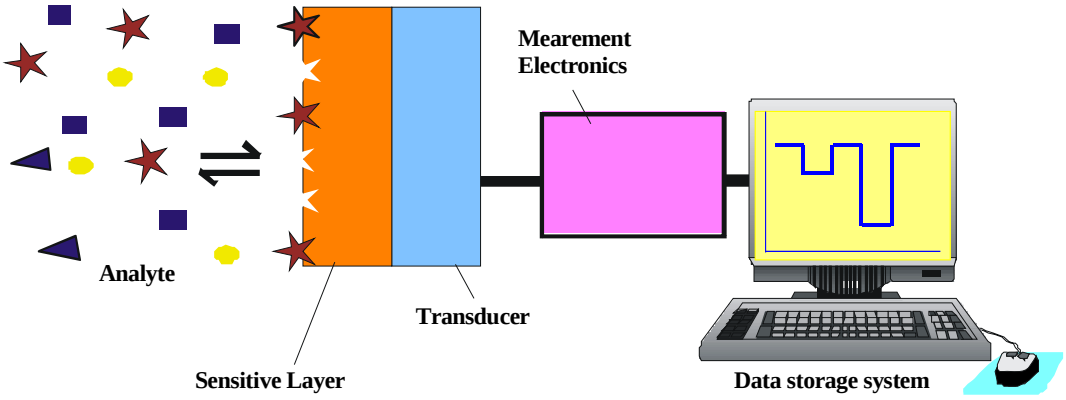

Figure 1.1 Schematic diagram of a chemical sensor.

The transducer system converts these physical changes into optical or electrical signals. The signals obtained from physical transducers are detected, amplified and processed by different electronics and software. After processing the data with suitable software, it is changed into a presentable form.

1.5 Acoustic Wave (or Mass) Sensors

Chemical sensors that measure change in mass on the surface of a chemically sensitive layer are known as mass sensors and are able to detect a large variety of analytes. These sensors can be employed to all types of biological and chemical species. Typical examples of this type of these sensors are surface acoustic wave devices (SAW) and bulk acoustic wave devices (BAW). The major advantage of mass sensitive sensors is their ability to detect neutral species [14]. The change in mass on sensor sensitive surface can be

detected by change in some physical parameters, such as frequency, amplitude, mechanical deformation or phase shift [15]. These changes in mass could be because of bulk interactions (absorption) or surface confined phenomenon (adsorption). The working principle of mass sensors is based on inverse piezoelectric effect. The most commonly used piezoelectric materials are quartz (SiO_2), lithium tantalate ($LiTaO_3$) and lithium niobate ($LiNbO_3$). Some other commercially available materials are gallium arsenide (GaAs), silicon carbide (SiC), langasite (LGS), zinc oxide (ZnO), aluminum nitride (AlN) , lead zirconium titanate and polyvinylidene fluoride (PVdF). Mass sensitive sensors are subdivided into bulk acoustic wave devices and surface acoustic wave devices, of which former will be discussed in more detail below.

Bulk Acoustic Wave (BAW) Devices

The most important and commonly used piezoelectric material in the field of chemical sensing is an AT-cut quartz plate with circular electrodes patterned on its both sides. Quartz crystal microbalance (QCM), the predominate term found in literature is the typical example of BAW devices and resonate in a thickness shear mode (TSM).

Figure 1.2 Quartz sheet with dual electrodes sketch on surface

A thickness shear waves are produced by applying an electric potential between the electrodes of a QCM. The AT-cut quartz sheet shows very low temperature dependence. Commercially, QCMs are available with resonance frequencies up to 20 MHz and sometimes up to 50 MHz [14]. Desired sketches can be printed on the quartz surface as shown in figure 1.2 and then a chemically sensitive recognition layer is coated on it to provide selectivity to the sensor. The coated QCM is placed into an oscillating circuit and is resonated with its fundamental frequency.

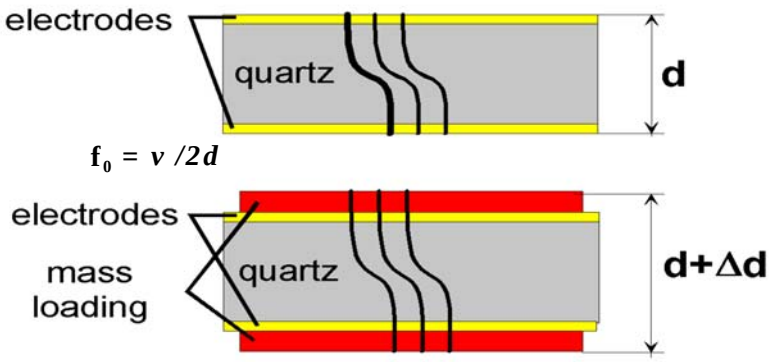

Figure 1.3 The principle of QCM

The mass of deposited analyte on QCM surface can be related to the change in resonance frequency of quartz crystal microbalance and this relationship is given by the Sauerbrey equation.

$$\Delta f = -f_o^2 \frac{2}{A_{cr}\left(\rho_m C_q\right)^{1/2}} \Delta m \qquad (1)$$

The equation (1) provides a relationship between the change in frequency and the change in mass on quartz surface, using the density of the chemical film, the shear modulus of the quartz crystal, the fundamental resonance frequency of

crystal and the area of the crystal. The above equation (1) relates the change in frequency to mass changes on QCM surface in gas phase only. On applying this equation to liquid phase the properties of the liquids are to be considered and the Sauerbrey equation is modified as given below by equation 2.

$$\Delta f = -f_o^{\,2} \frac{2}{\left(\rho_m C_q\right)^{1/2}} \sqrt{\frac{\rho_l \eta_l}{4\pi f_o}} \qquad (2)$$

The above equation represents the relationship of change in frequency to the density and viscosity of the surrounding liquid as well as to the density and shear modulus of the quartz crystal microbalance. Quartz crystal microbalance can be regarded as a highly sensitive scale and a 10 MHz QCM has a sensitivity of 1 $Hzng^{-1}$ mass loading. It means a QCM is able to detect an analyte up to 1 ng in worst case and even less than 1 ng detection is also possible.

1.6 Characteristics of a Chemical Sensor

Some basic characteristics to assess the quality of a chemical sensor are:

Sensitivity

It is the frequency change of quartz crystal microbalance per unit mass change of analyte. Sensitivity of a chemical sensor perceives the change in mass of the sensitive layer with respect to analyte concentration when it is exposed to analyte of interest. It depends on the sensitive layer, fundamental resonance frequency of quartz crystal and also on the damping of QCM. Sensitivity of a crystal is affected by temperature, type of cell used for measurement, viscosity, density of media and measuring electronics.

Response Time

Response time of a chemical sensor is the time required by the sensor to achieve constant frequency. A good sensor should have a fast response time and it is of substantial importance particularly for online and real-time monitoring of chemical reaction and process. It depends on the recognition layer material, layer height, temperature and the type of interaction existing between analyte and sensitive layer material.

Selectivity

It is the contribution of actual analyte response in total sensor signals with respect to other chemical species. There is no ideal sensor but a good sensor should be highly selective to its analyte of interest.

Noise Level

A good chemical sensor should bear low intrinsic level and high sensitivity because noise level directly influences the sensitivity of a chemical sensor. It is very important and significant especially in gas phase, where the concentrations of analytes are very low.

Drift

It is a slow and non-random change of sensor signal under unaltered experimental conditions. Drift is calculated by filtering a linear function to the data set collected in a given period of time. It is observed because of the continuous loss of mass sensitive layer from the electrode surface and sometimes several electrical reasons causes drift. A good and ideal chemical sensor should be drift free.

Reversibility and Reproducibility

Reversibility of a chemical sensor is the return of the sensor frequency to its original values after switching off the analyte concentration and the repeatability of the sensor is repetition of sensor signal with same values every time under the same conditions of temperature and analyte. The standard deviation of the measured signal in repeated measurements is called repeatability. The irreproducibility of a chemical sensor is directly related to the stability of sensor and sensors with harder and rigid sensitive layers are more stable.

1.7 Research Strategy and Goal

Chemical sensor technology is a most promising and suitable technique for environmental processes monitoring which offers higher sensitivities necessary for real-life environmental samples [16].

In preliminary studies [17] it is found that soft metal sulfide has substantial affinity interaction towards thiol based on so-called hard-soft acid and base concept of species introduced by Pearson. Thiols (RSH) are considered of great interest since long time because of their importance in many biological and non-biological processes. Thiols in biological systems undergo very important chemical reactions i.e. addition, substitution, elimination and oxidation to produce S-C, S –matel, S-S or S-O bond formation. The biological activity of thiols distinguishes them from other biomolecules with comparable nucleophilicity because of the existence of sulfur (S) in numerous oxidation states i.e. 2, 4 and 6. Thiols are the major component of antioxidant defense network of a biological system and act as redox-buffer to prevent oxidative damage. They act as a free radical scavenger and generate other antioxidants i.e.

vitamin E and C. Human diseases and metabolic disorders related to oxidative stress can be diagnosed and monitored by measuring the aminothiol concentrations in biological fluids. Non-biological thiols are of also substantial importance, especially from environmental point of view. Volatile sulfur compounds play a vital role in earth's radiation budget and climate forcing. Current methods for thiol determination in biological and non-biological samples differ from one another, because thiols and disulfides have no chromophores, they easily oxidize during sample manipulation and they are usually present in very low concentrations in sample. Many effective separation techniques are applied for thiols and disulfide by HPLC and CE in conjunction with different detection strategies. Fluorescence methods are most frequently used which need pre or post derivatization of –SH group with suitable and reactive fluorophore. There are also some –SH –reactive reagents commercially available for UV/Vis detection of thiols.

The development of direct and non-destructive method for thiols detection is a challenging and tedious task. Up till now only few gas sensors for thiols have been reported [17,18,19,20,21,22]. We used the idea of affinity interactions between soft metal and thiols but the direct use of soft metal nanoparticles as a recognition material for thiols shows irreversible interactions with gold. Preliminary experiments, with soft metals sulfides as recognition material for thiol detection revealed reversible and reproducible effects. This strategy is further extended to study the influence of Pearson hardness on sensitivity and selectivity by testing several metal sulfides, such as MoS_2, Cu_2S and Ag_2S. Finally, the testing of these materials in molecularly imprinted polymer composite to enhance the sensitivity towards analyte of interest was investigated.

2. Sensing of Thiols with Molybdenum Disulfide Nanoparticles

2.1 Introduction

Molybdenum disulfide (MoS_2) is a black crystalline compound and found as the mineral molybdenite. Molybdenum is mainly extracted from this ore and the natural amorphous form is called the rarer mineral jordisite. It is not as reactive as other transition metal chalcogenides. As the Van der Waals interactions between the sheets of sulfide atoms are very week [23] and because of these week forces MoS_2 has a low coefficient of friction which makes it as promising candidate to be used as lubricant. MoS_2 is diamagnetic and semiconductor. MoS_2 is used as a catalyst in petroleum refineries for hydrodesulphurization [24]. Together with cadmium sulfide it also causes to increase the rate of photocatalytic hydrogen production. Studies [17] showed that molybdenum disulfide is a soft material and yields affinity interactions with thiols which merits further investigation.

2.2 Experimental

Chemicals and Materials:

Molybdenum hexacorbonyl (Mo $(CO)_6$), diphenyl ether, oleic acid, n-hexane and sulphur were purchased from Fluka and Merck in highest purity available. Quartz crystal sheets (f = 10MHz) were purchased from Zheijiang, China, and the brilliant gold paste for screen printing of electrode structures from HERAEUS, Germany.

Synthesis of MoS_2 Nanoparticles

Method 1:

100ml of p-xylene solution is first degassed for 20-30minutes by heating it up to 100^{o}C with constant stirring. Then nitrogen gas is bubbled through the solution at 140^{o}C and 7.3 mg of sulfur (99%, 2.3x10^{-4} mol) is dissolved in it. Temperature of system is cooled down to room temperature with continuous flow of nitrogen through the solution. 30 mg of molybdenum hexacarbonyl (98%, 1.15x10^{-4} mol) is added leading to an atomic ratio of sulfur to molybdenum of 1:2. The temperature is again increased up to 140^{0}C and refluxed for 20 minutes. It is kept at same temperature for several hours, until brownish black powder of molybdenum sulfide is obtained, filtered, washed with acetone and dried [25]. The size of these particles is determined with atomic force microscopy, which resulted in sizes ranging 100-150 nm in diameter.

Method 2

In this method we prepared MoS_2 nanoparticles according to already reported procedure [26]. A slurry of $Mo(CO)_6$ with phenyl ether in presence of oleic acid was prepared and then heated to degas up to 310^{o}C for 35 minutes under inert atmosphere. After this reaction the white color of slurry converted to bright brown and finally black. The particles were separated by centrifugation at 4400 rpm and dispersed in hexane. In above colloidal solution, which is a mixture of Mo/MoO_x, elemental sulfur (2.5 equiv.) was added under inert atmosphere and heated up to 310^{o}C for 30 minutes. The solution turned to dark brown and particles were separated from reaction mixture by centrifugation at 4400 rpm. The average size of the particles measured with AFM was less than 50 nm, some of them even have size less than 10 nm.

Atomic Force Microscopy (AFM)

AFM measurements took place on a Veeco NanoScope IVa in contact mode at 1 Hz scan rate. 5 μl suspension of particles in THF (Tetrahydrofuran) was deposited on glass substrate and analyzed with contact mode scanning.

X-Ray Powder Diffractometry

Diffraction (XRD) data was obtained from a Guinier-Huber image plate employing monochromatic Cu $K\alpha_1$-radiation (1.54056 Å). The sample measurements were carried out at a voltage of 40 kV and a current of 30 mA. The diffraction pattern was recorded from 8° to 100° in 2θ geometry on an image plate. Particles were deposited on a polymeric sample holder by paraffinic adhesive material not interfering with the measurement.

Quartz Crystal Microbalance processing

As a transducer for the sensor measurements, we applied 10 MHz quartz crystal microbalance with dual electrodes printed on both sides of QCM sheet by screen printing. After electrode deposition, the QCM sheets were immersed overnight in 5-10% solution of 1-butanethiol in n-hexane so as to generate a monolayer of alkanethiolate on the gold surface. This prevents further interaction with thiol vapors during measurement. A suspension of 5mg of molybdenum disulphide nanoparticles in 500 μl of ethylenediamine was used for coating. Ethylenediamine was used for suspension because a better dispersion of nanoparticles was observed in it as compared to others solvents. On the respective working electrode, a layer of 2-3 kHz was generated by spin coating 5 μl of that suspension on both faces of the quartz at a speed of 2000rpm. QCM were dried overnight at 80^{o}C.

Calculation of concentrations of analytes.

(a)1-octanethiol

For concentrations from 1-30 ppm of 1-octanethiol ($CH_3(CH_2)_7SH$) with molecular mass 146.29, boiling point 197-200 °C, Melting point -49°C, purity ≥98.5%, density 0.843 g/ml at 25 °C, Flash Point 68 °C and Vapor pressure, kPa at 25°C: 0.06 table 2.1 gives the calculated gas stream.

Table 2.1 Calculation of concentrations of 1-octanethiol.

Conc. (ppm)	***Solvent (ml)***	***Air (l)***	***Conc. (ppm)***	***Solvent (ml)***	***Air (l)***
1	3.4	2.0	8	27	1.97
2	6.7	2.0	9	30.4	1.97
3	10.1	1.99	10	33.7	1.97
4	13.5	1.99	15	50.6	1.95
5	16.9	1.98	20	67.5	1.93
6	20.2	1.98	25	84.4	1.92
7	23.6	1.98	30	101.2	1.90

(b) 1-butanethiol

1-butanethiol or butyl mercaptan has molecular formula $CH_3(CH_2)_3SH$, molecular weight 90.19, vapor pressure 83 mmHg (37.7 °C), 60.6mbar (25°C), boiling point 98 °C, melting point −116 °C, purity ≥99% and density

0.842 g/mL at 25 °C. Different concentrations of 1-butanethiol with air are calculated as shown in Table 2.2.

Table 2.2 Calculation of concentrations of 1-butanethiol.

Conc. (ppm)	***Solvent (ml)***	***Air (l)***	***Conc. (ppm)***	***Solvent (ml)***	***Air (l)***
0	0	1.0	250	3.9	1.0
25	0.4	1.0	500	7.8	0.99
50	0.8	1.0	750	11.8	0.99
100	1.6	1.0	1000	15.6	0.99

(c) n-octane

n-octane has molecular formula $CH_3(CH_2)_6CH_3$, molecular weight 114.23, vapor pressure 14 mmHg/14.6mbar (25 °C), purity ≥99%, boiling point 125-127 °C, melting point −57 °C and density 0.703 g/mL at 25 °C. Different concentrations of n-octane with air are calculated and shown in Table 2.3 as below.

Table 2.3 Calculation of concentrations of n-octane.

Conc. (ppm)	***Solvent (ml)***	***Air (l)***	***Conc. (ppm)***	***Solvent (ml)***	***Air (l)***
100	6.8	0.99	600	40.9	0.96
200	13.6	0.99	700	47.7	0.95
300	20.4	0.98	800	54.5	0.94

400	27.2	0.97	900	61.3	0.94
500	34.0	0.97	1000	68.1	0.93

(d) Ethyl methyl ketone

Ethyl methyl ketone has purity >99% and vapor pressure 71 mmHg /94mbar at 25^0C and purchased from Sigma Aldrich. Different concentrations of ethyl methyl ketone with air are calculated and mentioned in Table 2.4 as below.

Table 2.4 Calculation of concentrations of ethyl methyl ketone.

Conc. (ppm)	***Solvent (ml)***	***Air (l)***	***Conc. (ppm)***	***Solvent (ml)***	***Air (l)***
100	1.0	1.0	600	5.8	0.99
200	1.9	1.0	700	6.8	0.99
300	2.9	1.0	800	7.8	0.99
400	3.9	1.0	900	8.7	0.99
500	4.8	0.99	1000	9.7	0.99

(e) Limonene

Limonene has vapor pressure 2.6656 mbar at 20 C^o. It was purchased from Sigma Aldrich with 96 % purity. Its different concentrations are calculated as below.

Table 2.5 Calculation of concentrations of d-limonene.

Conc. (ppm)	***Solvent (ml)***	***Air (l)***	***Conc. (ppm)***	***Solvent (ml)***	***Air (l)***

25	19.0	1.98	75	56.9	1.94
50	37.9	1.96	100	75.8	1.92

Experimental set up

For frequency measurements, a network analyzer (Agilent Technologies E5062A) and a two channel frequency counter (Agilent Technologies 53131A) were used. A custom-made oscillator circuit was used for operating the quartz. For data acquisition, WinSens, a software designed within the group, was used. Air streams with defined amounts of thiol were generated by a gas mixing apparatus based on mass flow controllers (Tylan-RO7020).

2.3 Results and Discussion

Characterization of MoS_2 Nanoparticles

First of all, the feasibility of the synthetic procedure had to be checked.

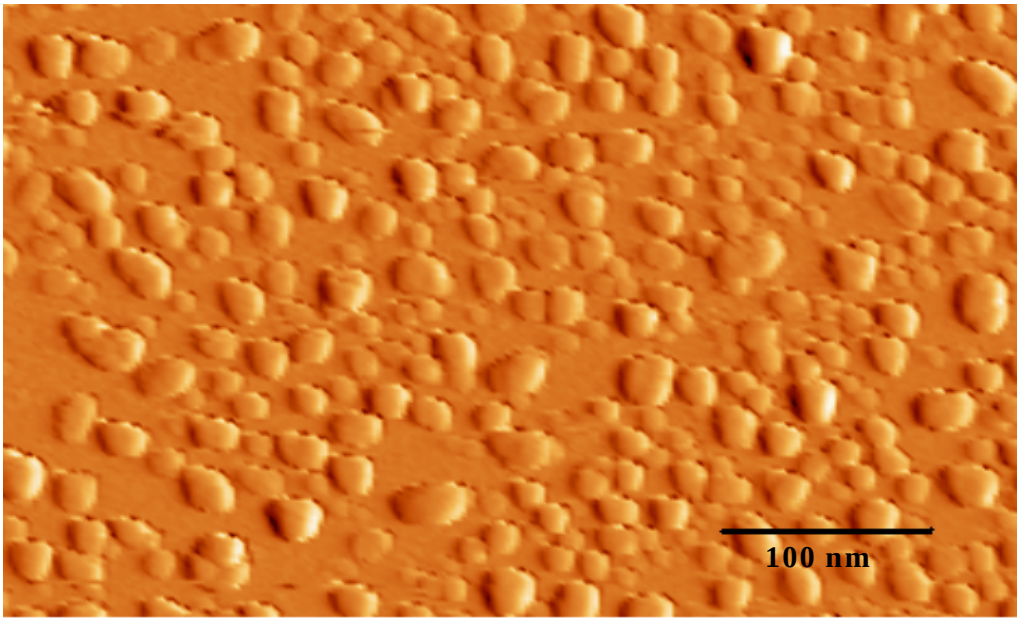

Figure 2.1 AFM images of MoS_2 nanoparticles on glass substrate.

For this purpose, AFM images of MoS_2 nanoparticles deposited on glass substrate were recorded and the particle sizes analyzed. Figure 2.1 indicates that most of the particles are with diameter less than 50 nm. Nanoparticles are uniformly distributed and of same visual symmetry.

In order to achieve an optimal interaction between sensor material and analyte, the stoichiometry of the particles plays a potent role. Therefore, we applied XRD analysis of nanoparticles to ensure purity and figure 2.2 is showing the XRD pattern of MoS_2 nanoparticles.

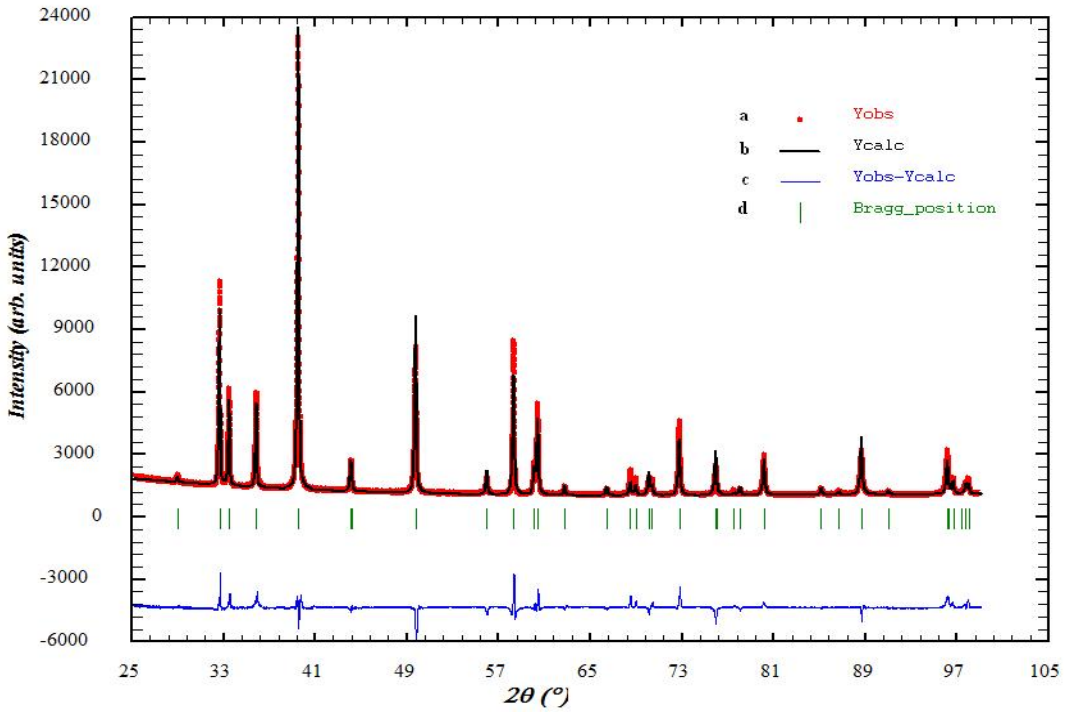

Figure 2.2 XRD powder diffraction pattern of MoS_2 nanoparticles where (a) is the sample peaks; (b) is the reference from database, (c) is the difference between sample and reference peaks and (d) shows the Bragg-positions.

It is obvious from the figure that the main diffraction peaks of the sample almost perfectly match the reference peaks obtained from database and there is no additional peak visible, therefore indicating that pure MoS_2 had been synthesized. It is also clear from the diffraction pattern that the sample peaks has

the complete agreement with reference peaks. The sample peaks shows complete agreement with standard peaks value obtained from literature. The informations obtained from XRD pattern about geometry and atomic parameters of Molybdenum disulfide (MoS_2) are given below in table 2.6.

Table 2.6 Rietveld refinement of MoS_2 nanoparticles.

Parameter	***XPD Refinement***
Space group	$P6_3/mmc$
a, c [nm]	0.31610(1), 1.23023(2)
$R_F = \Sigma\|F_0\text{-}F_c\|/\Sigma F_0$	0.0836
$R_I = \Sigma\|I_0\text{-}I_c\|/\Sigma I_0$	0.0937
$R_{wP} = [\Sigma w_i\|y_{0i}\text{-}y_{ci}\|^2/\Sigma w_i\|y_{0i}\|^2]^{1/2}$	0.1670
$R_P = \Sigma\|y_{0i}\text{-}y_{ci}\|/\Sigma\|y_{0i}\|$	0.1710
Atomic parameters	
Mo; 2*c* (1/3, 2/3, 1/4); Occ.;	1.00
B_{iso} (10^2 nm^2)= 0.65(3)	B_{iso} (10^2 nm^2)= 0.12(3)
S; 4*f* (1/3, 2/3, z); Occ., z;	1.00, 0.6210(1)
B_{iso} (10^2 nm^2)= 0.75(3)	B_{iso} (10^2 nm^2)= 0.40(2)

The atomic environments of molybdenum and sulfur atoms are given below is figure 2.3. From the XRD powder diffraction pattern the structure of S1

is triangle and center outside while of Mo1 has anti-cubooctahedron structure. The Molybdenum atoms are sandwiched between two layers of sulfur atoms.

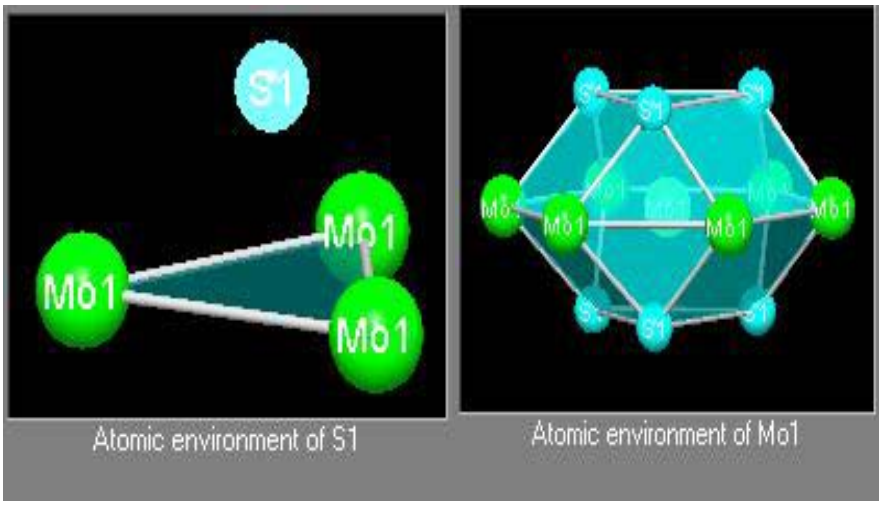

Figure 2.3 3D atomic environments of molybdenum and sulfur.

3D crystal structure of molybdenum disulfide molecules obtained from the XRD analysis is shown in figure 2.4. The cell parameters are a = 0.316 nm, b= 0.316 nm, c= 1.229 nm, while bond angles are given below as, α= 90°, β= 90°, γ= 120°.

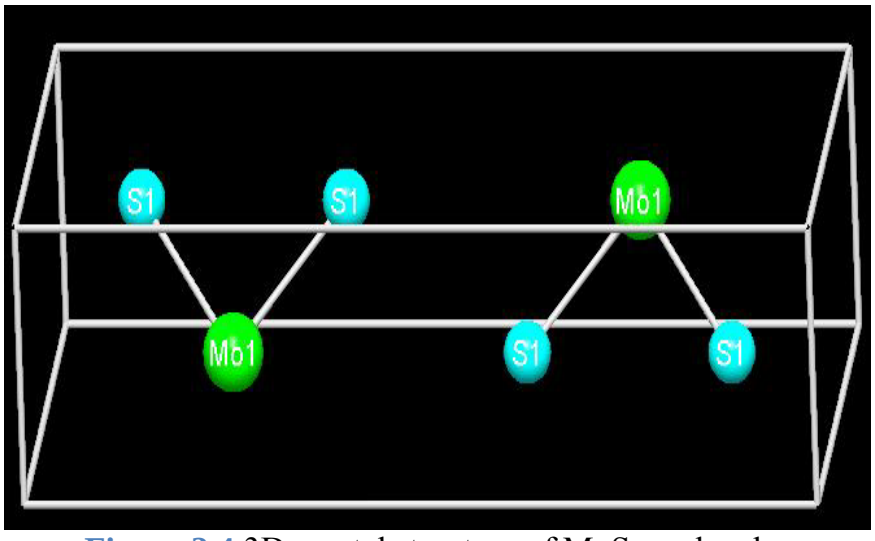

Figure 2.4 3D crystal structure of MoS_2 molecule.

Mass sensitive measurements with Molybdenum Disulfide nanoparticles:

After assuring the composition, purity and particle size of molybdenum disulfides, it was used as a recognition material for thiols. Molybdenum disulfide consists of two parts: one is the metal, which is a soft acid and other the sulfide group, which acts as a soft base according to hard and soft acid base concept. Similarly in case of alkanethiols there are two groups i.e. alkyl and –SH, acting as soft acid and soft base respectively. On exposing MoS_2 nanoparticles to alkanethiols, a so-called soft acid-base interaction is established. This principle should allow for mass effects on QCM electrode surface.

Mass sensitive measurement of 1-Octanethiol with Molybdenum disulfide Nanoparticles (MoS_2 NPs)

On exposing the molybdenum disulfide nanoparticles based sensor to different concentrations of 1-octanethiol, it gives reversible and reproducible signals as shown in figure 2.5.

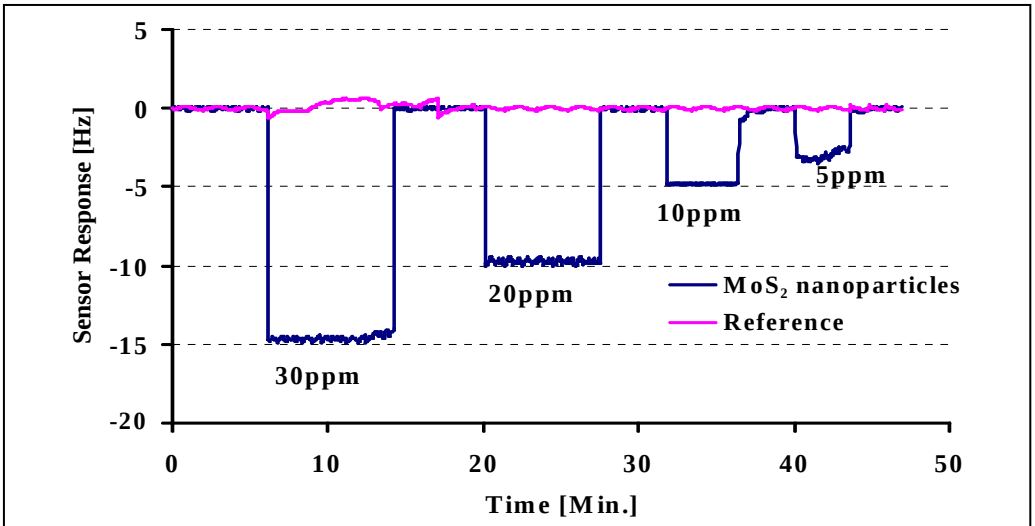

Figure 2.5 Sensing of 1-octanethiol with MoS_2 NPs

As the thiol molecules pass through the chamber they show an affinity interaction with molybdenum disulfide layer and due to deposition of thiol molecules on electrode surface, it shows a frequency shift based on Saurbery's effect. Figure 2.5 presents the normalized (at 1 kHz = 40 nm) sensor response MoS_2 nanoparticles against different concentrations of 1-octanethiol ranging from 30 ppm to 5 ppm respectively.

At the concentration of 30ppm it shows approximately 15 Hz response and 3.5 Hz for 5 ppm with 0.1 Hz noise level only. The limit of detection of the sensor is approximately 430 ppb.

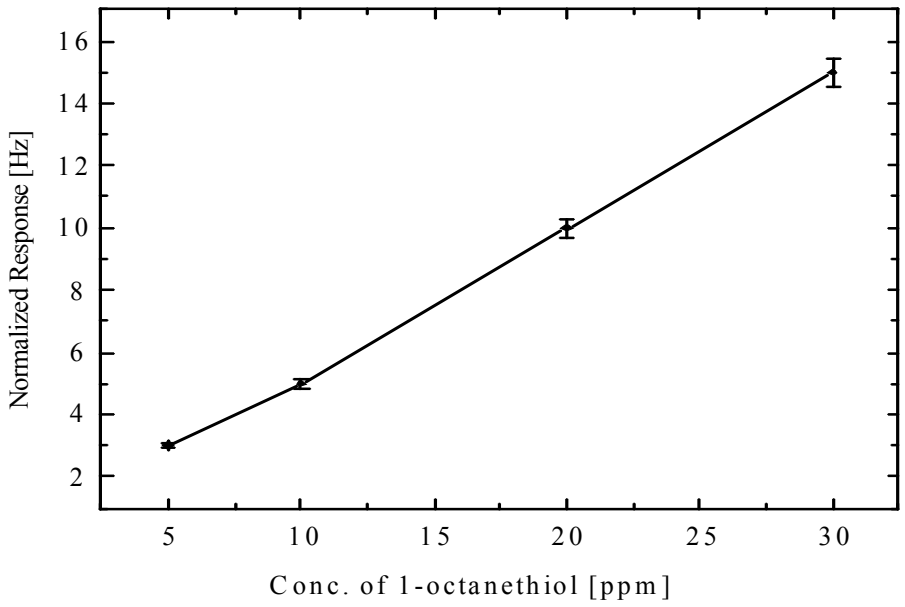

Figure 2.6 Normalized response of MoS_2 nanoparticles against 1-octanethiol.

There is linear relationship between the concentration of 1-octanethiol and sensor response as can be observed in figure 2.6 where the sign of bars at 5ppm, 10ppm, 20ppm and 30ppm indicates the repeatability error of our sensor. The error is less

than 3 percent which indicates efficient reproducibility characteristics of molybdenum disulfide nanoparticles.

Implementation of this strategy to short chain thiol (1-Butanethiol)

In order to assess the feasibility of this strategy to short chain thiols, we exposed our sensor to 1-butanethiol. These nanoparticles have also a reversible and reproducible response for short carbon chain thiols too, which strongly indicates that the recognition indeed takes place via thiol functionality. As the sensor was subjected to different concentrations of 1-butanethiol, an affinity interaction takes place between 1-butabethiol molecules and molybdenum disulfide and a mass change occurs on working electrode surface resulted in frequency shift. Sensor was exposed to different concentrations of 1-butanethiol ranging from 250-750 ppm as shown by figure 2.7.

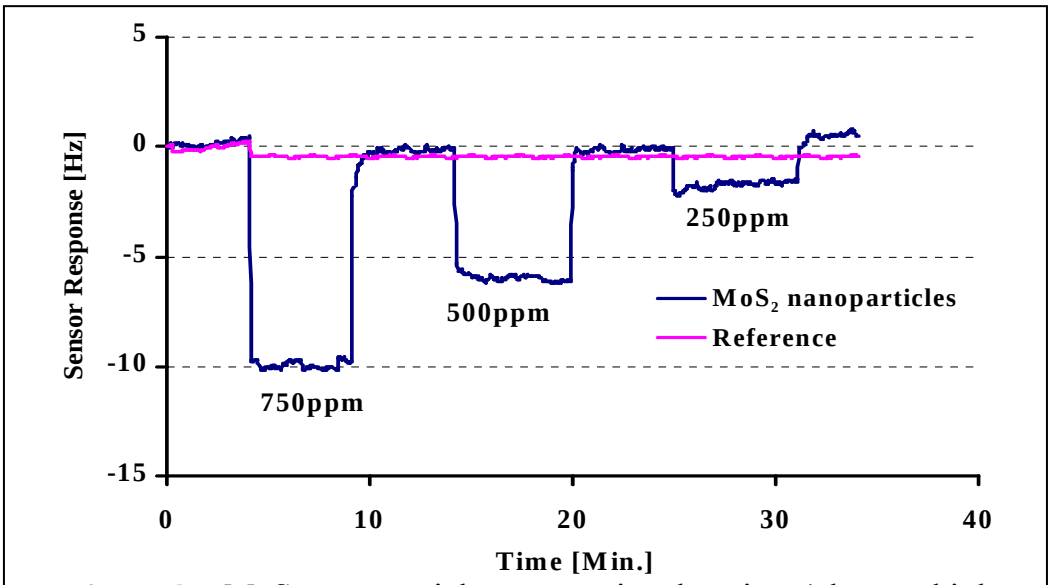

Figure 2.7 MoS_2 nanoparticles sensor signal against 1-butanethiol

Here in figure 2.7, we can see a sensor response of 10 Hz for 750 ppm, 6 Hz for 500 ppm and 3 Hz for 250 ppm at a noise level of 0.11 Hz. The limit of detection

of our sensor for 1-butanethiol is roughly 30 ppm, which represents a 5 times better sensitivity achievement as compared to already reported with same material [17]. Normalized response of MoS_2 nanoparticles sensor against 1-butanethiol is shown in figure 2.8. The R^2 value is 0.9841 that represents linear relationship between the concentration of analyte and sensor signal.

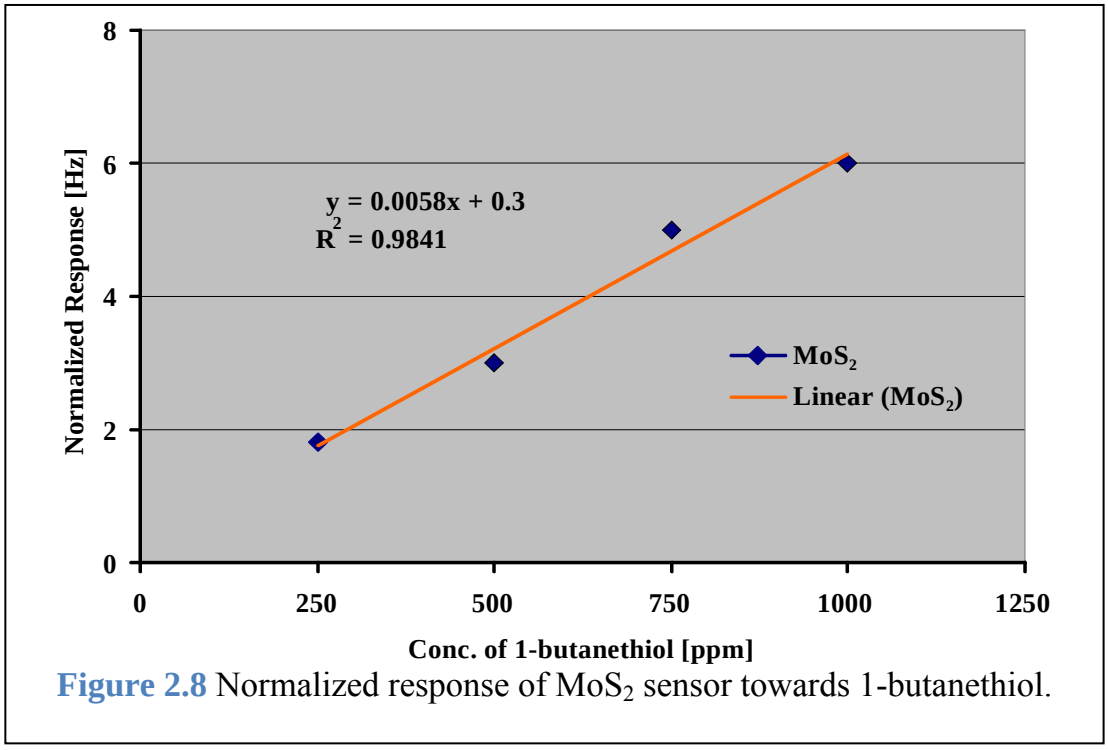

Figure 2.8 Normalized response of MoS_2 sensor towards 1-butanethiol.

Cross Sensitivity and Selectivity Measurements:

Selectivity and sensitivity are of great importance in the field of chemical and biochemical sensor. These two parameters play a key role to assign quality and reliability of a sensor. In order to see the selectivity of designed sensor, it was exposed to n-alkane with same number of carbon atoms.

(i) n-octane

In order to investigate the fact whether recognition is either because of carbon chain interaction or thiol functionality, sensor was subjected to different

analytes differing in functional group but with same number of carbon atoms. On exposing the sensor to different concentrations of n-octane, it shows insensitivity less than 100ppm concentration which indicates the high sensitivity and selectivity of designed sensor towards thiols. It also reinforces and supports the basic strategy and work hypothesis of sensor. Figure 2.9 shows the sensor signal against n-octane at different concentrations.

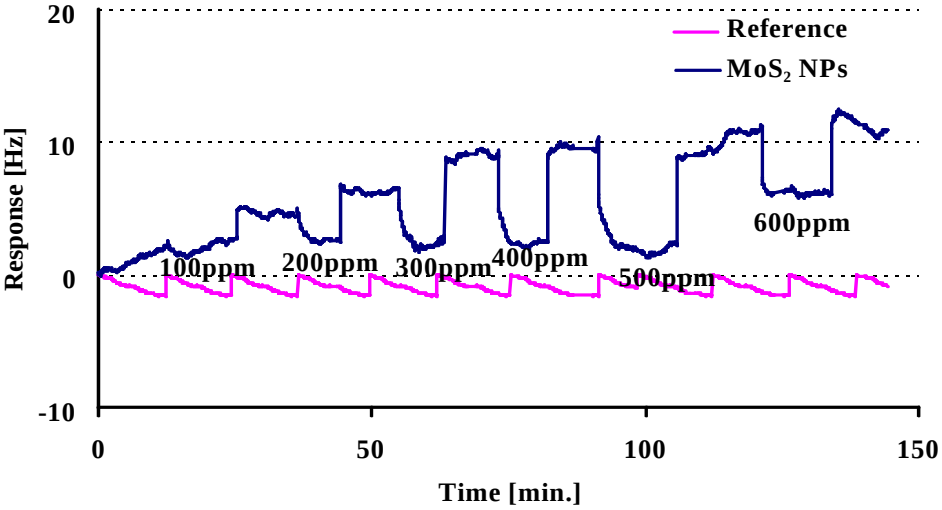

Figure 2.9 MoS_2 nanoparticles sensor response against n-octane.

There is only less than 1 Hz response at 100 ppm concentration of n-octane and even up to 500 ppm there is 7 Hz frequency shift only. As both thiols i.e. 1-butanethiol and 1-octanethiol, yield higher responses than n-octane which have hydrophobic interaction with MoS_2 nanoparticles due to carbon chain indicates that recognition takes place via soft-soft interaction phenomenon. For 40 ppm of 1-octanethiol, sensor yields a response of 10 Hz while 40 ppm of n-octane does not have any frequency change. Even up to 100 ppm of n-octane, there is only 1 Hz response, which is strong indicative for affinity interactions between MoS_2 and thiols. We exposed our sensor to different compounds with molecular mass/number of carbon near or same to respective thiols, but the

sensor shows very minute and ignorable interactions with these compounds indicating the selectivity towards thiols. Figure 2.10 shows the comparison of sensor signals against 1-octanol and n-octane and, where one can directly observe the huge difference in their responses.

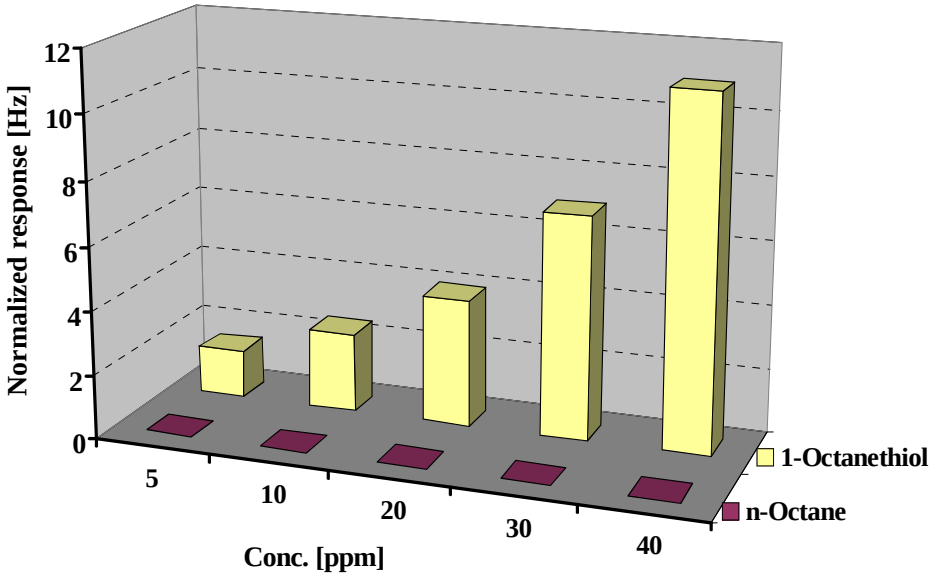

Figure 2.10 Selectivity pattern of MoS_2 nanoparticles

This further supports the model that selectivity is reached by soft-soft interaction between the thiol group and the substrate.

(b)Ethyl methyl ketone

After observing its sensitivity with specific alkanethiol, sensor was also exposed to other organic compounds with same number of carbon but different functional groups. Figure 2.11 represents the sensor response of molybdenum disulfide nanoparticles against 800 ppm and 1000 ppm of ethyl methyl ketone. There is minute response of 1.5 Hz at 1000 ppm of ethyl methyl ketone, while on the other hand 1-butanethiol with same number of carbon atoms but with thiol functionality yields as much as 2.5 Hz at 250 ppm. The molybdenum disulfides nanoparticles base sensor shows 10 times higher response for 1-butanethiol as

compared to ethyl methyl ketone which further indicates that the interactions take place via soft acid-base interactions existing between thiol and MoS_2 nanoparticles.

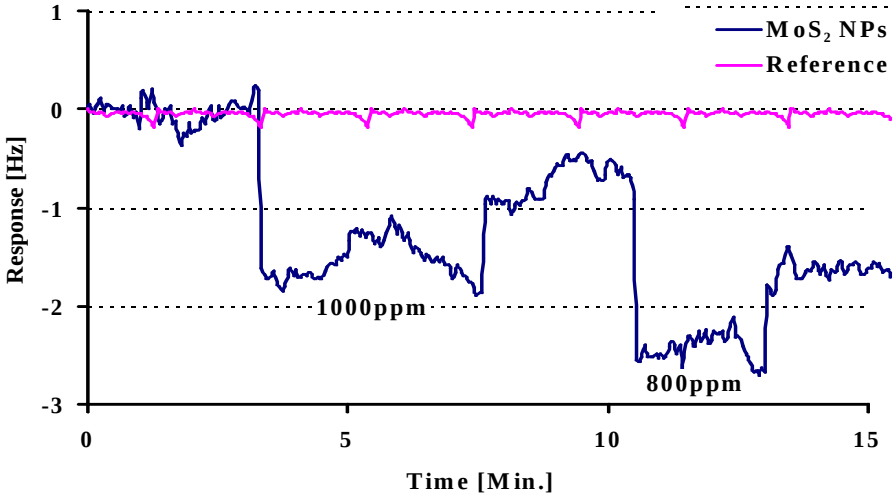

Figure 2.11 MoS_2 nanoparticles sensor response towards ethyl methyl ketone.

(c)Terpenes

Sensors were also exposed to cyclic odorous compounds for selectivity purpose. For this purpose we choose terpenes, a family of maturely accuring odorous compounds and limonene was used as an analyte to see sensor selectivity. It was observed that MoS_2 nanoparticles based sensor has no such appreciable response against limonene. Figure 2.12 shows the sensor response against 100ppm and 50ppm concentrations of limonene and it shows only 3 Hz change in frequency for 100 ppm and 2 Hz for 50 ppm of limonene. A frequency change on reference electrode is also observed along with working electrode. The large effect on the reference electrode indicates that interaction mainly takes place with the aliphatic monolayer used for electrode modification.

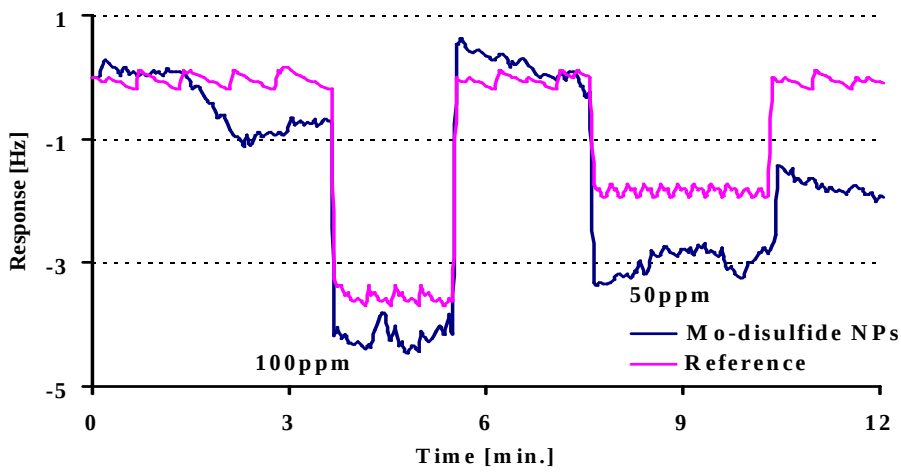

Figure 2.12 Sensor response of MoS_2 nanoparticles against Limonene.

So, theoretically being soft material MoS_2 nanoparticles layer shows interaction with thiols only, which is itself a soft species and not to other compounds. It can be seen in figure 2.13 that the sensor response of MoS_2 nanoparticles towards

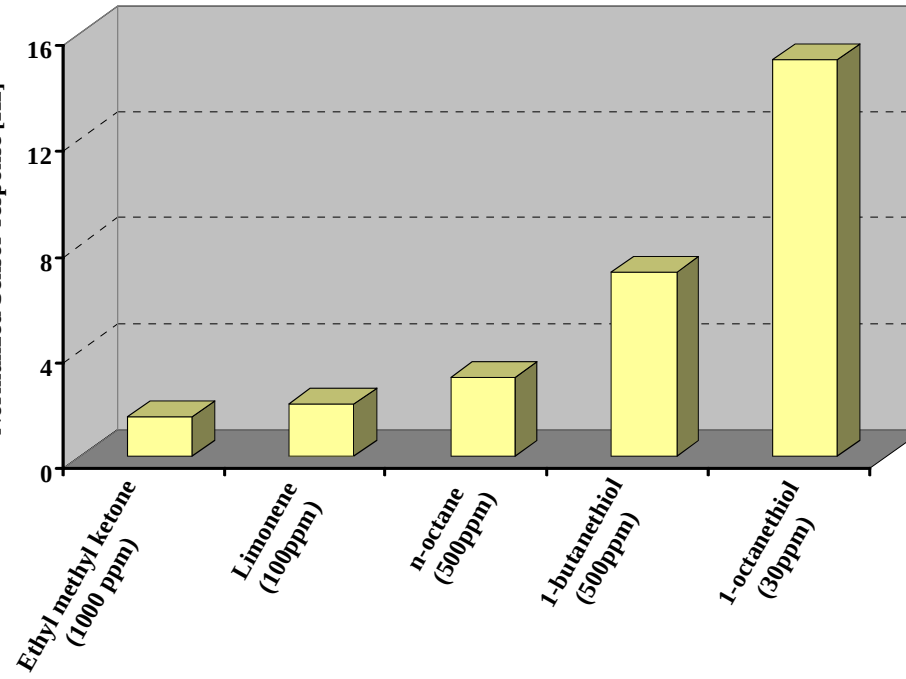

Figure 2.13 Sensitivity and selectivity pattern of MoS_2 nanoparticles.

thiol is substantially higher as compared to n-octane, limonene and ketone. In figure 2.13 we can see that there is a response of 15 Hz for 30 ppm of 1-octanethiol, 7 Hz for 500 ppm of 1-butanethiol, 3 Hz for 500 ppm of n-octane, 2 Hz for 100 ppm of limonene and 1.5 ppm for 1000 ppm of ethyl methyl ketone. Sensor response for 1-octanethiol is 80 times more than n-octane having same number of carbon atoms but lack of thiol functionality, similarly on comparing thiols responses with other analytes a substantial difference has been observed. So, MoS_2 nanoparticles based sensor offers the unique possibility of independently sensing the thiol group containing compounds. Therefore, as we see above our sensor is highly sensitive and selective towards thiols.

Affinity interaction comparison of MoS_2 nanoparticles with different polymers:

After comparing the sensor responses of MoS_2 nanoparticles with compounds having similar number of carbon atoms but different symmetry and functionality, we extended our approach by comparing them to layers showing mainly to polar, hydrophobic and unsaturated compounds functionality such as polyvinyl alcohol, polystyrene and polyvinyl chloride. The respective sensor responses obtained towards different concentrations of 1-octanethiol are summarized in figure 2.14. As polyvinyl alcohol is highly polar and yields 4 Hz response only towards 30 ppm of 1-octanethiol, indicating no appreciable interaction of thiol with polar system. On the other hand polystyrene is an unsaturated system, shows 2 Hz sensor signals towards 30 ppm of 1-octanethiol and is less than MoS_2 system by a factor of more than 7 which means that thiol has no interaction with saturated system. Similarly, polyvinyl chloride being hydrophobic yields 1.5 Hz response only for 30 ppm of 1-octanethiol which is 9 times less than that of MoS_2 nanoparticles. As none of these polymers has low

Pearson hardness, this further underpins the importance of that factor for recognition.

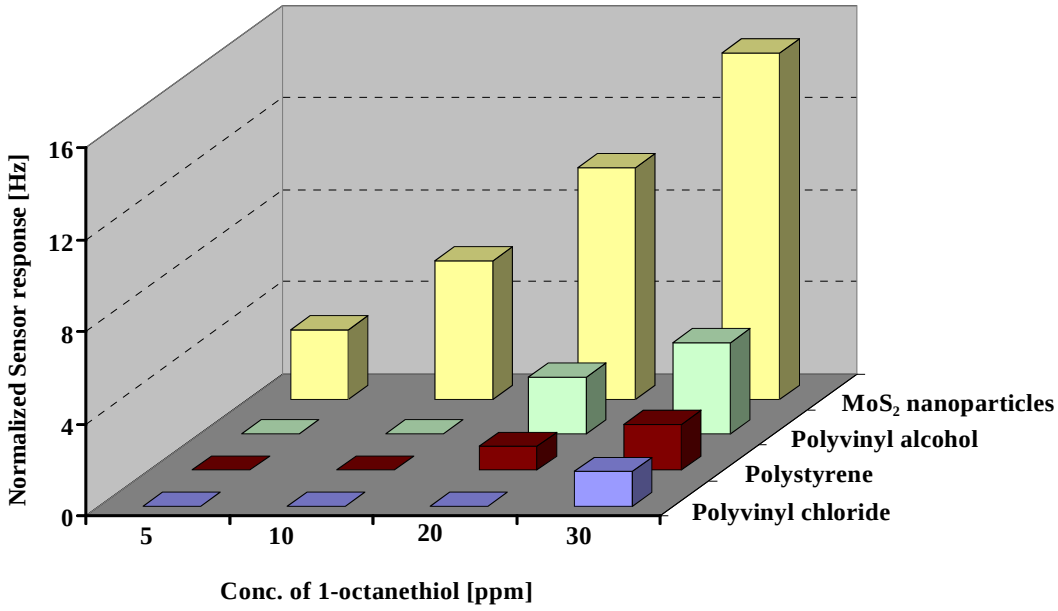

Figure 2.14 Comparison of sensor signals of polyvinyl alcohol, polystyrene and polyvinyl chloride with MoS_2 nanoparticles

2.4 Conclusion

The use of nanoparticles as a recognition layer material enhances the sensitivity and detection limit of a sensor because of availability of substantial increased surface area. Thus soft metal-sulfide nanoparticles approaches have proven themselves to be highly suitable for designing sensor materials to detect pollutants for both environmental and process control applications. Molybdenum disulfide nanoparticles interact reversibly with organic thiols and therefore can be used to detect highly smelly and toxic to human via affinity interactions between “soft” sulfur atom of the analyte and “soft” layer material, where “soft” refers to Pearson concept of hard and soft materials. By decreasing the

nanoparticles size, the sensitivity of sensor increases and there is a direct relationship between particles size and sensor limit of detection. For 1-butanethiol and 1-octanethiol the limit of detection is 30 ppm and 0.5 ppm respectively, which shows the application of this newly developed sensor in that areas where on-line and continuous monitoring of thiols is mandatory. So this strategy has proved itself as suitable, highly sensitive and selective recognition material for thiols.

3. Sensing of Thiols with Copper Sulfides Nanoparticles

3.1 Introduction

To further elucidate the influence of Pearson hardness on the sensor effects, different metal sulfides were assessed according to their properties as sensor layers. In this, copper is of special interest, because some of the most important copper ores are sulfides [27], namely chalcopyrite ($CuFeS_2$), boronite (Cu_5FeS_4), covellite (CuS), Chalcocite (Cu_2S). Copper sulfides are a particularly interesting class of metal sulfides because of their ability to form various stoichiometrical products [28]. Sulfides of copper have substantial importance in field of acid-base chemistry, as Cu^{+2} has Pearson hardness (η_A) of 8.3 and Cu^{+1} with Pearson hardness (η_A) of 6.3, is soft species [29].

3.2 Experimental

Material and Method:

Sodium thiosulfate ($Na_2S_2O_3.5H_2O$), copper sulfate ($CuSO_4.\ 5H_2O$), and surfactant to minimize the coagulation of particles were purchased from Merck and Fluka with the highest purity available and used as received.

Synthesis of Copper Sulfide Nanoparticles

Method 1

Copper sulfide (Cu_xS) particles were synthesized via photochemical method from an aqueous solution containing copper sulfate ($CuSO_4$) and Sodium thiosulfate ($Na_2S_2O_3$) [30]. In a typical experiment, 5 ml $CuSO_4$ solution (1

mol/l) was mixed with 15 ml $Na_2S_2O_3$ solution (1 mol/l) drop wise resulting in a bright-green solution. This was kept at ambient conditions for a week without stirring. After mixing both precursor solutions (i.e. sodium thiosulfate and copper sulfate), the resultant solution remained transparent and clear. After two days nanoparticles formation started but yielding optimal results after one week. These black-green particles were collected from the solution by centrifugation and washed several times with distilled water to remove all other unwanted byproduct and impurities. Particles were dried at 60^0C overnight. The possible way of formation of Cu_xS can considered as follow,

$$xCu^{2+} + S_2O_3^{2-} + 2H_2O \rightarrow [Cu_x(S_2O_3)(H_2O)_2]$$
$$[Cu_x(S_2O_3)(H_2O)_2] \rightarrow SO4^{2-} + Cu_xS + 2H^+ + H_2O$$

Method 2

An aqueous solution of 300 ml containing Sodium thiosulfate ($Na_2S_2O_3$) in range of 0.025-0.1 mol/l and copper sulfate ($CuSO_4$) with concentration of 0.0025-0.05 mol/l was stirred up to one hour at ambient conditions. Initially, the pH of the solution was 6, which was then lowered to 3 by adding drop wise dilute H_2SO_4. Then solution was kept under constant UV light for two hours. Copper sulfide particles were filtered and washed with dilute HCl aqueous solution (v/v HCl:H_2O = 1:4) to remove unwanted material. The particles with different sizes were separated by centrifugation and dried at 60^0C in an oven over night [30]. If aqueous solution of thiosulfate ions $S_2O_3^{2-}$ are exposed to UV light, it becomes excited and acts as a reductant. This sulfur atom is thereby converted to sulfide ion. The metal ions precipitate with sulfide ions and in this way form copper sulfide in the irradiated region.

$$S_2O_3^{2-} + h\upsilon \rightarrow S + SO_3^{-2}$$

$$2S_2O_3^{2-} + h\upsilon \rightarrow S_4O_6^{-2} + 2e^-$$

$$2Cu^{2+} + S + 4e^- \rightarrow Cu_2S$$

$$Cu^{2+} + S + 2e^- \rightarrow CuS$$

This assumed reaction mechanism shows that at excess thiol sulfate is needed (1.5 fold for Cu_2S and three fold for CuS).

The presence of Cu_xS nanoparticles is confirmed by analysis of these particles with XRD and the size of particles is calculated through atomic force microscopy (AFM). The procedure of microscopy, XRD analysis and particles coating is same as discussed already in chapter 2.

3.3 Results and Discussion

Nanoparticles Characteristics by XRD Analysis

To verify the feasibility of synthesis of copper sulfide nanoparticles XRD technique was used, working with Cu $K\alpha_1$-Radiation (1.54056Å). The measurement of the samples is executed at a voltage of 40 kV and a current of 30 mA. Figure 3.1 given below, represents the XRD pattern of CuS nanoparticles. It can be seen from diffraction pattern that there is no additional peak of any impurity. There is a complete agreement of sample peaks with reference peaks. The pattern obtained indicates the purity of nanoparticles and also about the phase of copper sulfide i.e. copper is present in Cu^{2+} form. Therefore, it is assured that the CuS nanoparticles are with highest purity.

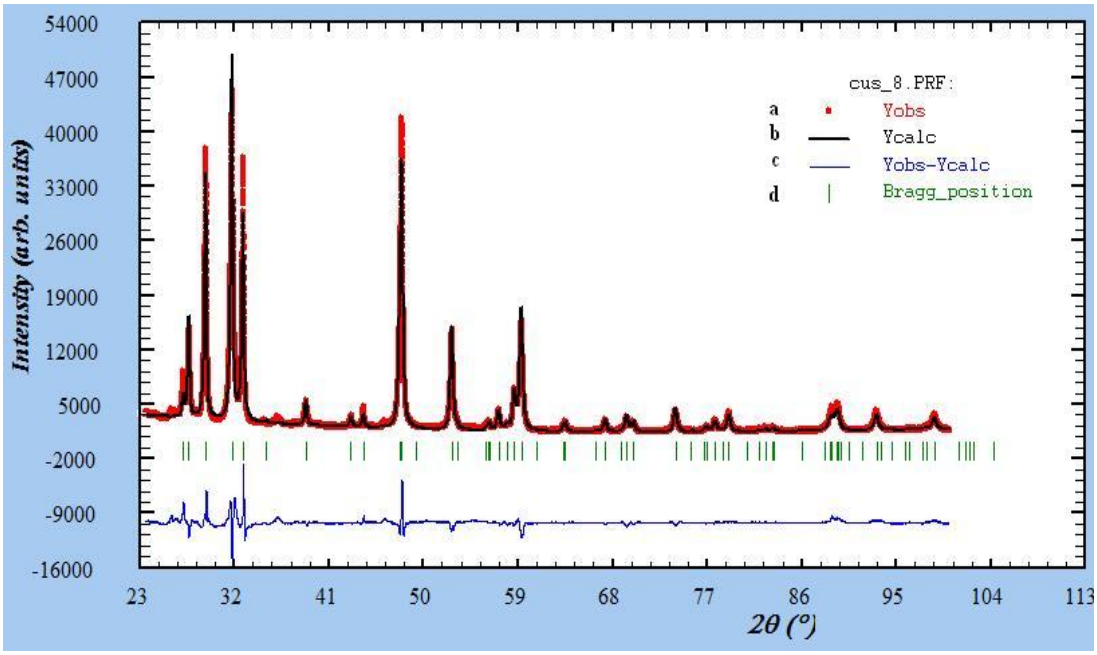

Figure 3.1 XRD powder diffraction pattern of CuS Nanoparticles where (a) is the sample peaks; (b) is the reference from database, (c) is the difference between sample and reference peaks and (d) shows the Bragg-positions.

Covelite CuS has remarkably complex crystal structure and the structure of CuS is already reported in literature [31]. Figure 3.2 shows its 3D structure as below.

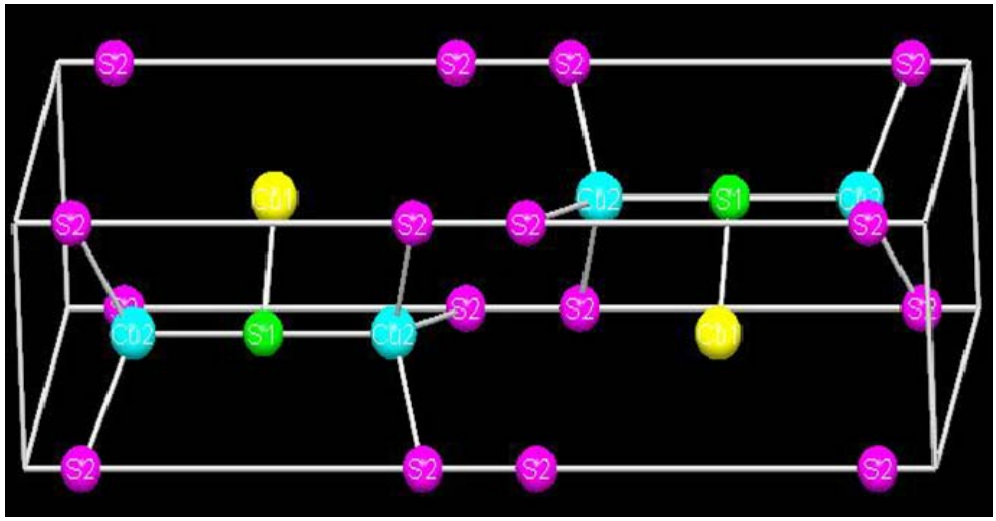

Figure 3.2 Three dimensional crystal structure of CuS [31]

XRD analysis provides the informations related to atomic environments of copper and sulfur in CuS. The copper atom in CuS has two different atomic environments and exists in triangle, center inside and tetrahedron shapes. But sulfur atom also has two atomic environments as tetrahedron and tetragonal bi-pyramid. The atomic environments of Cu and S atoms are shown in figure 3.3.

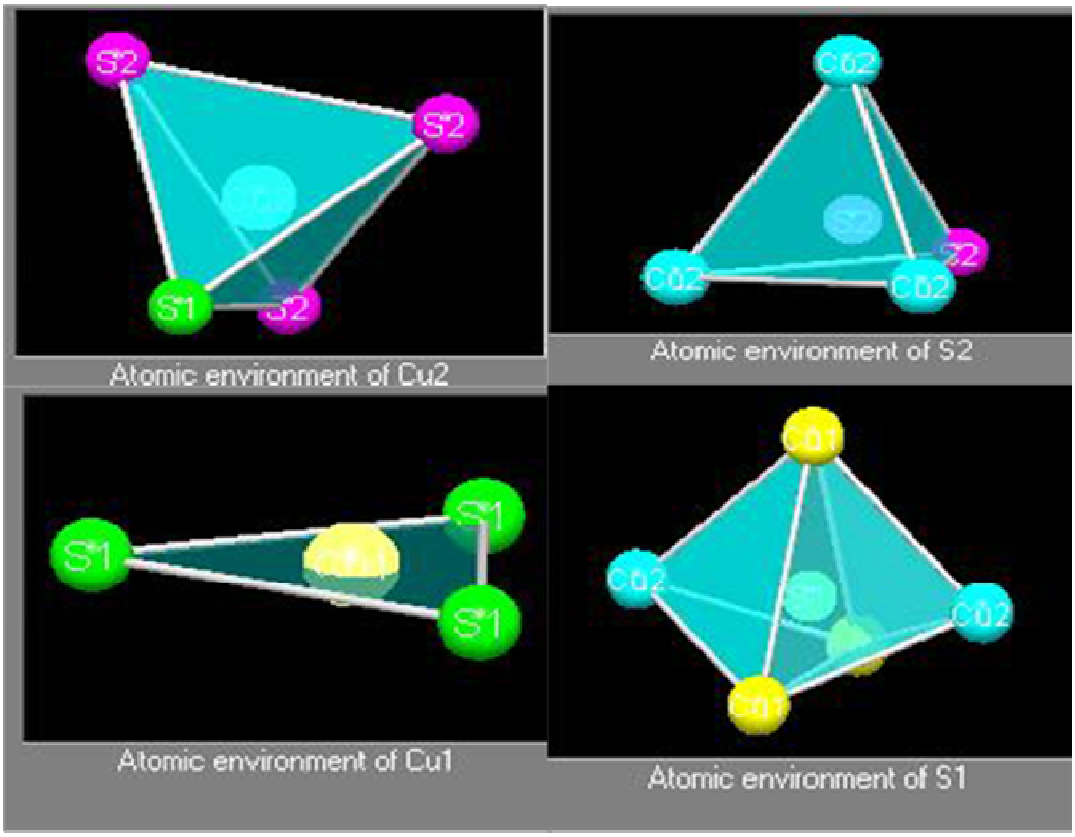

Figure 3.3 3D environments of sulfur and copper atoms in CuS [31].

As the sulfides of copper occur in both forms as Cu_2S and CuS, one is very soft material and other one hard. So, the use of both materials as recognition layer for thiol and comparison of the results provides a good chance to verify the hypothesis of soft-soft interaction. Therefore before using the Cu_2S nanoparticles as sensor material their stoichiometry and purity was also verified by XRD

analysis. The experimental procedure and method was same as mentioned above in case of CuS. Figure 3.4 illustrates the X-ray diffraction pattern of Cu_2S nanoparticles. From diffraction pattern we can see that there is no additional peak of any impurity and all sample peaks have complete agreement with reference peaks obtained from data base which insures the purity of Cu_2S. The data obtained is given below, which is similar to already reported [32].

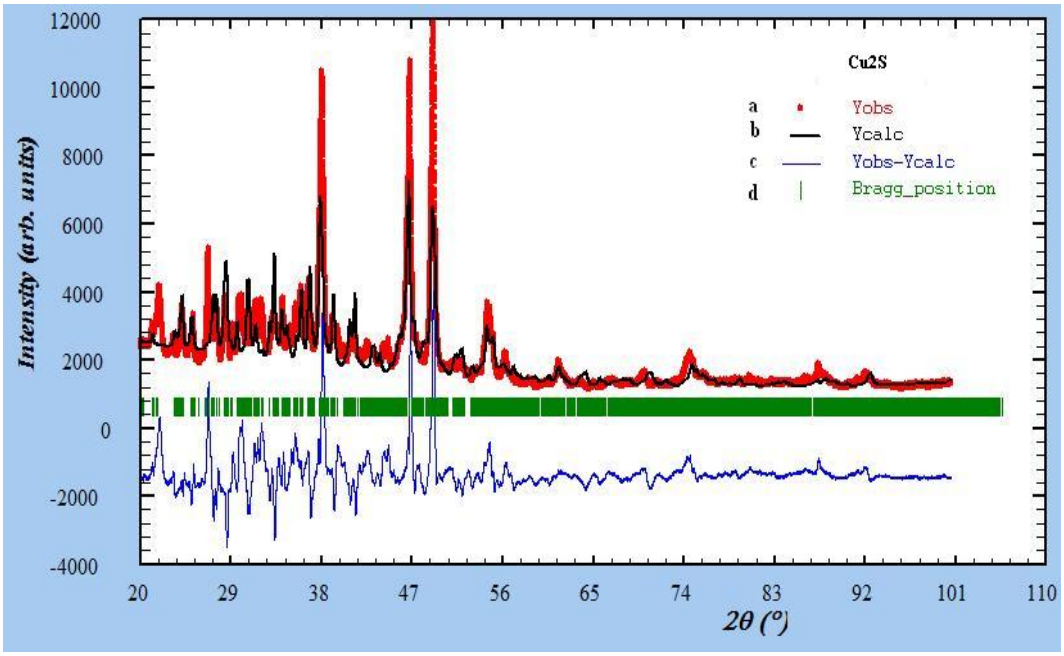

Figure 3.4 XRD pattern of Cu_2S where (a) is the sample peaks; (b) is the reference from database, (c) is the difference between sample and reference peaks and (d) shows the Bragg-positions

The 3D structure of Cu_2S obtained from XRD analysis is shown in figure 3.5 with very complex geometry having copper and sulfur atoms with different atomic environments. The atomic environments of some Cu and S atoms in the Cu_2S are also shown with different planes in figure 3.6.

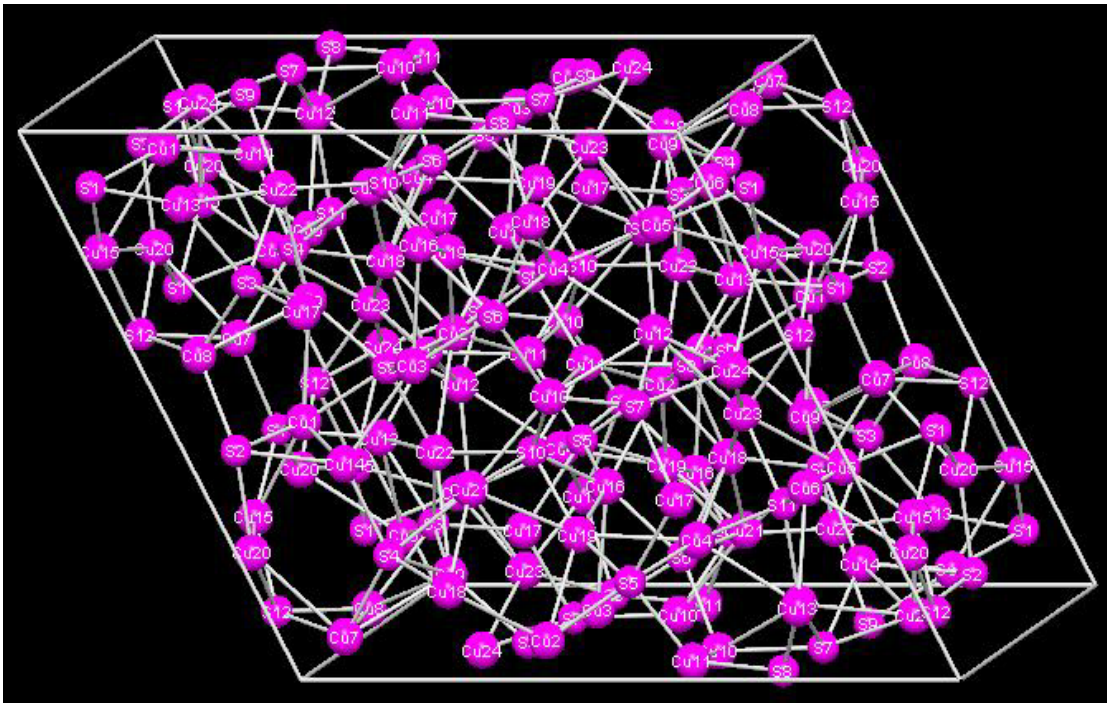

Figure 3.5 3D structure of Cu_2S crystal [32]

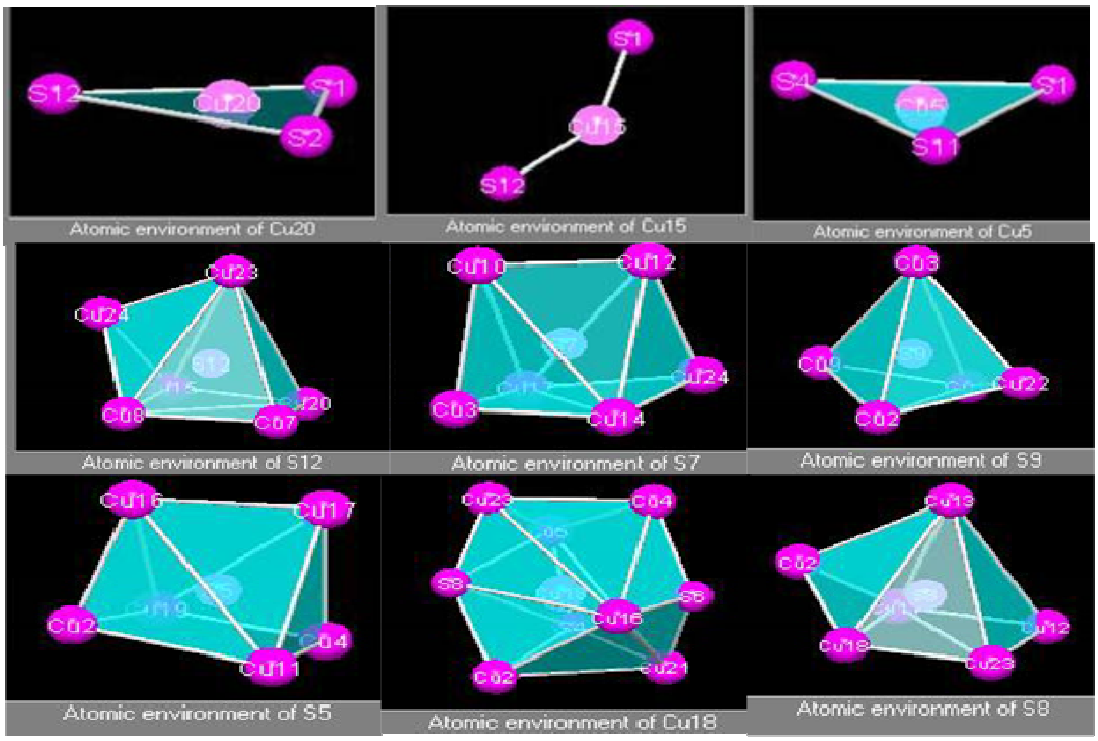

Figure 3.6 3D environments of copper and sulfur atoms in Cu_2S crystals [32]

Atomic Force Microscopy of Copper Sulfide Nanoparticles

In order to check the feasibility of synthesis procedure the particle size had to be checked. For this purpose AFM images of copper sulfide particles were recorded after depositing particles on a glass substrate. Figure 3.7 illustrates the size of nanoparticles; (a) shows the particles of smaller size all having less than 50 nm and (b) represents the image of particles with size less than 100 nm respectively. The particles with different sizes were separated by centrifugation at different speed and time. The size of nanoparticles is of crucial importance because small particles offer greater surface area.

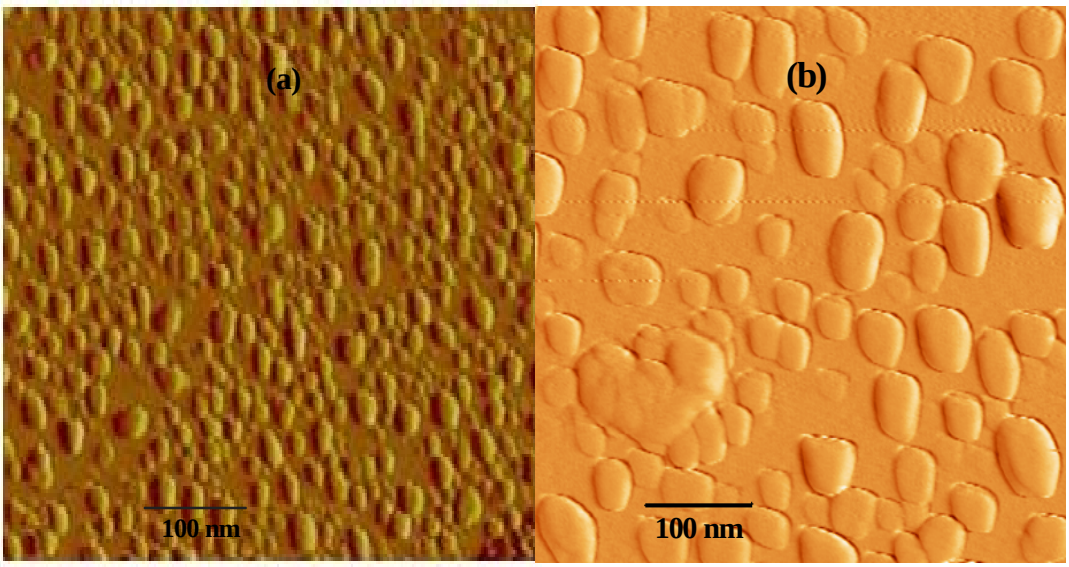

Figure 3.7 AFM images of Cu-sulfide nanoparticles (a) particles with size less than 50 nm and (b) particles having size less than 100 nm

It can be seen from above figure that the majority of the particles are of rounded shape.

Preparation of QCM and Mass Sensitive Measurements

For thiol sensing a 10 MHz quartz crystal microbalance was prepared as mentioned in case of molybdenum disulfide. 10 mg of copper sulfide nanoparticles were mixed together with 500 µl ethylenediamine which results into a suspension of nanoparticles. 5 µl of suspension was coated on electrode each surface by spin coating method at 2000 rpm and dried at 80^{o}C for overnight. A rigid, thin and compact layer of nanoparticles with layer height of 5-6 kHz (1 kHz = 40 nm) was resulted.

Sensing of 1-octanethiol

In order to test these hypothesis, Cu_2S nanoparticles coated QCM was exposed to first of all 1-octanethiol at different concentrations in air. Figure 3.8 shows the resulting sensor response of between 3-18 ppm for particles being 50-100 nm in diameter. It is evident from the figure that Cu_2S nanoparticles yield a reversible and reproducible sensor signal against 1-octanethiol. The nanoparticles for coating have sizes ranging from 50-100 nm.

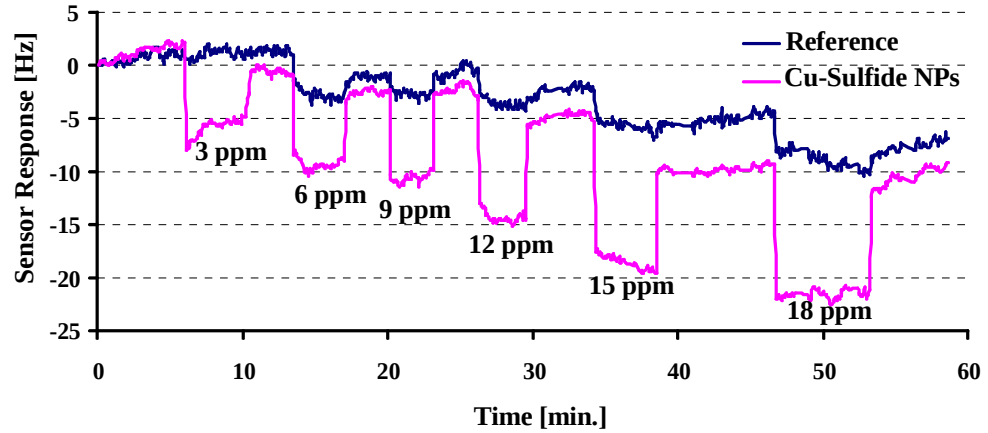

Figure 3.8 Sensor signal of Cu_2S nanoparticles layer against 1-octanethiol

From the figure we can see that there is a response 5 Hz for 3 ppm with 0.3 Hz noise level and its limit of detection is less than 1 ppm. This change in frequency is due to the selective interaction of Cu_2S nanoparticles with thiol, most probably based on HSAB theory of softness and hardness. This proves the principal versatility of the approach for sensing purposes.

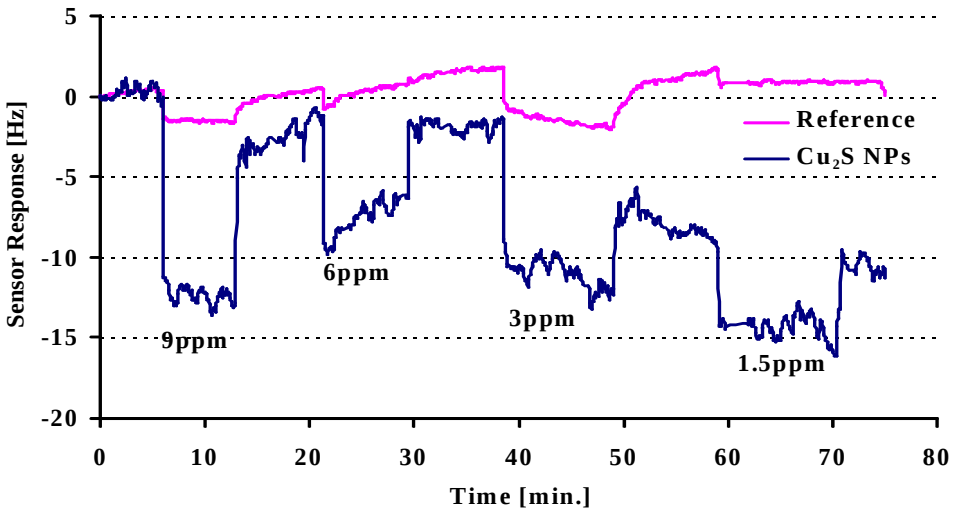

Figure 3.9 Sensing of 1-octanethiol with Cu_2S nanoparticles (<50nm)

Figure 3.9 represents the sensor response of a QCM sensor coated with nanoparticles of diameter less than 50 nm to assess the influence of particle size on sensitivity. The sensor shows a response 4 Hz for 1.5 ppm of 1-octanethiol with the detection limit of 50 ppb. As compared to sensor signal of particles having diameter 100 nm the sensor response, sensitivity and limit of detection is increased by the factor of two. The reason of this increased sensitivity is the increase in surface area of particles with size less than 50 nm. This is further supported by the fact that sensitivity increases by the same factor as overall surface of particles increases (half the diameter leads to twice the surface area when keeping the amount particle material constant). Furthermore, sensor layers composed of smaller nanoparticles has lower surface roughness and better

homogeneity which leads to better electronic quality of the oscillator (i.e. lower noise) and therefore improved sensor signals.

Another Cu_2S sensor curve obtained at 10-60 ppm concentrations of 1-octanethiol is shown by figure 3.10

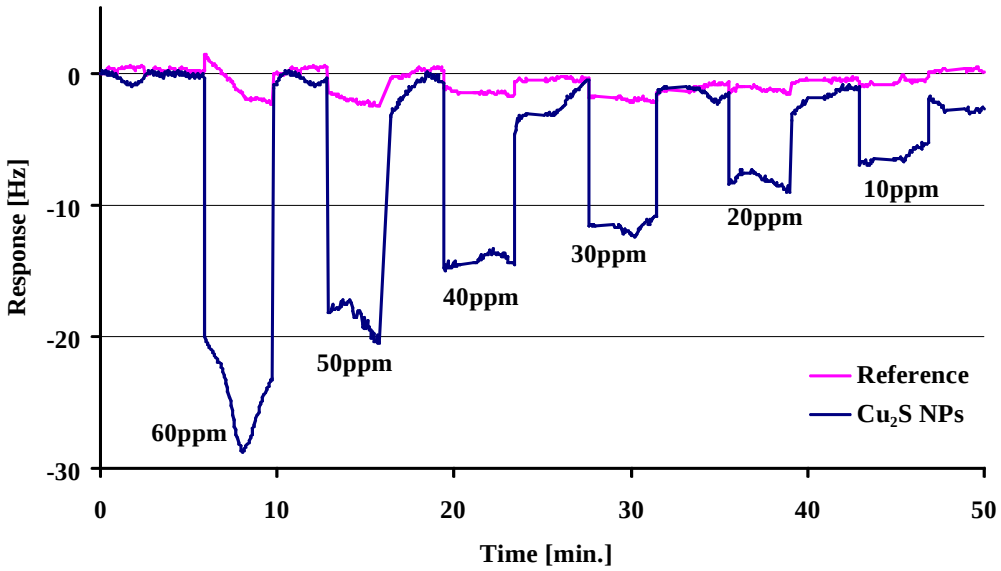

Figure 3.10 Sensor Response of Cu_2S NPs (50-100 nm) towards 1-octanethiol

It can be seen from figure 3.10 that there is a linear relation between sensitivity and concentration of 1-octanethiol. At the concentration of 10 ppm there is a response of 6 Hz, for 20 ppm of 9 Hz, for 30ppm of 12 Hz, for 40 ppm of 15 Hz, for 50ppm of 20 Hz and for 60 ppm of 28 Hz response has been recorded. This indicates the concentration dependence sensitivity behavior of Cu_2S nanoparticles towards 1-octanethiol.

Normalized response of Cu_2S nanoparticles against 1-octanethiol is shown in figure 3.11. It can be seen that there is a good relationship between the concentration of 1-octanethiol and sensor response. The correlation coefficient

(R^2) value is 0.9863 which indicates the linear tendency of all the data points. So it is proved that our sensor response is concentration dependent.

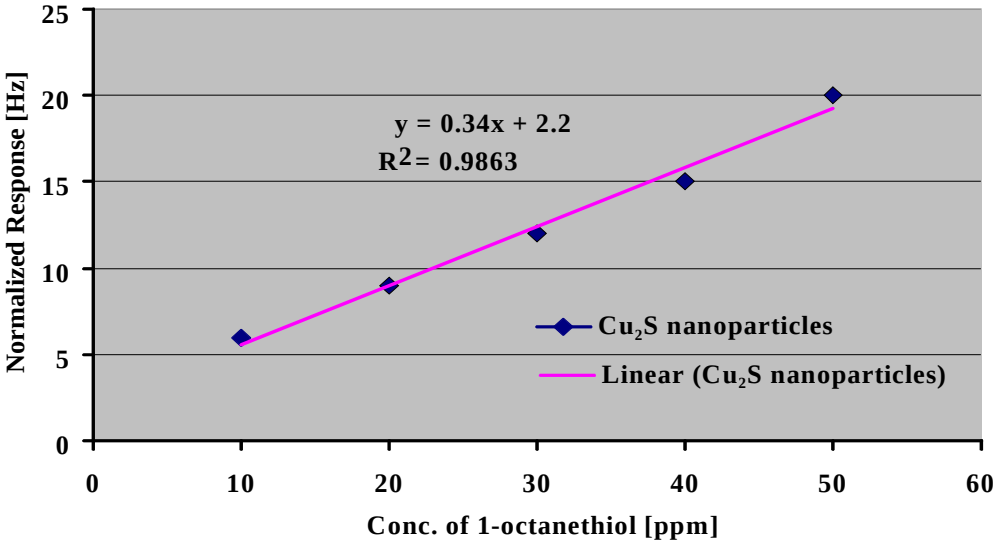

Figure 3.11 Normalized sensor response of Cu_2S nanoparticles towards 1-octanethiol

1-butanethiol sensing

Of course, it is also of interest to assess the influence of chain length on the sensor signals. Therefore, we exposed the sensor to 1-butanethiol. The figure 3.12 represents the sensor response of Cu_2S nanoparticles with size ranging 50-100 nm towards 1-butanethiol at concentrations of 500-2500 ppm. A reversible and reproducible sensor behavior could be observed. As can be seen from figure 3.12 there is a sensor response of 6 Hz for 500 with a 0.2 Hz noise and the detection limit of sensor is 50 ppm.

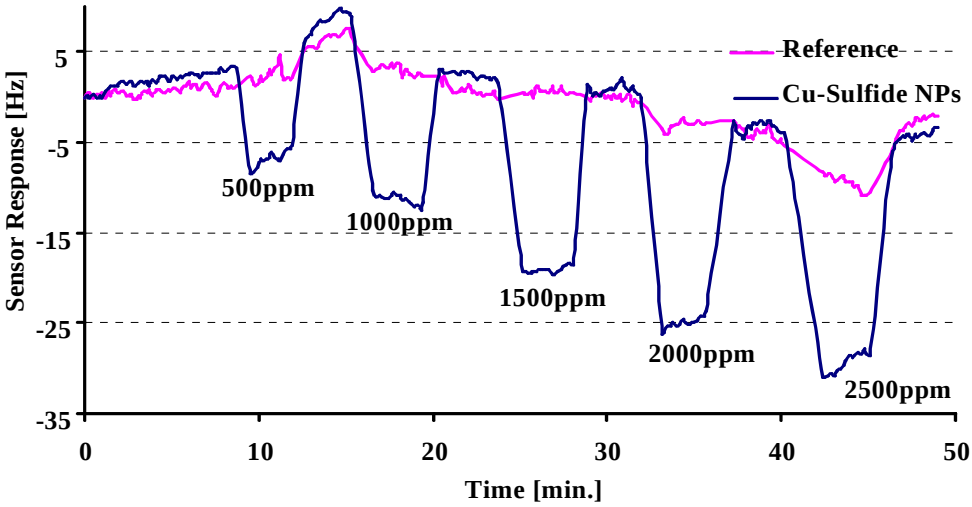

Figure 3.12 Sensor response of Cu_2S nanoparticles (50-100nm) against 1-butanethiol

Again, nanoparticles with smaller diameter offer substantially increased interaction area. Figure 3.13 shows the sensor response of Cu_2S nanoparticles with less than 50 nm diameter towards the different concentrations of 1-butanethiol ranging from 100-1000 ppm.

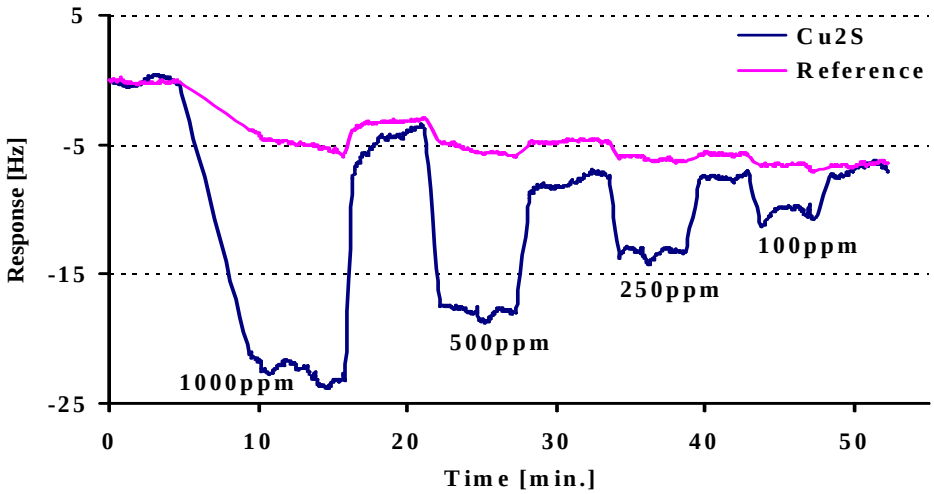

Figure 3.13 Sensor response of C_2S nanoparticles (<50nm) towards 1-butanethiol

There is a sensor response of approximately 4 Hz for 100 ppm of 1-butanethiol with 0.15 noise level and the detection limit is 12 ppm. So the detection limit is increased by a factor of more than 4. The sensitivity of the sensor is also increased by the factor of more than four. This increase of sensor sensitivity is because of the availability of the substantial increased surface area provided by small nanoparticles.

The normalized sensor response of Cu_2S nanoparticles against 1-butanethiol is shown in figure 3.14. A linear and reversible behavior of sensor can be observed from this figure. The regression analysis indicates that there is a linear relationship between sensor signals and concentrations of 1-butanethiol. The correlation coefficient (R^2) value is 0.9897 and the percentage error less than 3 percent has been observed.

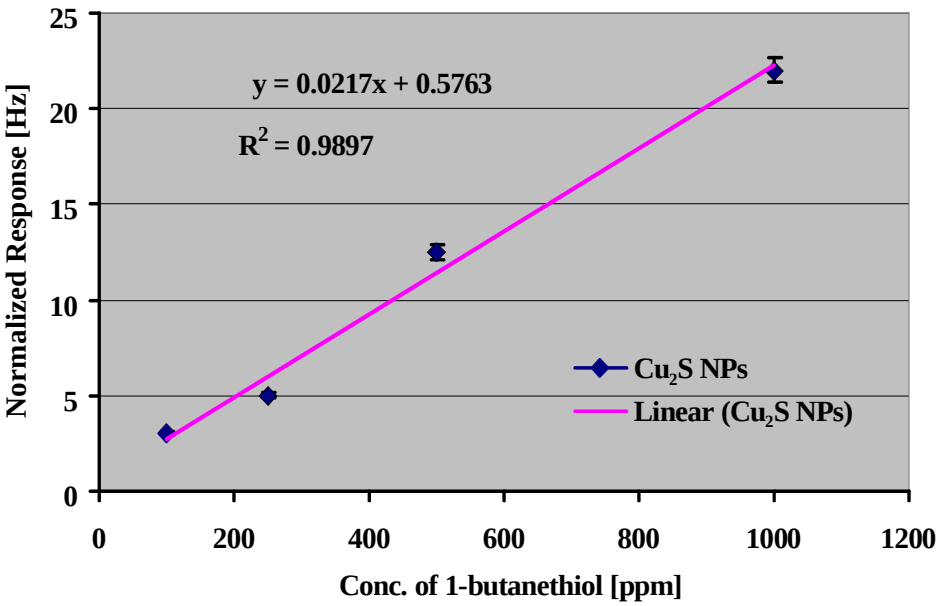

Figure 3.14 Normalized response of Cu_2S NPs against 1-butanethiol with percentage error bars

Selectivity and Cross Sensitivity of Cu_2S nanoparticles

As with MoS_2, we further checked the under lying mechanisms by exposing our sensor to vapors with different functionality i.e n-octane, ethyl methyl ketone and limonene.

(a) n-octane

Figure 3.15 shows the sensor signal of Cu_2S nanoparticles against n-octane at different concentration ranging from 100-500 ppm. The sensor gives no frequency shift below 100 ppm; for 100 ppm there is a small response of only 2.0 Hz. On the other side the sensor response for 1-octanethiol (that has the same amount of carbon atoms) at 1.5 ppm is 4 Hz. It verifies the fact that sensitivity of the sensor is due to the thiol functionality not because of possibly hydrophilic interactions between the carbon chain and the nanoparticles.

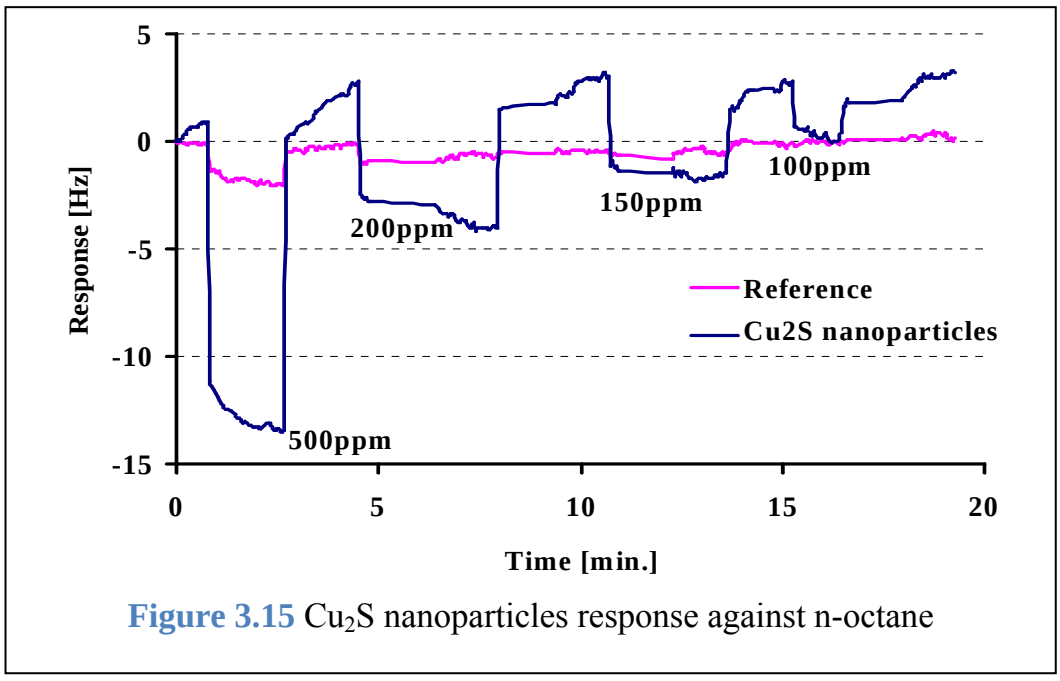

Figure 3.15 Cu_2S nanoparticles response against n-octane

(b) Ethyl methyl ketone

Ethyl methyl ketone has different functionality and number of carbons, so it can be used to assess the effect of carbon chain and functional group. The sensor response of Cu_2S nanoparticles towards different concentrations ranging 200-1000 ppm of ethyl methyl ketone is shown by the figure 3.16. Sensor gives a small shift of 1 Hz only for 200 ppm and 5 Hz for 1000 ppm. The molar mass ratio between ethyl methyl ketone and 1-butanethiol is 1:1.25 respectively. However, the ratio between their sensor responses is as high as 1:4. This four time increase of sensor response at same concentration of 100 ppm of each analyte also strongly indicates that the mass effect on the sensors can be traced back to soft-soft interaction between Cu_2S and thiols.

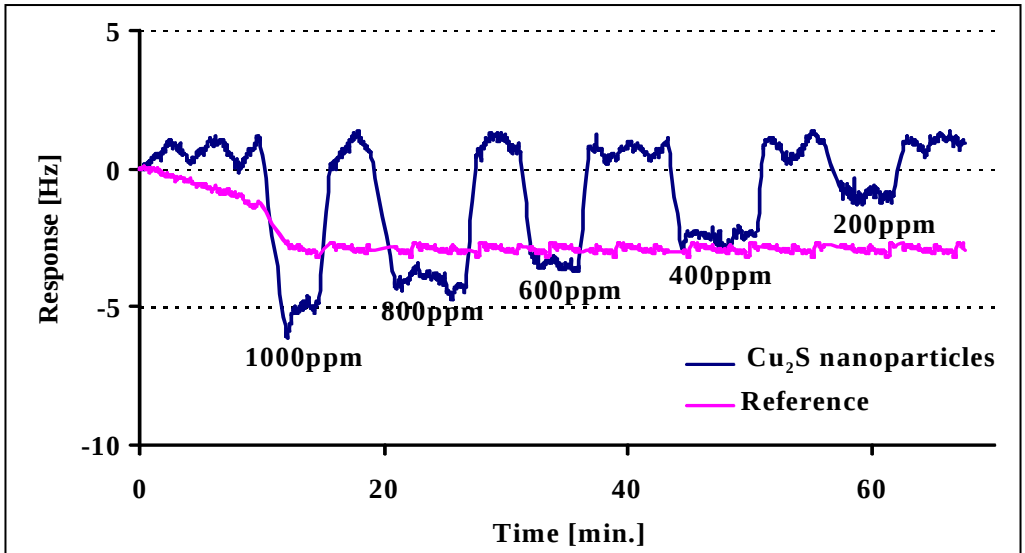

Figure 3.16 Cu_2S nanoparticles response against ethyl methyl ketone

(c) d-Limonene

Aside of functionality and differences in the aliphatic chain, it is also of great interest to assess cyclic and/or unsaturated compounds. For this purpose we

exposed our sensor to terpenes combining these two properties. Figure 3.17 shows the sensor response of Cu_2S towards 50-100 ppm of limonene. There is a sensor response of 1.5 Hz only for 50 ppm of limonene with molecular mass of 136.23 g. The molar mass ratio between 1-octanethiol and limonene is 1:1.07 respectively but the sensor response of 1-octanethiol is 20 times more than limonene which also indicates that this difference is due to thiol functionality.

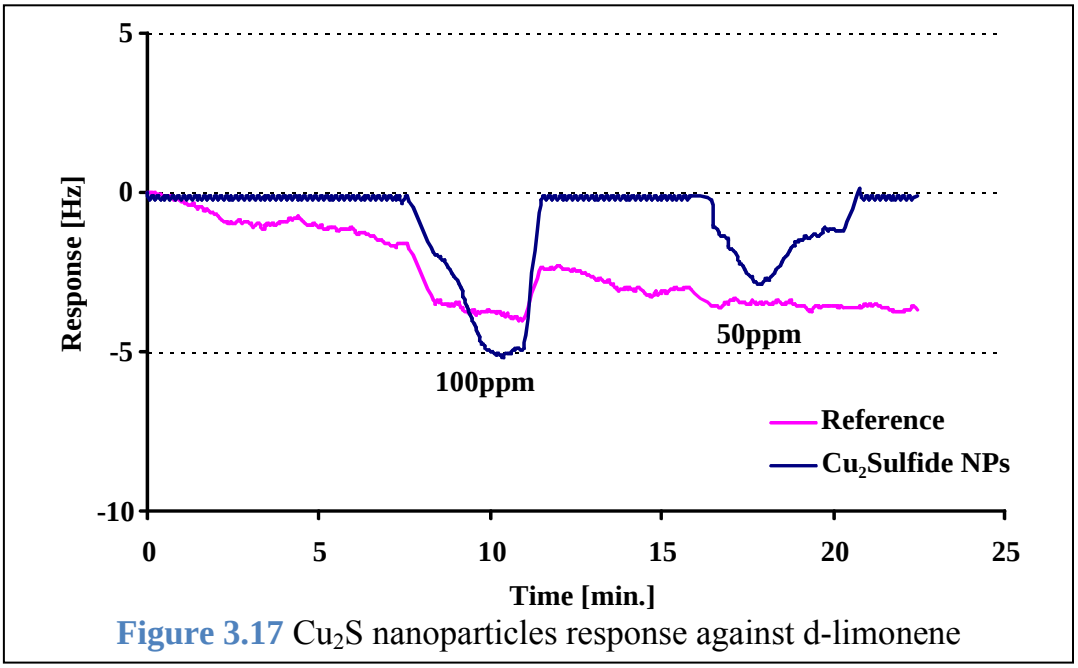

Figure 3.17 Cu_2S nanoparticles response against d-limonene

The overall selectivity pattern of the Cu_2S nanoparticles is shown in figure 3.18. In this figure Cu_2S response against 1-octanethiol, 1-butanethiol, n-octane, limonene and ethyl methyl ketone at 30 ppm, 500 ppm, 500 ppm, 100 ppm and 1000 ppm respectively is shown. The n-octane and 1-butanethiol have same number of carbon atoms differ from one another only by their functionality. However; the sensor response for 1-octanethiol is 100 times more than that of n-octane.

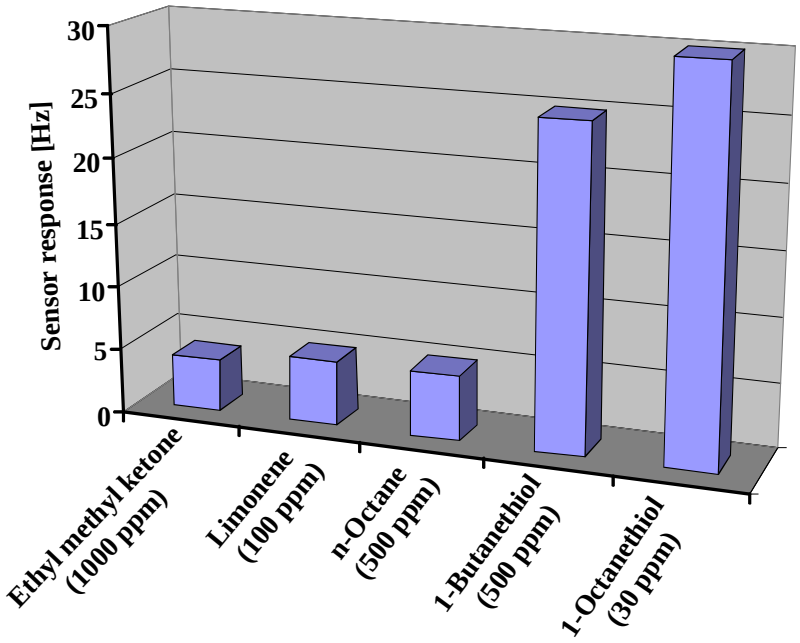

Figure 3.18 Selectivity pattern of Cu_2S nanoparticles

Similarly, 1-btanethiol has less molecular weight than n-octane but yields five times large frequency shifts than n-octane with double number of carbon atoms. The sensor behavior for ethyl methyl ketone and limonene is also similar to that of n-octane and yielded 3 and 4 Hz for 1000 and 100 ppm of ketone and limonene respectively. So this comparison convincingly shows that the Cu_2S nanoparticles are suitable recognition materials for thiol sensing.

Comparison of Cuprous sulfide (Cu_2S) and cupric sulfide (CuS) nanoparticles:

There exist two different types of copper sulfides: one with copper Cu^{1+} and other with Cu^{2+}. As the charge on species increases its hardness also increases. In this case C^{1+} has lower Pearson hardness as compared to Cu^{2+}, therefore Cu_2S nanoparticles should interact more strongly with thiol species as

compared to CuS nanoparticles. In order to verify this basic strategy behind the working principle of our sensor, we have compared the sensor response of Cu_2S nanoparticles with CuS nanoparticles at same concentrations of 1-octanethiol. The results are summarized in figure 3.19.

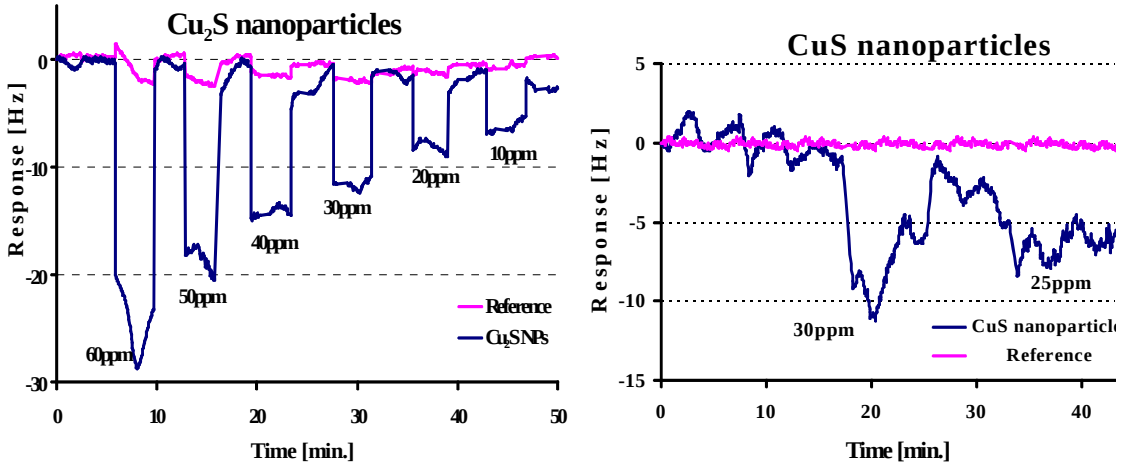

Figure 3.19 Sensor responses of Cu_2S and CuS nanoparticles

It can be seen from the figure that Cu_2S nanoparticles based sensor shows a frequency shift of 12 Hz for 30 ppm of 1-octanethiol and is fully reversible but in case of CuS nanoparticles there is small irreversible change in frequency and shows no further frequency change for 25 ppm of 1-octanethiol. The reason behind this sensor behavior is the hardness difference, CuS bears more hardness as compared to Cu_2S, so it shows hardly any interaction with thiol, whereas Cu_2S being a soft material interacts with thiol reversibly. This comparison between hard and soft materials of same metal provides further strong evidence of soft-soft affinity interaction between Cu_2S and thiols.

Finally, figure 3.20 compares the sensor responses between MoS_2 and Cu_2S nanoparticles. As one can see the sensor response of Cu_2S is higher by

the factor of 3 than that of MoS_2 for both 1-octanethiol and 1-butanol, which corresponds to their difference in hardness.

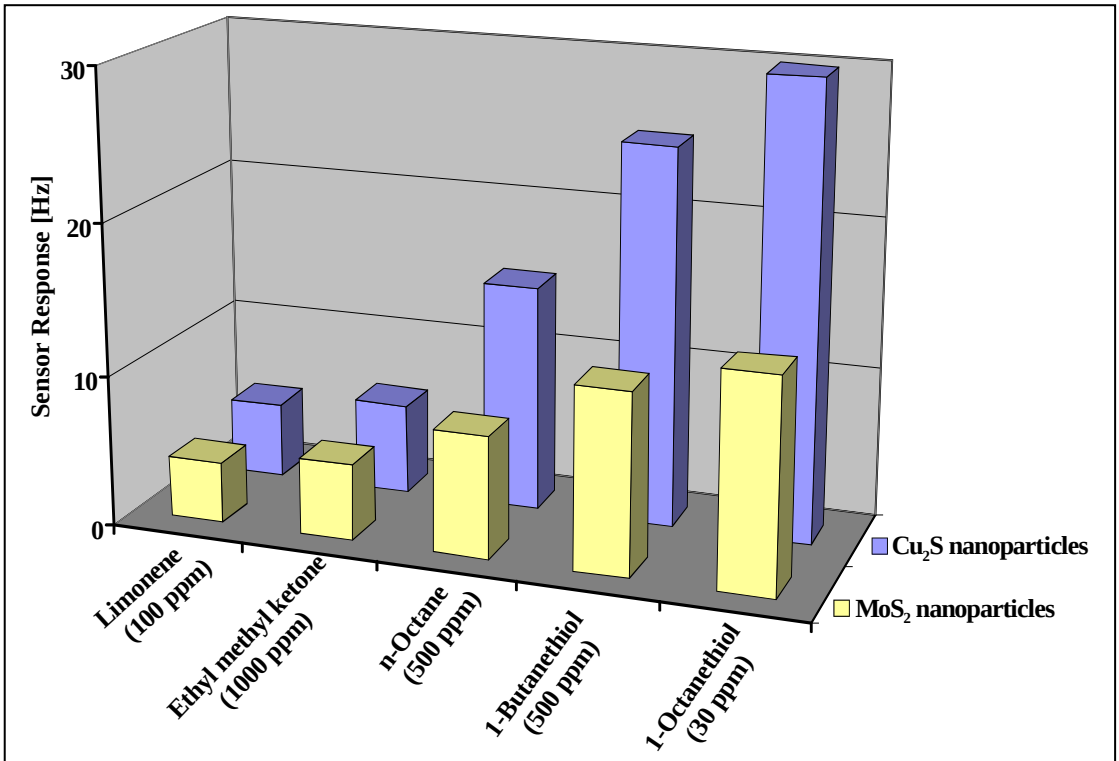

Figure 3.20 Comparison of sensor responses of Cu_2S with MoS_2

As we can see from figure 3.21, the sensor response of Cu_2S is higher by the factor of 3 than that of molybdenum disulfide for both 1-octanethiol and 1-butanethiol and this difference is because of the difference in their hardness. An interesting evidence of hardness dependent behavior of sensor is the same sensor response towards ethyl methyl ketone and limonene because none of them falls in soft species category. This pronounced sensitivity difference is due to more interaction of copper sulfide (Cu_2S) nanoparticles with thiol as compares to molybdenum disulfide (MoS_2) nanoparticles which is because of the fact that soft species will tend to make more interaction with soft and vice versa.

3.4 Conclusion

Following the differences in Pearson hardness, copper sulfide (Cu_2S) has proven even better sensor material for detecting the organic thiols than molybdenum disulfide. This is further supported by the selectivity studies yielding basically similar sensor responses of both materials towards other compounds, such as n-octane, ethyl methyl ketone and limonene. The fact that cupric sulfide (CuS), which is harder than cuprous sulfide (Cu_2S) yields hardly any response.

4. Sensing of thiols with Silver Sulfide Nanoparticles

4.1 Introduction

Silver sulfide (Ag_2S) is a black color sulfide of silver, found in nature as relatively low temperature mineral acanthite due to instability at room temperature is present in form of the pseudomorphosis of acanthite after argentite. 3D space filling structure of silver sulfide is given below in figure4.1 [33].

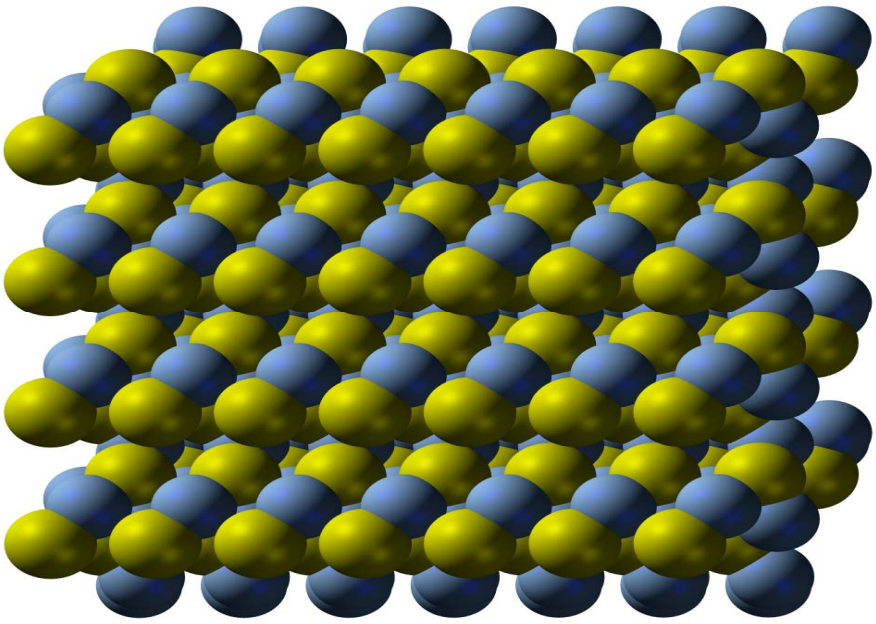

Figure 4.1 3D space filling structure of Ag_2S [33].

As we have observed in chapter 3 that with the increase of softness of metal sulfide their interaction with thiols also increases. For this purpose we are going to prolong our studies towards more soft metal sulfides to obtain more

suitable recognition material for thiols. After copper sulfide Ag_2S looks suitable candidate for these trails. The possible affinity interaction between silver sulfide nanoparticles and thiol can be explained as below,

$$\text{Silver-S} + \text{alkyl-SH} \leftrightarrow \text{Silver-SH} + \text{alkyl-S}$$

4.2 Experimental

Materials

Silver nitrate, ethanol, H_2S gas and these all are purchased from Merck and Fluka with highest purity available used as received.

Synthesis of Ag_2S Nanoparticles:

Silver sulfide powder particles were produced via precipitation method following an already published procedure [34]. 0.5 g of Silver nitrate was dissolved in 100 ml of anhydrous ethanol in rounded bottom flask. H_2S gas was bubbled through this solution until it turned colorless to black due to the formation of silver sulfide nanoparticles. The nanoparticles of silver sulfide were precipitated. Silver sulfide nanoparticles were produced via following reaction,

$$AgNO_3 + H_2S \rightarrow Ag_2S + 2HNO_3$$

These particles were washed with anhydrous ethanol and separated by centrifugation. Nanoparticles with different sizes were separated from each other by centrifugation at 4000 rpm as the function of time i.e. particles with larger size sediment. The nanoparticles were dried at 80^0C for 24 hours.

Preparation of QCM and Ag_2S Nanoparticles Coating.

Dual electrode QCM was prepared as discussed in chapter 2. A suspension of Ag_2S NPs was prepared by mixing 6mg of particles in 500 µl of

ethylenediamine. 5 µl of this black color suspension was coated on QCM electrode by spin coating at the speed of 15-2000 rpm. As a result a layer with 80 nm (2kHz) thickness was obtained and dried at 80C^{o} overnight before use.

4.3 Results and Discussion

Nanoparticles Characterization

In order to check the feasibility of synthesis procedure the particles size had to be analyzed by atomic force microscopy (AFM). A thin layer of Ag_2S nanoparticles was deposited on glass substrate and then AFM images were recorded. A typical AFM image of Ag_2S nanoparticles is shown by figure 4.2. It can be seen from figure that vast majority of particles are ball-shaped. The particles with different sizes were separated from one another by centrifugation at different speed and time.

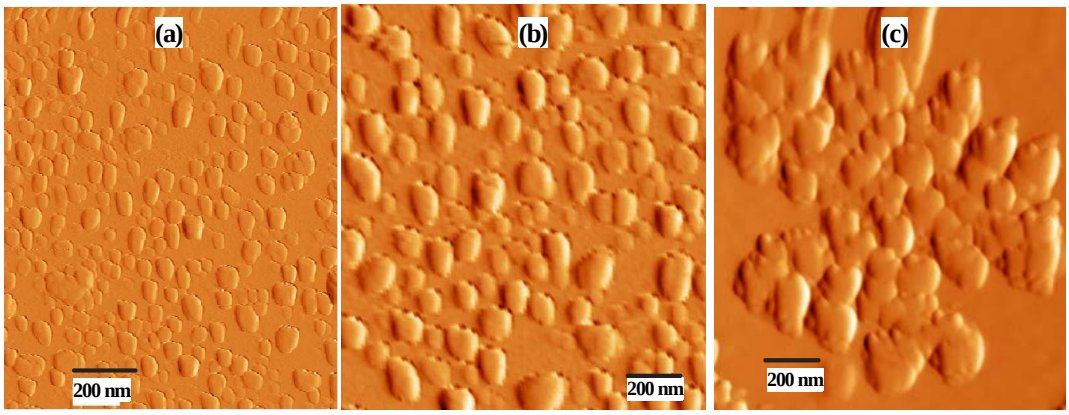

Figure 4.2 AFM images of Ag_2S nanoparticles deposited on glass substrate (a) particles with diameter <50 nm (b) particles with diameter 50-100 nm and (c) particles with diameter 100-150 nm

XRD analysis of nanoparticles has been conducted to ensure the feasibility of synthesis procedure and stoichiometry of Ag_2S. It can be clearly

seen from the figure 4.3, representing the XRD pattern of Ag_2S nanoparticles that there is no impurity peak and observed peaks of the sample match perfectly with reference peaks obtained from data base.

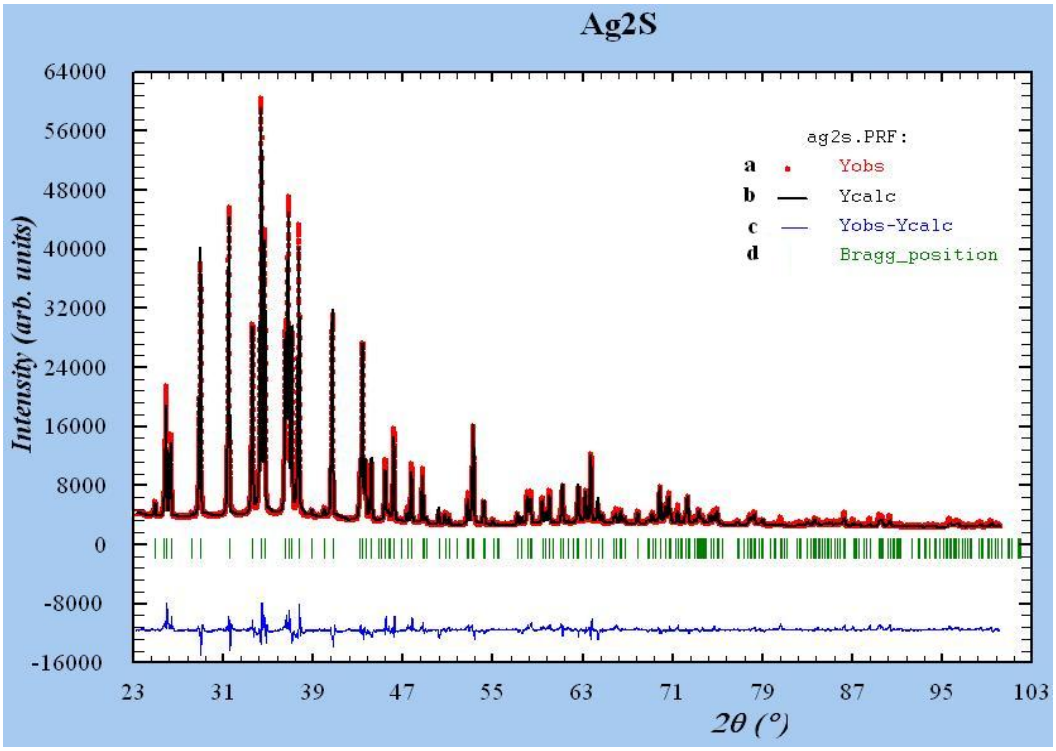

Figure 4.3 XRD powder diffraction pattern of Ag_2S nanoparticles where (a) is the sample peaks; (b) is the reference from database, (c) is the difference between sample and reference peaks and (d) shows the Bragg-positions.

So the feasibility of Ag_2S nanoparticles synthesis approach has thus been proved. The 3-D structure of Ag_2S is given below in figure 4.4, obtained from the XRD powder diffraction analysis which is similar to already reported in literature [35]. The crystal structure of Ag_2S is of mP12,14 type and the space group $P12_1/c1$ (14).

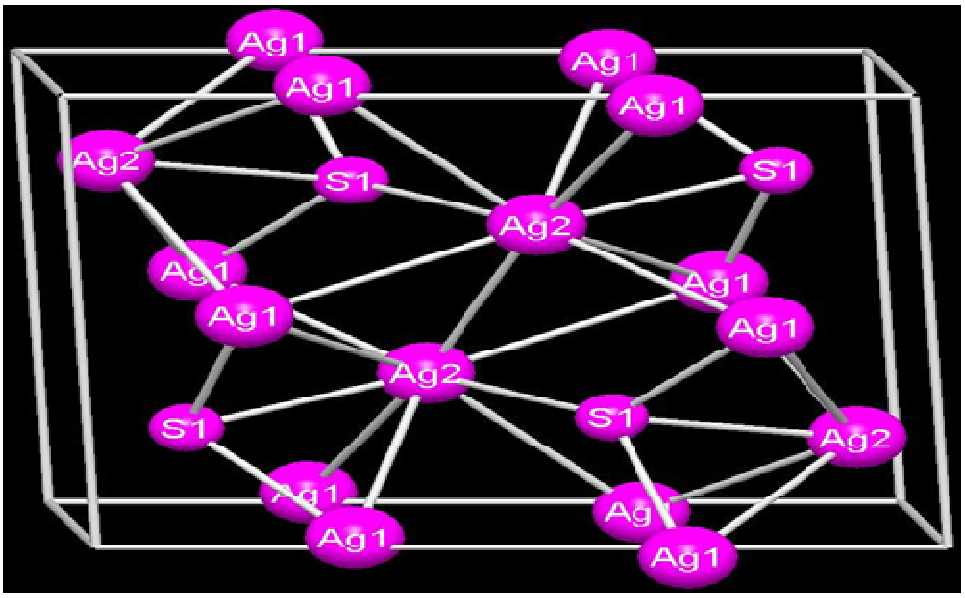

Figure 4.4 3D structure of Ag_2S crystal [35].

Figure 4.3 shows the 3D atomic environment of silver (Ag) and sulfur (S) atoms. In Ag_2S crystal silver atom exists in two types of 3D environments, Ag1 as Pseudo Frank-Kasper (18) and Ag2 as Pseudo Frank-Kasper (11) atomic environment types and sulfur has only one atomic environment named as equatorially mono-capped trigonal prism [35].

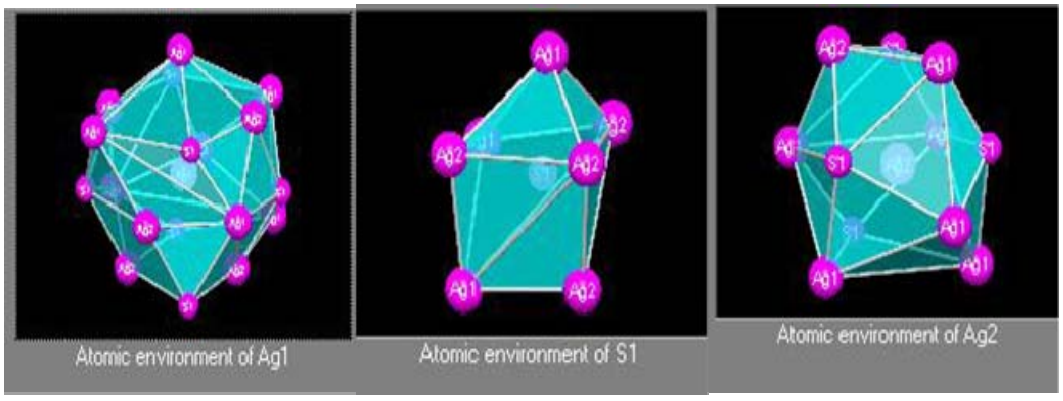

Figure 4.5 3D atomic environments of silver and sulfur atoms in Ag_2S [35].

QCM Sensor Characteristics

As we have already discussed in chapter 3 that the affinity interaction of metal sulfide towards thiols is associated with the hardness, so we extend our approach from copper sulfide to silver sulfide. After assuring the synthesis procedure, shape and stoichiometry of silver sulfide nanoparticles, the feasibility of Ag_2S as recognition material is to be checked.

Sensing of 1-Octanethiol

The sensor coated with Ag_2S nanoparticles with diameter of 100-150 nm was exposed to different concentrations of 1-octanethiol ranging from 30 ppm to 50 ppm respectively, as can be seen in figure 4.6 given below.

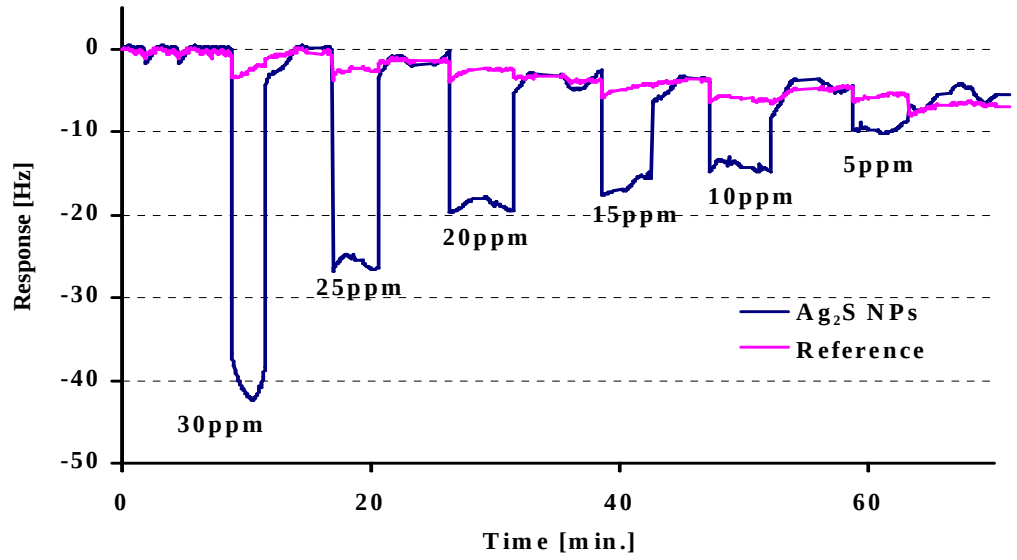

Figure 4.6 Sensing of 1-octanethiol with Ag_2S nanoparticles with size (100-150nm).

As one can see, there is response 42 Hz for 30 ppm and 5 Hz for 5 ppm of 1-octanethiol with noise level of 0.1 Hz. The detection limit of the sensor with particles size 100-150 nm diameters is near to 350 ppb. Compared to MoS_2 and Cu_2S, this means sensitivity is substantially increased.

To assess the influence of particle size on sensitivity, another QCM coated with Ag-sulfide nanoparticles of diameter 50-100nm, was exposed to different concentrations of 1-octanethiol again as given by figure 4.7. An increase of sensitivity could be observed. One can see that there is sensor response 10 Hz for 2 ppm with noise level of 0.10 Hz resulting in detection limit of 60 ppb. This increase of sensitivity is because of decreased particles size and increased surface area exposed to analyte.

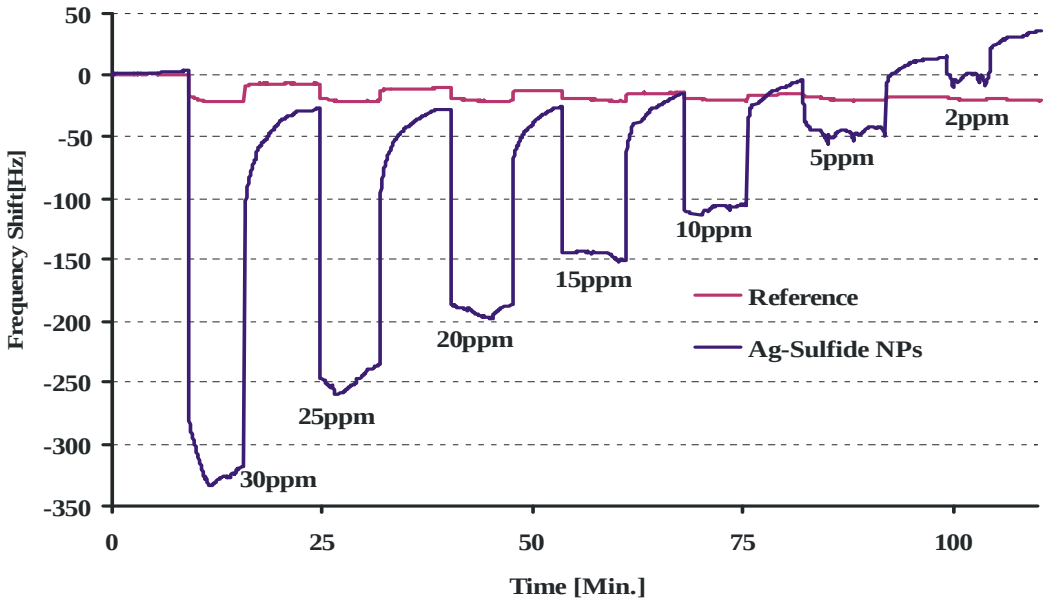

Figure 4.7 Sensing of 1-octanethiol with Ag-sulfide NPs with size 50-100nm.

Furthermore silver sulfide nanoparticles with size less than 50 nm were coated on QCM and it was exposed to different concentrations of 1-octanethiol. The figure 4.8 shows the sensor signal of nanoparticles towards 1-5 ppm concentrations of 1-octanethiol. It can be seen from the figure that the sensor yielded a response of 25 Hz for 1 ppm with noise level of 0.10 Hz and the detection limit of sensor is approximately 12 ppb. This substantially increased

signal is due to the more available surface area provided by smaller size nanoparticles.

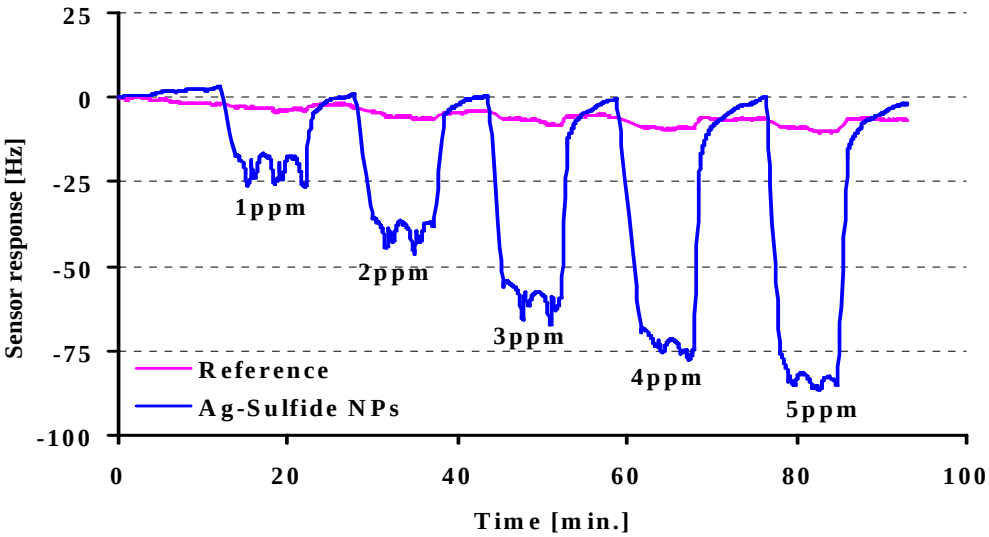

Figure 4.8 Sensing of 1-octanethiol with Ag_2S NPs with size <50nm

The normalized response of Ag_2S nanoparticles (<50 nm) towards 1-5 ppm of 1-octanethiol is shown in figure 4.9. One can see from the figure that there is linear relationship between the sensor signals and concentrations of 1-octanethiol.

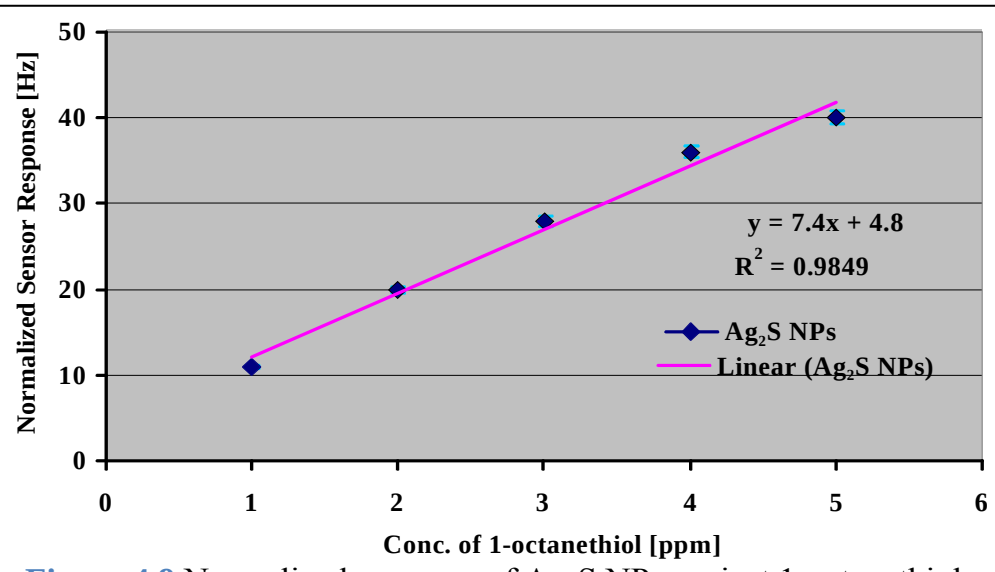

Figure 4.9 Normalized response of Ag_2S NPs against 1-octanethiol.

The regression analysis of the sensor also represents the linear behavior of sensor in concentration range of 1- ppm with correlation coefficient (R^2) of 0.9849. An error of only 2.5 percent was observed after several repetitions of experiment which indicates the efficient and appreciable reversibility and repeatability characteristic of sensor.

In order to see the particles size influence on sensitivity, a comparison has been made between the sensor responses of Ag_2S particles with diameter 100-150 nm, 50-100 nm and <50 nm as shown by figure 4.10.

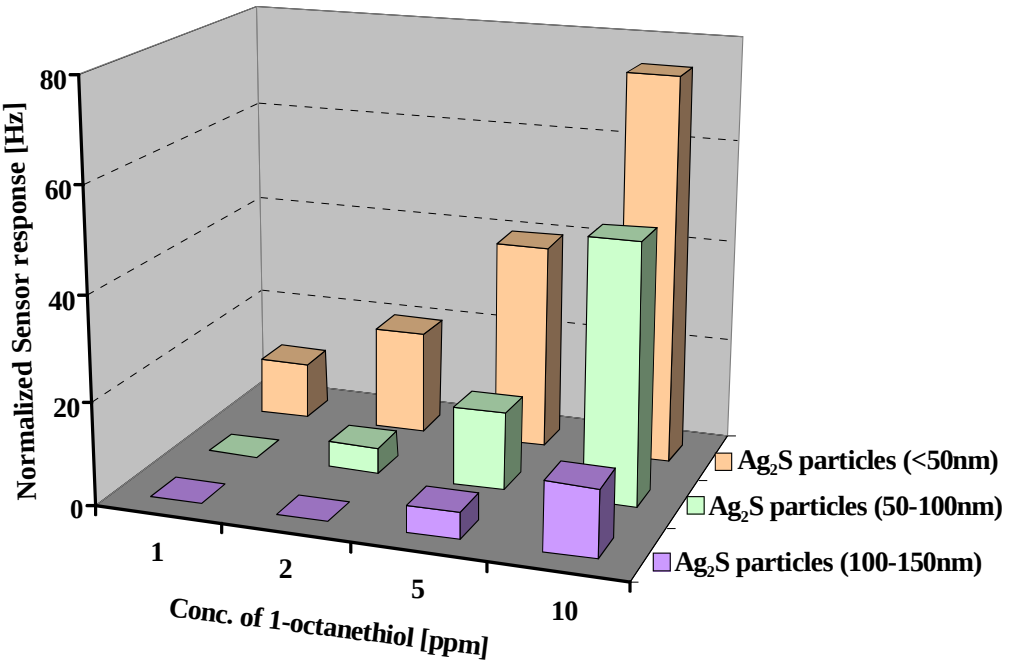

Figure 4.10 Comparison of sensor responses of Ag_2S nanoparticles against different concentrations of 1-octanethiol

It is clear from figure 4.10 that the nanoparticles of diameter less than 50nm are able to sense the 1-octanethiol with limit of detection up to 12ppb with a quite appreciable sensor signal of 25 Hz for 1 ppm, while the particles with size ranging 50-100nm has limit of detection up to 60 ppb and particles which are of

bigger size with diameter 100-150nm has limit of detection of 350 ppb of 1-octanethiol. The limit of detection of particles with diameter less than 50 nm is quite higher than that of particles with diameter 50-100 nm by the factor of 5. Similarly, the limit of detection between particles with size 50-100 nm and 100-150 nm is 1:5.8 respectively. This limit of detection difference should be up to 3 times higher and this could be due to different surface reactivities depending on the surface diameter of particles. So, this will need further investigations.

Sensing of 1-Butanethiol with Ag_2S Nanoparticles

As with previous sulfide nanoparticles, for the confirmation of claim that the interaction is only due to the affinity of thiol functionality with Ag_2S nanoparticles, the sensor was exposed to thiols with different number of carbon atoms. Sensor was exposed to different concentrations of 1-butanethiol ranging from 50-500 ppm as shown by figure 4.11. It can be seen from figure that there is sensor response of 7 Hz for 50 ppm of 1-butanethiol with noise level of 0.2 Hz and limit of detection up to 4.3 ppm. The sensor response is fully reversible.

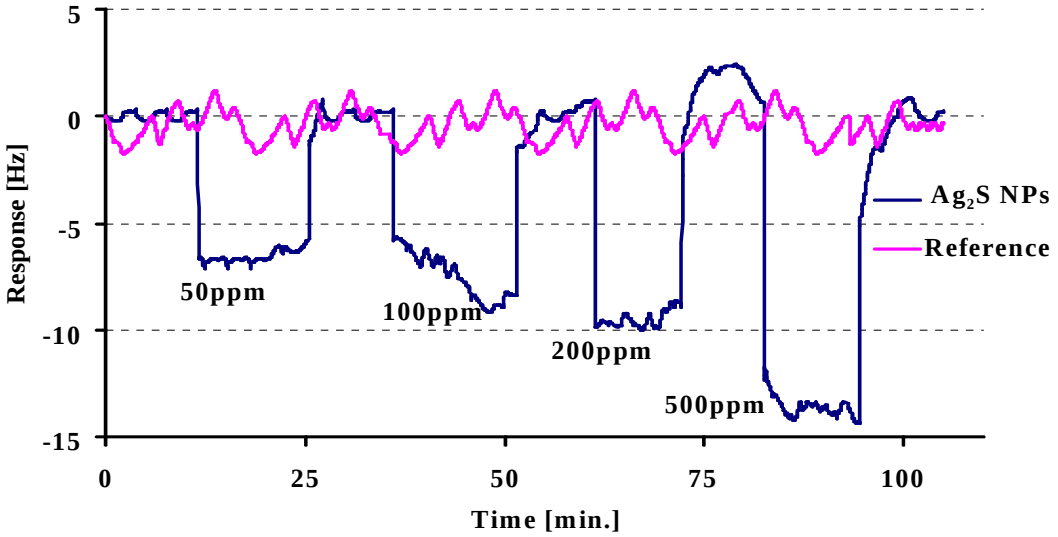

Figure 4.11 Sensing of 1-butanethiol with Ag-sulfide NPs (50-100nm).

For the assessment of nanoparticles size effect on sensitivity of 1-bitanethiol, the sensor with nanoparticles of <50 nm diameter was exposed to 1-butanethiol and a sensor response has been observed as shown by figure 4.12. There is a sensor response of 12 Hz for 50 ppm of 1-butanethiol with noise level of 0.15 Hz and the limit of detection is 1.9 ppm. As the particles diameter ratio used in figure 4.11 and 4.12 is 1:2 respectively and a similar ratio in their limit of detection can also be seen.

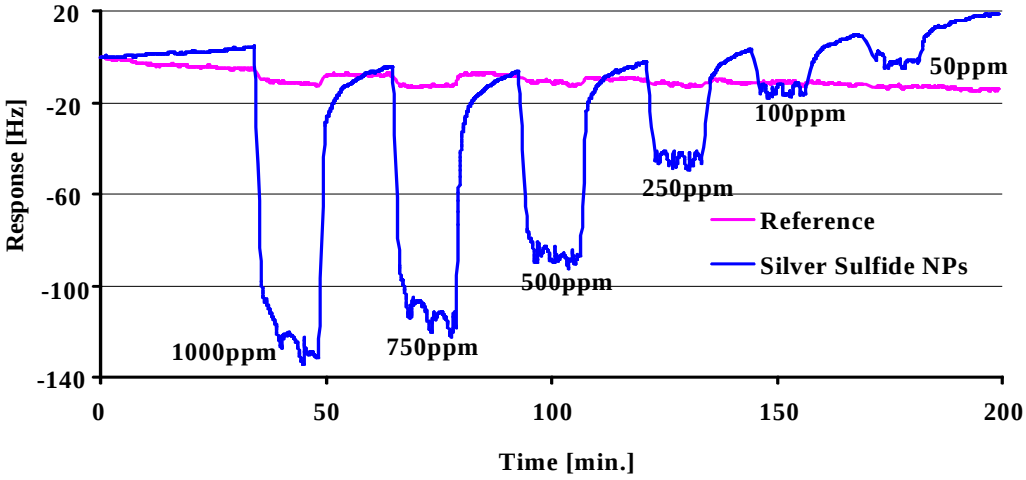

Figure 4.12 Sensing of 1-butanethiol with Ag-sulfide NPs of size <50nm.

The sensor response was reversible and limit of detection up to 1.9 ppm. The normalized responses of Ag_2S nanoparticles against different concentration of 1-butanethiol is given in figure 4.13 below along with correlation coefficient. There is complete linear relationship between the sensor signals and concentration of 1-butanethiol. The regression analysis of the sensor responses yields a correlation coefficient (R^2) of 0.9869. The percentage error between different measurements was observed less than 3. The quantitative comparison between the sensor responses of 1-butanethiol and n-octane with double number of carbon atoms will be discussed later on in selectivity pattern diagram.

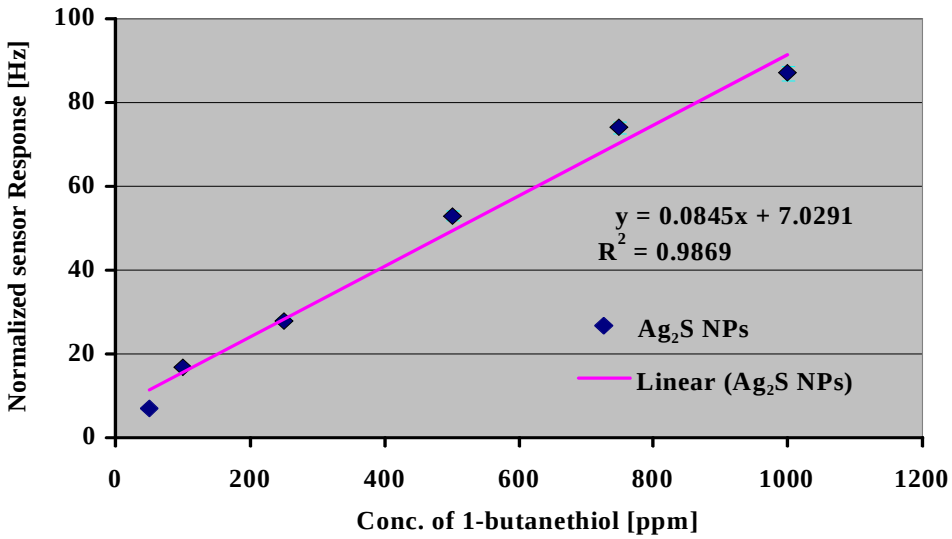

Figure 4.13 Normalized response of Ag_2S nanoparticles towards 1-butanethiol (50-1000 ppm).

Cross Sensitivity and Selectivity of Sensor with different compounds

For complete comparison, Ag_2S nanoparticles were also exposed to same analytes, as in case of MoS_2 and Cu_2S nanoparticles and are discussed as below.

(a) n-octane

The result of exposing the sensor to different concentrations of n-octane is shown by the figure 4.14. The sensor yields no frequency shift for concentrations below 100 ppm. Even at 600 ppm there is response of 21 Hz. But on comparing with 1-octanethiol with similar carbon chain there is a response of 25 Hz for only 1 ppm, it means that sensor is 600 times more sensitive towards thiol as compared to n-octane even both bear same number of carbon atoms. It strongly proves the soft-soft affinity interaction between Ag_2S nanoparticles and thiols.

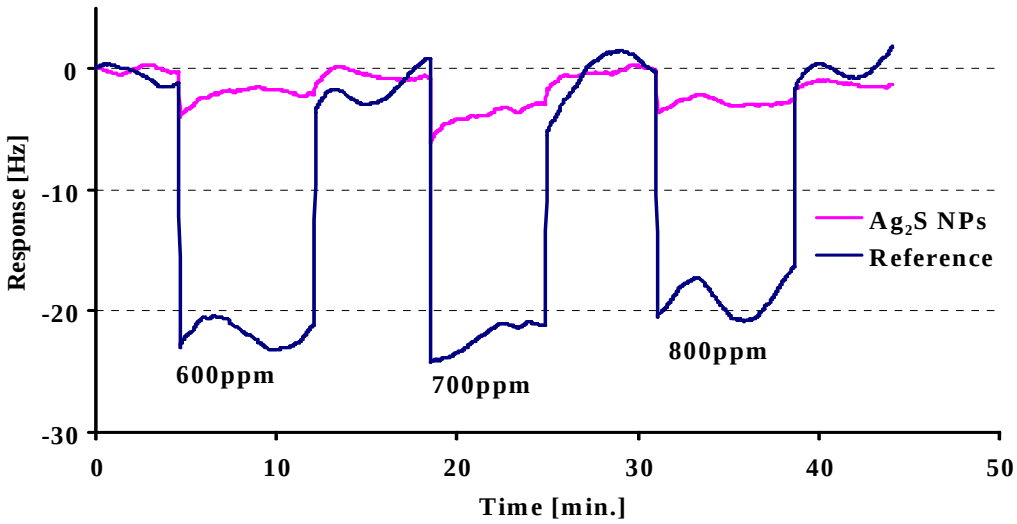

Figure 4.14 Sensing of n-octane with Ag-sulfide NPs (50nm)

(b) Ethyl methyl Ketone

Sensor was exposed to different concentrations of ethyl methyl ketone and sensor signals are recorded as shown by figure 4.15. One can see that there is no response for concentrations less than 500 ppm. There is a response 3 Hz for 500 ppm and even up to 1000 ppm it shows a change in frequency of only 8 Hz which shows that silver sulfide has no affinity interaction with ketone group.

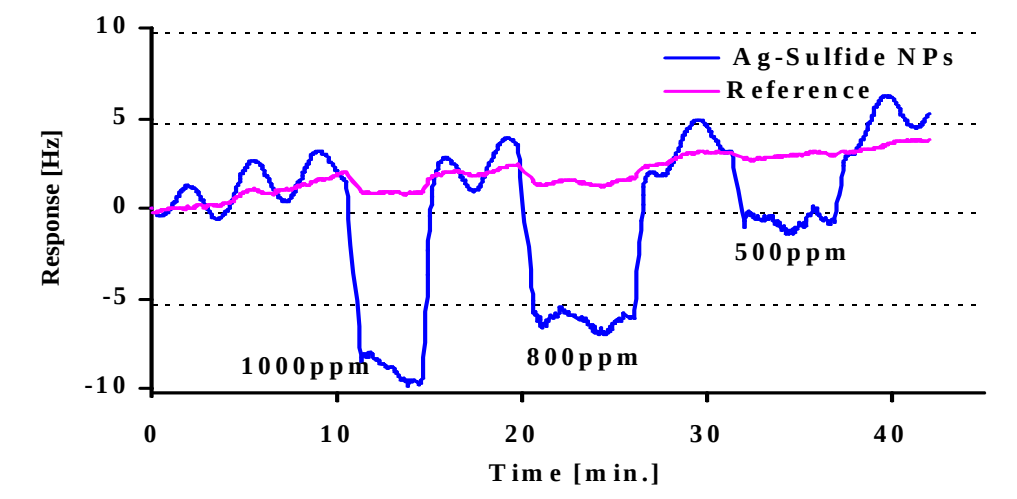

Figure 4.15 Sensing of ethyl methyl ketone with Ag-sulfide NPs (<50nm).

As ethyl methyl ketone does not fall in hard and soft acid-base category so, theoretically it should have no affinity interaction with soft metal sulfide. This too less sensitivity of thin layer of nanoparticles towards ethyl methyl ketone provides the evidence of existence of so-called HSAB principle based interaction.

(c) Terpenes:

As mentioned above newly designed sensor shows no remarkable response toward different concentrations of n-octane and ethyl methyl ketone, which are acyclic compounds and then we extended our studies to the odorous cyclic compounds. For this purpose we have chosen limonene, a member of terpenes group of cyclic odorous compounds.

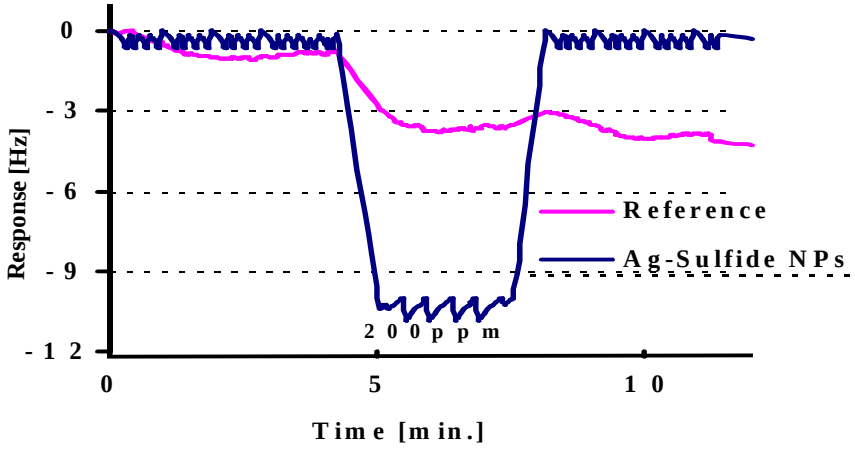

Figure 4.16 Sensor response of Ag_2S nanoparticles against Limonene.

At a concentration of 200 ppm of limonene sensor has response of only 10 Hz, as illustrated by figure 4.16.

Figure 4.17 shows the selectivity diagram of our sensor in which the sensor response of Ag_2S nanoparticles towards 1-octanethiol at 30 ppm, 1-butanethiol at 500 ppm, n-octane at 600 ppm, ethyl methyl ketone at 1000 ppm and limonene at 200 ppm respectively.

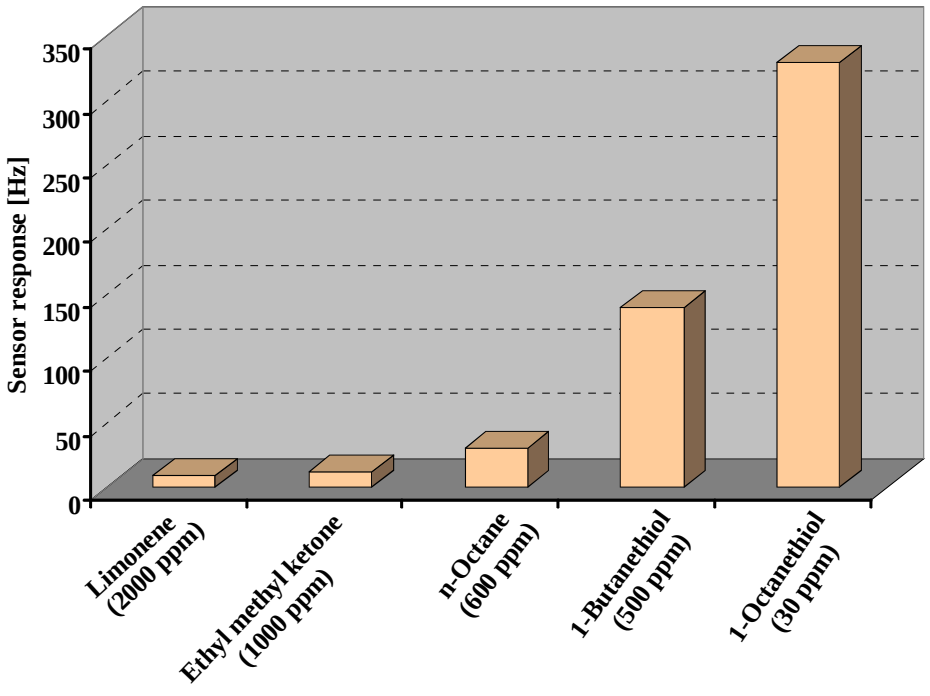

Figure 4.17 Selectivity pattern of silver sulfide nanoparticles based sensor.

It can be seen from figure 4.17 that there is a sensor response of 320 Hz for 30 ppm of 1-octane thiol, while n-octane with same number of carbon have only 21 Hz for 600 ppm and similarly 1-butanethiol with half number of carbon atoms than n-octane has four times higher response than that of n-octane. The sensor response difference between 1-butanethiol and 1-octanethiol is because of their vapor pressure and molar mass differences. The sensor response of Ag_2S against ethyl methyl ketone for 1000 ppm is 8 Hz and towards limonene for 200 ppm is 10 Hz only which shows that the recognition takes place via thiol functionality only.

Comparing affinity interaction of Ag_2S nanoparticles and different polymers towards thiols

The figure 4.18 given below shows the comparison between the sensor responses of silver sulfide nanoparticles and that of obtained from polystyrene, polyvinyl alcohol and polyvinyl chloride. We have observed that for 30 ppm of 1-octanethiol sensor responses of Ag_2S nanoparticles, polyvinyl alcohol, polystyrene and polyvinyl chloride are 320 Hz, 4 Hz, 2Hz and 1.5 Hz respectively.

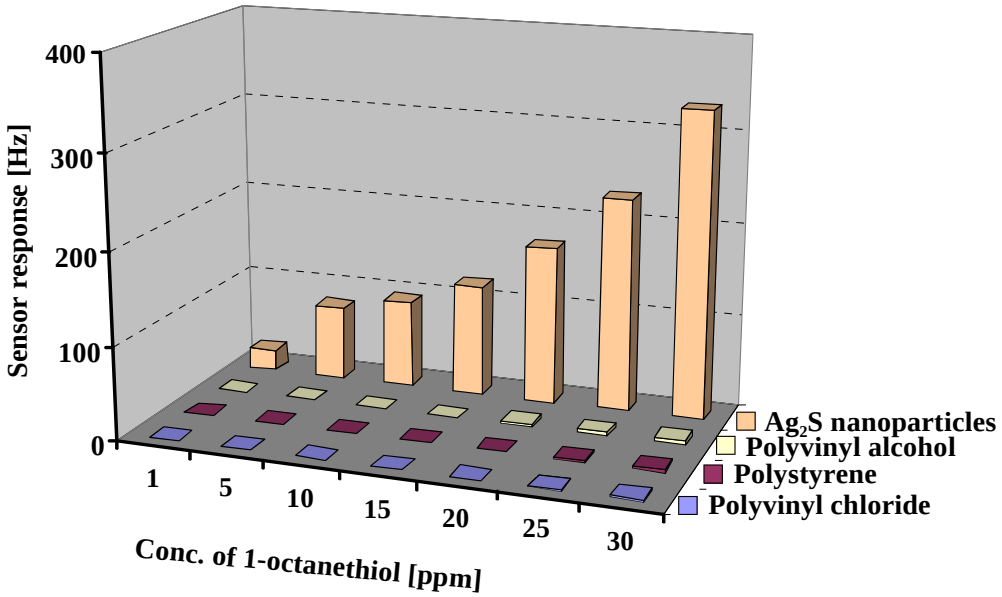

Figure 4.18 Comparison of sensor responses of different recognition materials against 1-octanethiol.

As the polyvinyl alcohol is highly polar, polystyrene is unsaturated and polyvinyl chloride is hydrophobic in nature but none of them is able interact with thiols which means that in case of Ag_2S nanoparticles the recognition takes place via soft-soft acid and base interaction.

Effect of hardness of metal on sensitivity of metal sulfide nanoparticles

With the increase of softness of metal sulfide the affinity interaction with thiols also increases. So-called soft-soft acid based interaction strategy behind the basic principle of metal sulfide was verified by comparing the sensor responses of metal sulfides particles with different softness of metals. In figure 4.19, a comparison between molybdenum sulfide and silver sulfide is given. As molybdenum is has higher hardness as compared to silver and gold, therefore the interaction of silver is more as compared to molybdenum.

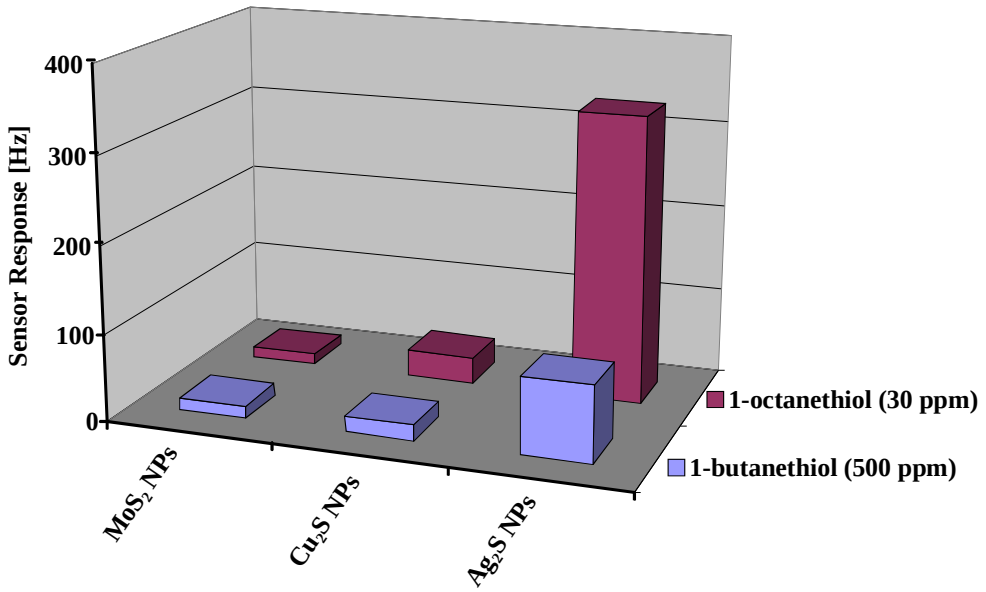

Figure 4.19 Comparison of Ag_2S and Cu_2S nanoparticles sensitivities against thiols.

In MoS_2 molybdenum is present in Mo^{4+} form and in Cu_2S copper is present in Cu^{1+} while in Ag_2silver is present in Ag^{1+} form, the softness of Ag^{1+} is more as compares to Cu^{1+} and Mo^{4+} has more hardness as compared to Cu^{1+}, as with the increase of charge on metal its softness decreases and also the number of valence electrons decreases which plays an important role in affinity interaction with thiols. Therefore Ag^{1+} and Cu^{1+} are softer than Mo^{4+} and that is why the affinity

interaction of MoS_2 is less than others. The atomic hardness (η^d) of Cu is 3.25 and that of Ag is 3.14 [29], as silver is softer as compared to copper, so thiol will prefer to bind strongly via affinity interaction with silver sulfide as compared to copper sulfide. While the sulfur atom has hardness 4.12 and it will tends to interact with less hard metal silver rather than copper.

4.4 Conclusion

Nanoparticles approaches have proven to be highly suitable for generating sensor materials for both environmental and process control applications. The use of nanoparticles as a recognition layer is a promising strategy for the sensitivity enhancement of a chemical sensor and there is direct relation between the particle size and limit of detection. Soft metal sulfides nanoparticles are highly promising candidate for recognition sensor coatings and interact reversibly with organic thiols and therefore can be utilized to detect the outstanding smelly and toxic to human beings class of organic compounds. Recognition takes place via affinity interactions between the "soft" sulfur atom of analyte and the "soft" metal of layer material. As silver is a sufficiently soft metal, it has greater affinity interaction towards thiols as compared to molybdenum and copper. So, it has proven itself as a promising recognition material candidate for the detection of different thiols with very good limit of detection ranging up to ppb level. By comparing the sensor signals of silver sulfide with that of molybdenum disulfide and copper sulfide, it is observed that with the decrease of hardness of metal sulfide, the affinity interaction towards thiol increase substantially which reinforce and support the fundamental principle of strategic approach for thiol sensing.

5. Mass Sensitive Measurement of Alcohols with Metal Sulfides Nanoparticles

5.1 Introduction

The detection of volatile organic compounds (VOCs) like esters, alcohols, ethers, halocarbons, ammonia, nitrogen dioxide, warfare agent stimulants and toxic gases, is of special importance in sensor technology [36,37,38]. Analyzing alcohol contents is of great interest in industrial and biochemical fields and also in the beverage industry. For the measurement of ethanol and other alcohols, many analytical methods have been developed during the last few years including chromatographic and enzymatic methods. Chromatography is very powerful technique being used to detect ethanol and other alcohols on the order of 0.005% v/v[39], however, it comes along with some drawbacks including high cost, necessary to pretreat the sample, long operation time, difficulty in moving the apparatus from one place to other as well as need of expert operators. On the other hand the use of some enzymes i.e. alcohol oxidase and alcohol dehydrogenase provides a rapid method to determine alcohol concentration by monitoring O_2 consumption or H_2O_2 formation [40,41]. The drawback of this method is the denaturing of protein at high temperature and pressure and also extreme pH thus somewhat limiting the operation range. The change in optical and/or electrical properties of some recognition materials on exposure to volatile organic compounds (VOCs) is measured in order to detect organic vapors [42]. For the detection of methanol in air infrared spectroscopy is being in use [43]. However, these methods are expensive, time requiring and unable to do on-line monitoring of these toxic and harmful organic vapors. Therefore the development of chemical sensors with high sensitivity,

reproducibility, rapidly, reliability and sufficient selectivity is of substantial interest for an analytical chemist. Recently, lifetime-based [44] and fluorescence-based [45,46,47,48,49] sensors for alcohol have been designed by using various alcohol-sensitive dyes with good sensitivity but also with lack of high temperature stability and autofluorescence interference. Among these all sensors and devices the quartz crystal microbalance is of great interest for the sensing of volatile organic compounds [50,51,52]. Polypyrrole as a recognition material for the detection of alcohols and other organic vapors has been reported but it is less sensitive and shows incomplete desorption of the gas molecules [53]. Polyaniline (PANI) due its good environmental stability, electrical conductivity was also used as a sensing material for volatile organic vapors including alcohols by some researchers [54,55]. We have fabricated a novel sensor for alcohol detection based on interactions between soft metal sulfides and alcohols.

5.2 Experimental

Chemicals, method and QCM preparation

1-propanol, 1-butanol and 1- propanol were purchased from Merck and Fluka Chemicals. MoS_2, Cu_2S and Ag_2S were prepared as discussed in chapter 2, 3 and 4, respectively. Duel electrodes quartz crystal microbalance were coated and processed as mentioned in previous chapters.

Vapor pressure based Calculation of Different concentrations of Alcohols:

(a)1-propanol

Different concentrations of 1-propanol from 250-1000 ppm, were calculated by mixing these analytes with dry air and these calculations were made by using software “P6” designed by our group totally based on vapor

pressure of respective analyte. The concentrations calculations for 1-propanol are given as below in table 5.1 and all these calculations are made at 20°C with vapor pressure of 15 mmHg/19.99 mbar and purity of 1-propanol is 99.99%.

Table 5.1 Vapor pressure dependent calculation of different concentrations of 1-propanol.

Conc. (ppm)	***Solvent (ml)***	***Air (l)***
0	0.0	1.0
250	12.5	0.99
500	25	0.97
750	37.4	0.96
1000	49.9	0.95

(b)1-butanol

For 1-butanol with purity 99.99% (Merck) and vapor pressure 5 mmHg/6.7 mbar at 20°C, the calculated air to solvent ratio for different concentrations is given as below in table 5.2.

Table 5.2 Vapor pressure dependent calculation of different concentrations of 1-butanol.

Conc. (ppm)	***Solvent (ml)***	***Air (l)***
0	0.0	1.0
100	15.0	0.98
200	30.0	0.97
300	45.1	0.95
400	60.1	0.94
500	75.1	0.92
600	90.1	0.91
700	105.1	0.89
800	120.0	0.88

(c) 1-octanol

Similarly, different concentrations of 1-octanol are given below in table 5.3 by mixing analyte with air. These all calculations are made at 99.99 % of 1-octanol with vapor pressure 0.07mmHg/0.093 mbar at 25^{o}C.

Table 5.3 Vapor pressure dependent calculation of different concentrations of 1-octanol.

Conc. (ppm)	***solvent (ml)***	***Air (l)***
0	0.0	1.0
1	10.9	0.99
2	21.7	0.98
3	32.6	0.97
4	43.4	0.96
5	54.3	0.95
6	65.1	0.93
7	76.3	0.92
8	86.9	0.91
9	97.7	0.90
10	108.6	0.89

By using above calculated concentrations of 1-propanol, 1-butanol and 1-octanol, sensor measurements were taken by using MoS_2, Cu_2S and Ag_2S nanoparticles as recognition materials.

5.3 Results and Discussion

Sensing of Alcohols with Molybdenum Disulfide Nanoparticles:

Alcohols are highly polar and hydrophilic organic compounds and the hydrophilicity decreases with the increases of carbon chain. This hydrophilicity

and polarity make them to interact with others polar compounds. By using these polar-polar interactions strategies, a suitable recognition material for alcohols can be fabricated. To check the feasibility of metal sulfides as recognition material for alcohol sensing, we exposed different metal sulfides nanoparticles based sensor to different alcohols. Figure 5.1 shows the sensor response of MoS_2 nanoparticles towards different concentrations of 1-propanol ranging from 250-1000 ppm. It has a high sensitivity and fast response time. At concentration of 250 ppm it shows a response of 10 Hz with 0.10 Hz noise level and limit of detection is 7.5 ppm. It can be seen that from 250 ppm to 1000ppm of 1-propanol, the sensor shows linearity in response.

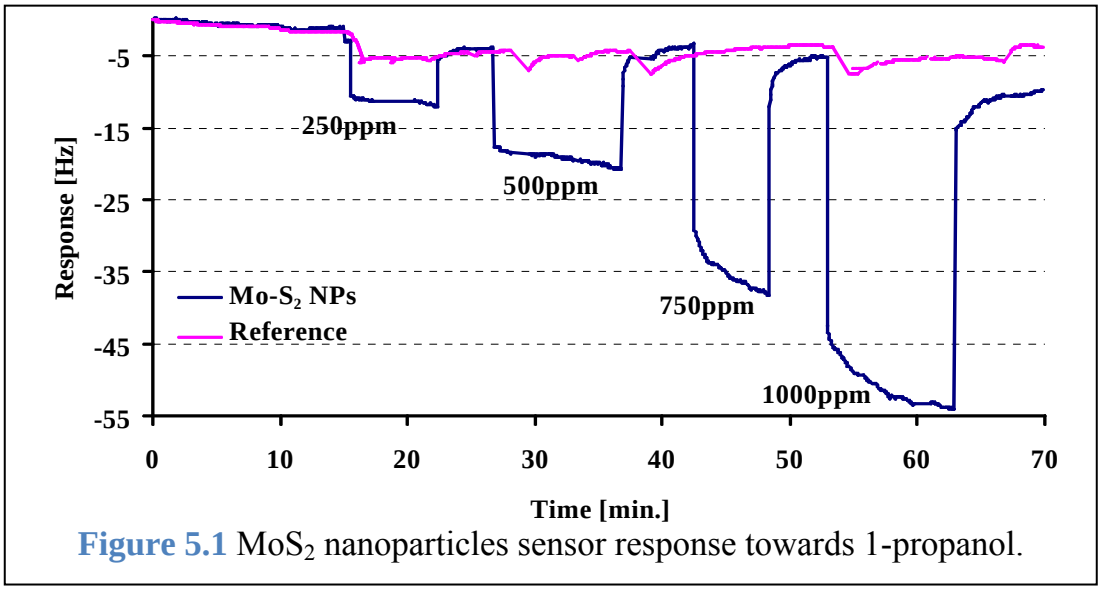

Figure 5.1 MoS_2 nanoparticles sensor response towards 1-propanol.

The same experiment was carried out for different concentrations of 1-butanol. The sensor response was appreciable with increased sensitivity and reproducibility as shown by figure 5.2. Sensor is able to detect the 1-butanol from 100ppm to onward and it has also linearity in response. For 100 ppm of 1-butanol the response is 13 Hz with 0.1 Hz with noise resulting in a limit of detection of 4.7 ppm.

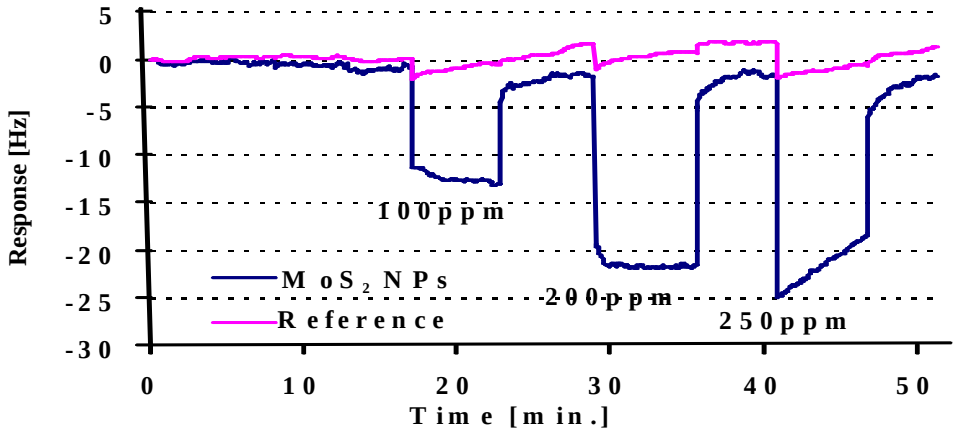

Figure 5.2 MoS_2 nanoparticles sensor signal towards 1-butanol.

The sensor was exposed to different types of alcohol varying in number of carbon atoms. As the number of carbon atoms increases the sensor signal also increases which is due to the different mass of the carbon chains. With increasing carbon chain the vapor pressure of alcohol decreases.

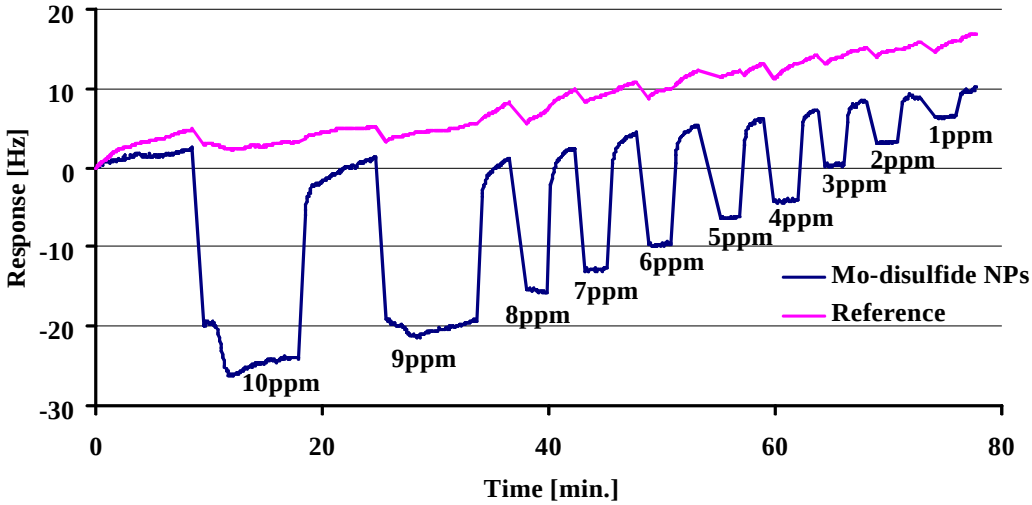

Figure 5.3 MoS_2 nanoparticles sensor response towards 1-octanol.

Affinity layers therefore promote condensation on the respective surface further. The sensor response of MoS_2 nanoparticles based sensor towards 1-octanol is

shown by figure 5.3as below. There is sensor response of 3 Hz for 1 ppm of 1-octanol with 0.1 Hz noise level and the detection limit is 100 ppb which is appreciable enough.

The normalized response of MoS_2 sensor against 1-octanol is shown in figure 5.4. It can be seen from figure that the sensor shows a good reproducibility and reversibility with correlation coefficient values 0.9735.

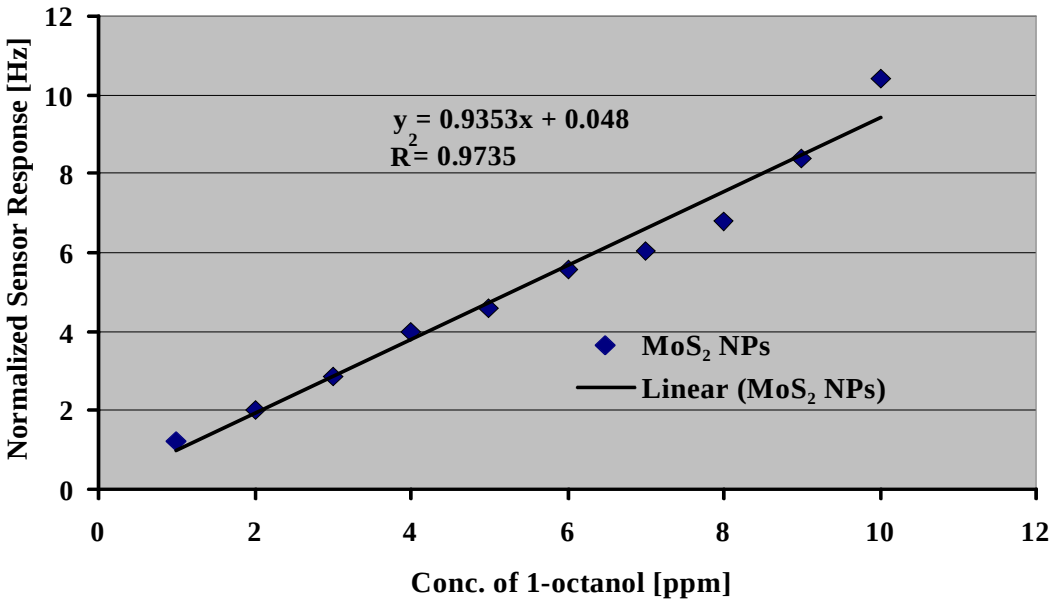

Figure 5.4 Normalized response of MoS_2 nanoparticles against 1-octanol.

It can be seen from figure 5.1 to 5.4 that with increase of carbon chain in alcohol the limits of detection of MoS_2 sensor decreases to lower concentrations. The possible reason is the molar mass effect, vapor pressure effect and the strongest reason is the increase of hydrophobic character of alcohol with long carbon chain. As MoS_2 is highly hydrophobic, the interaction between MoS_2 and alcohol increases following the decrease of hydrophilic properties of alcohols.

Alcohols Sensing with Copper Sulfide (Cu_2S) Nanoparticles:

Although giving appreciable sensor results, MoS_2 is hydrophobic. However, most alcohols are hydrophilic in nature therefore, in case of metal

sulfides; they should show more interactions towards less hydrophobic metal sulfides. As in Cu_2S, copper is present in Cu^{1+} form and as compared to MoS_2, Cu_2S is less hydrophobic because of less charge density and larger atomic radii of copper than molybdenum. Therefore, Cu_2S could be expected to have more interactions towards alcohol as compared to MoS_2 nanoparticles. To assess this hypothesis, we exposed copper sulfide nanoparticles based sensor to different alcohols e.g. 1-propanol, 1-butanol and 1-octanol respectively. Figure 5.5 shows the sensor response of Cu_2S nanoparticles against 1-butanol. The sensor response was fully reversible and reproducible with an appreciable sensitivity with limit of detection of 3 ppm at 0.10 Hz noise level.

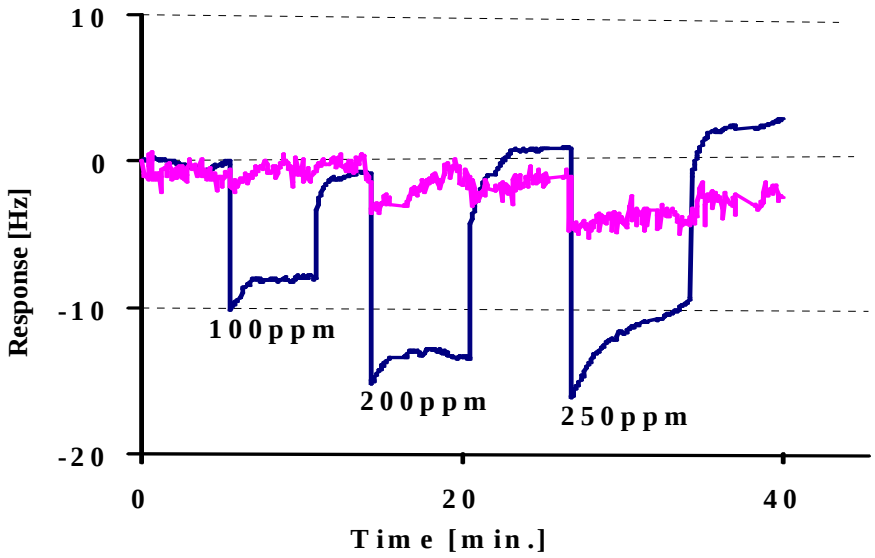

Figure 5.5 Cu_2S nanoparticles sensor response towards 1-butanol.

Figure 5.6 depicts the sensor response of Cu_2S nanoparticles towards different concentrations of 1-octanol ranging from 1-10 ppm. It shows a frequency shift of 33 Hz for 10ppm and 6 Hz for 1 ppm of 1-octanol with a noise level of 0.11 Hz. The limit of detection is 55 ppb. The sensor response against 1-octanol is also fully reversible and the sensitivity is better as compared to MoS_2

nanoparticles sensor by a factor of 2. So with the decrease of hydrophobicity of metal sulfide the sensor response increases.

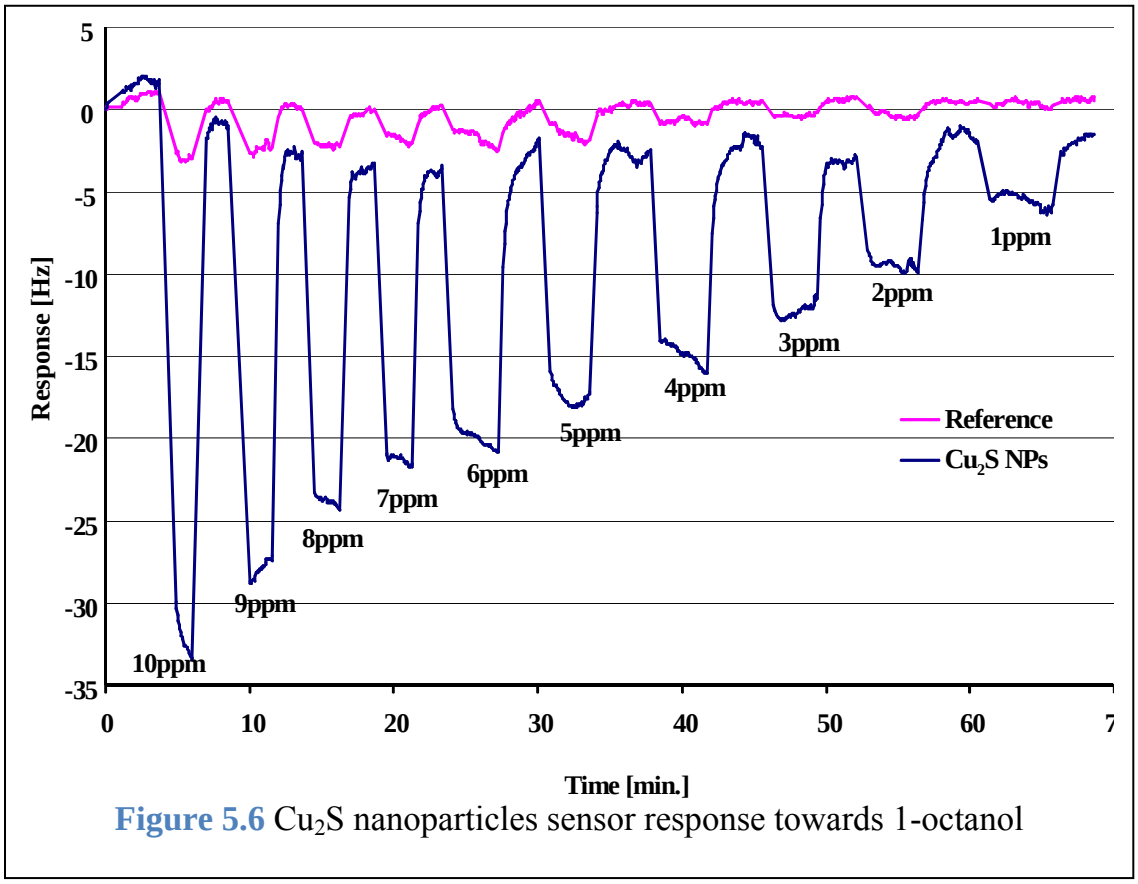

Figure 5.6 Cu_2S nanoparticles sensor response towards 1-octanol

The normalized response of copper sulfide nanoparticles against 1-octanol is shown in figure 5.7. The regression analysis of the sensor characteristics shows a linear behavior in concentration range from 1-10 ppm of 1-octanol with the value of correlation coefficient of 0.9866. Again the lower sensor detection limit for the long chain alcohol can mainly be traced to its hydrophobic behavior leading to chain-chain interactions, molar mass and vapor pressure effects supporting condensation.

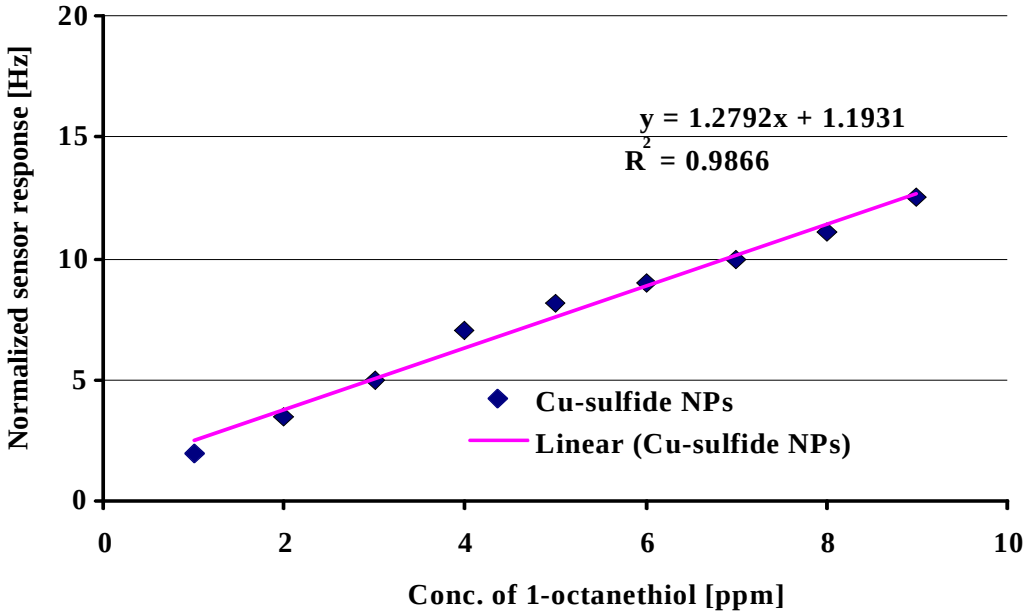

Figure 5.7 Normalized sensor response of Cu_2S nanoparticles towards 1-octanol.

Mass Sensitive Measurement of Alcohols with Silver Sulfide (Ag_2S) Nanoparticles:

As the sensor response of Cu_2S nanoparticles is higher as compared to MoS_2 nanoparticles because of its comparably higher hydrophilicity. So it provides us a powerful to tool to select the promising candidates for sensing of alcohol vapors in air. Therefore, we extend our strategy towards other, least hydrophobic metal sulfides as compared to molybdenum disulfide and copper sulfide. In this regards, silver sulfide seems an optimal candidate. Figure 5.8 summarizes the sensor response of Ag_2S towards different concentrations of 1-propanol ranging from 250 to 1000 ppm. There is sensor response of 14 Hz for 250 ppm of 1-propanol with 0.11 Hz noise level and the limit of detection is up

to 5.9 ppm. The sensor shows reversible, reproducible and linear response from 250-1000 ppm of 1-propanol.

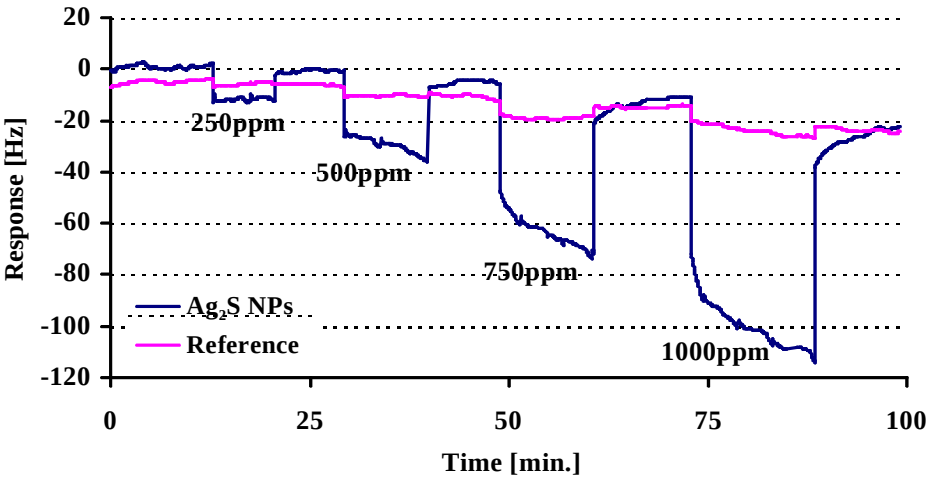

Figure 5.8 Sensor response of Ag_2S nanoparticles towards 1-propanol.

We also obtained an appreciably sensitive and fully reversible sensor signal, when sensor was exposed to different concentrations of 1-butanol. Figure 5.9 shows a reversible and linear response of silver sulfide nanoparticles against 1-butanol with different concentrations ranging from 100ppm to 500ppm.

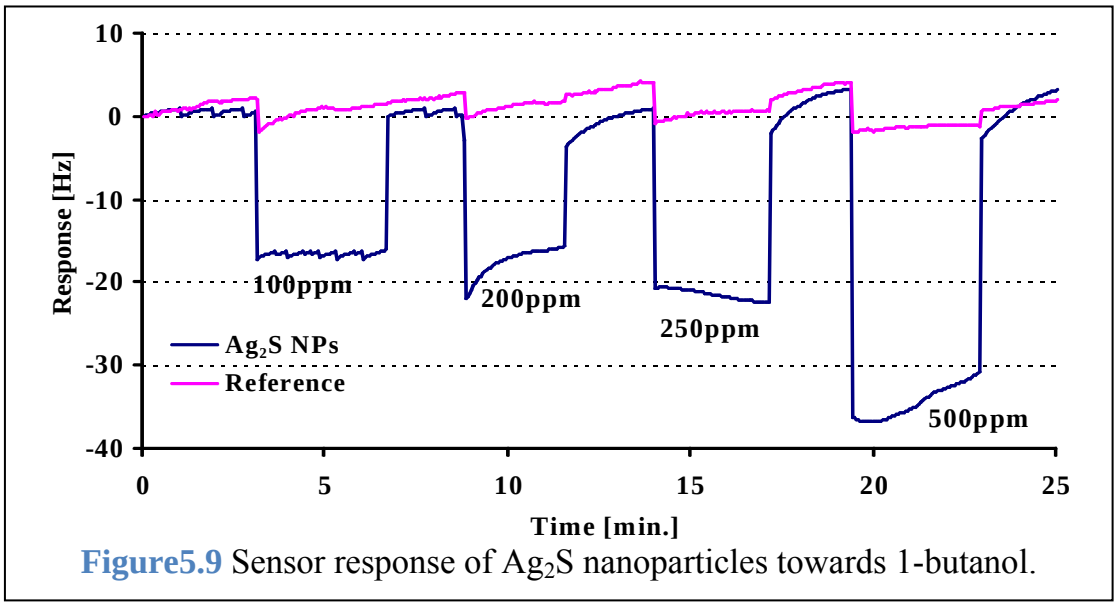

Figure5.9 Sensor response of Ag_2S nanoparticles towards 1-butanol.

Sensor yielded a response 17 Hz for 100 ppm of 1-butanol with 0.11 Hz noise level and the detection limit is 1.95 ppm. The sensor shows a concentration dependent linear behavior.

When sensor was exposed to different concentrations of 1-octanol, a reversible sensor signal was obtained showing the interaction of soft recognition material with 1-octanol molecules. It has ability to sense the 1-octanol less than 1ppm in air and at 1ppm has the sensor signal of more than 10 Hz. Figure 5.10 shows silver sulfide sensor response against different concentrations of 1-octanol. The detection limit of Ag_2S nanoparticles is 330 ppb which shows a better sensitivity achievement.

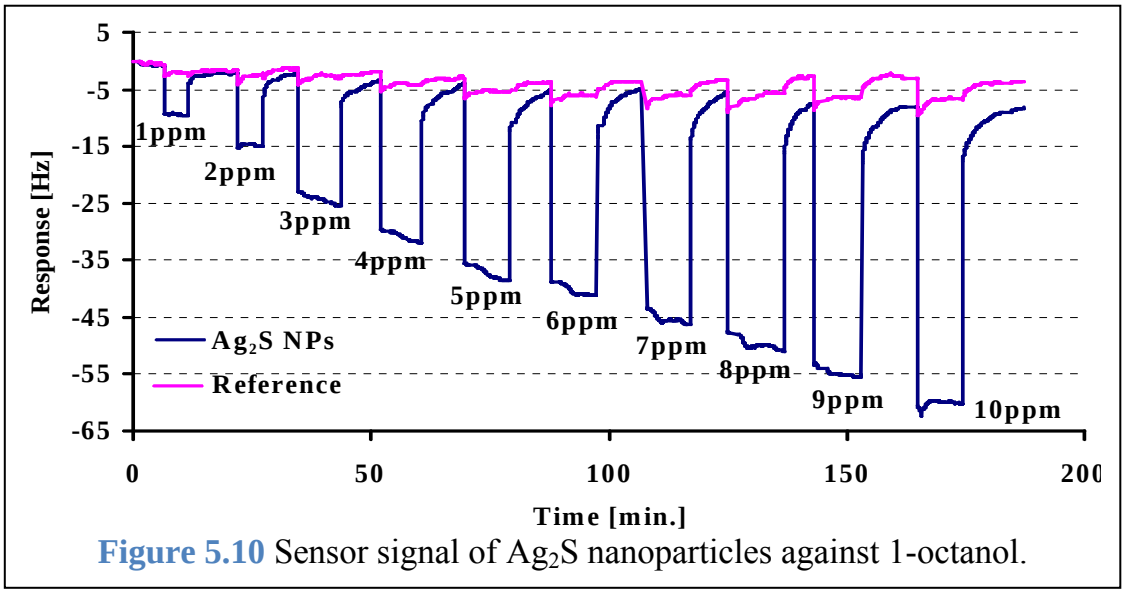

Figure 5.10 Sensor signal of Ag_2S nanoparticles against 1-octanol.

The normalized response of Ag_2S nanoparticles against 1-octanol is shows in figure 5.11, which indicates that silver sulfide nanoparticles based sensor have a linear response for a concentration of 1-9ppm of 1-octanol. The regression analysis of sensor characteristics shows also linear behavior with a correlation coefficient value of 0.9846.

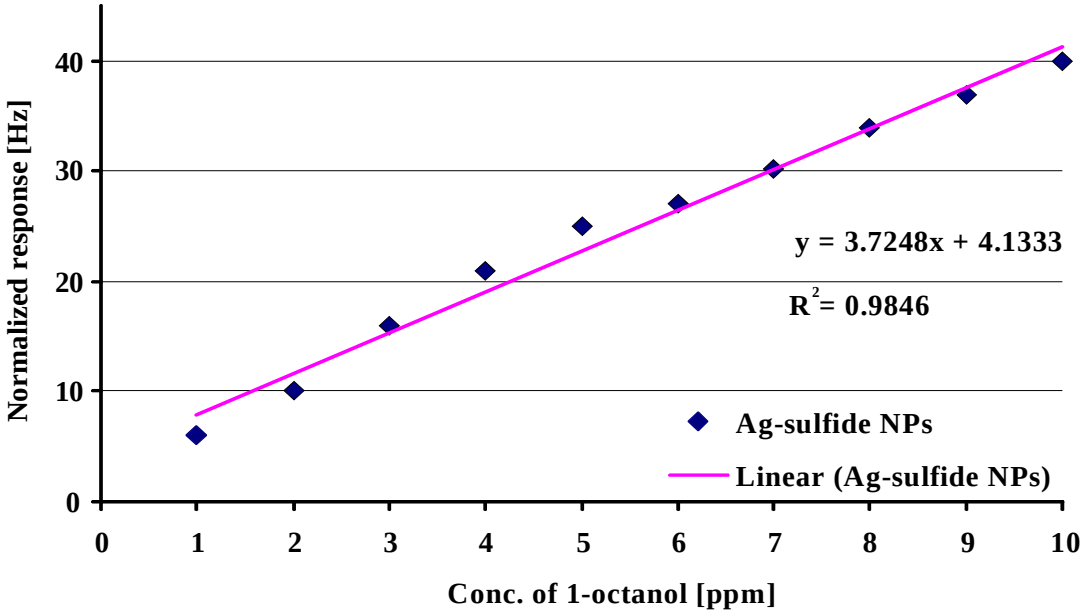

Figure 5.11 Normalized response of Ag_2S nanoparticles against 1-octanol.

The difference in sensor responses of Ag_2S nanoparticles towards 1-butanol and 1-octanol is because of the reasons as we have already discussed in case of MoS_2, and Cu_2S, i.e. vapor pressure, etc.

Comparison of Sensor Responses of Metal Sulfides nanoparticles

Figure 5.12 shows the comparison of sensor responses of molybdenum disulfide, copper sulfide and silver sulfide nanoparticles towards different concentrations of 1-octanol. At 5 ppm concentration of 1-octanol, the sensor responses of MoS_2, Cu_2S and Ag_2S are 4.6Hz, 8.15Hz and 25 Hz respectively. It is clear from the figure that sensor response of Cu_2S is twice than that of MoS_2 nanoparticles and silver sulfide nanoparticles is prominent over copper sulfide and molybdenum disulfide by the factor of 5 and 3 respectively. The reason behind this difference in sensor response is that MoS_2 is highly hydrophobic as compared to copper sulfide and copper sulfide is more hydrophobic than Ag_2S.

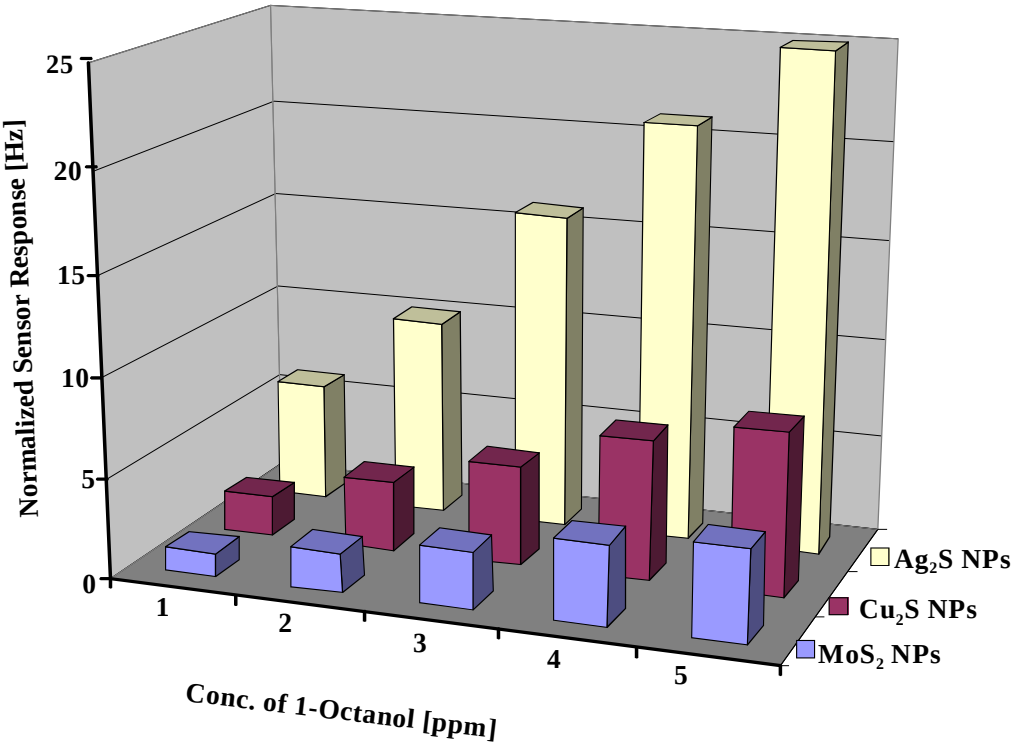

Figure 5.12 Sensor response comparison of MoS_2, Cu_2S and Ag_2S nanoparticles towards 1-octanol.

Therefore, the interaction between least hydrophobic silver sulfide is more as compared to MoS_2 and Cu_2S. The other reason for the much more pronounced responses of silver sulfide is its larger atomic radius and charge density on Ag^{1+} in Ag_2S. So this difference in hydrophobicity, charge density and atomic radii makes the silver sulfide nanoparticles as most promising recognition material for the detection of alcohols.

Selectivity Pattern of different Alcohol Sensors

We have studied the sensor response to an extended list of the volatile organic compounds. High selectivity of the nanopaparticles based sensor for alcohol detection has been demonstrated. A dramatic response difference was

observed between alcohol and other analyte with different functional groups including n-octane, ethyl methyl ketones and limonene. Figure 5.13 summarizes the sensor responses of MoS_2, Cu_2S and Ag_2S nanoparticles towards 1-octanol at 10 ppm, n-octane at 500 ppm, ethyl methyl ketone at 1000 ppm and limonene at 200 ppm. On comparing the sensor response of 1-octanol with other above mentioned analytes, the sensitivity of nanoparticles for other compounds is far less than that of alcohol.

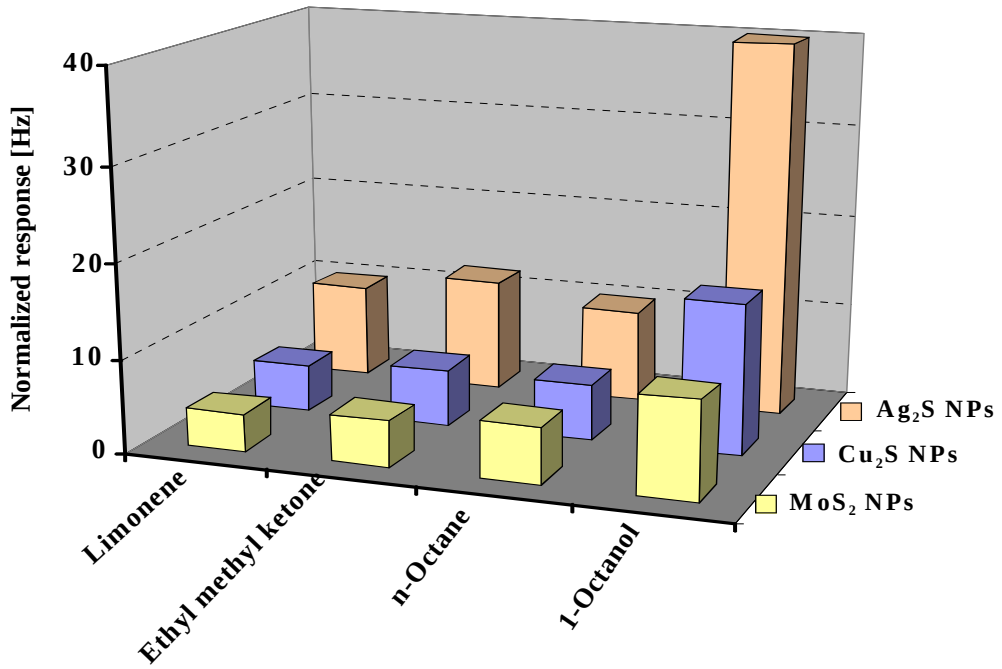

Figure 5.13 Sensitivity and selectivity pattern of nanoparticles

The sensor response of 1-octanol is 25 Hz, which is higher by the factor of more than three in case of Ag_2S as compared to the sensor signal towards n-octane, ethyl methyl ketone and limonene. In case of Cu_2S nanoparticles the sensor response towards 1-octanol is higher than that of others compounds by the factor of more than 2.5. Similarly, MoS_2 nanoparticles yield a sensor response of 4.6 Hz for 1-octanol which differs from that of n-octane, ethyl methyl ketone and

limonene by the factor 2. It means that least hydrophobic metal sulfides nanoparticles have more interactions towards alcohols.

5.4 Conclusion

The high sensitivity of designed sensor towards alcohol is due to interactions between alcohol and metal sulfide nanoparticles based on their respective hydrophilic or hydrophobic properties. The use of least hydrophobic metal sulfides nanoparticles for the detection of different alcohols seems to be the most promising approach for online monitoring of alcohols via affinity materials. The metal sulfides nanoparticles based sensor is highly selective to alcohols and provides better response towards alcohols as compared to other analytes, such as ketones or alkanes. High sensitivities of sensor can be achieved by decreasing the hydrophobicity and charge density on metal of metal sulfides compound.

6. Silver Sulfide-MIP Nanocomposite, Recognition Material for Alcohols

6.1 Introduction

Molecularly imprinted polymers are of substantial interest in synthesizing recognition sites optimized towards a specific analyte because of providing a very straightforward method for that purpose [56]. Chemical sensing in real-life environment often needs high sensitivies and selectivities. On mass sensitive chemical sensor (e.g. quartz crystal microbalance, QCM) these properties can be enhanced by generating a large number of interaction sites within the available respective recognition material and or by increasing the accessibility of the interaction centers [17]. Therefore, it may be of substantial interest to generate composites of metal sulfide nanoparticles with molecularly imprinted polymers (MIP) to make use of the best of two worlds, namely appreciable sensitivity provided by the former and selectivity/pre-concentration ability from the latter.

In these days inorganic-organic composite microspheres are of intensive research interest because of their importance in a wide-range of potential applications [57]. Recently, substantial efforts have been made to integrate inorganic nano-particles into the interior of polymer microspheres. The resulting inorganic-organic composite microspheres bear novel collective mechanical, thermal, optical, magnetic and electronic properties [58]. The high specific surface area of nanosized recognition materials offers a potentially large analyte-recognition material interface than a planar thin-film sensing materials such as metal nanoparticles semiconductor, or polymer-thin-film based sensors [59,60,61,62]. Sensitivity and selectivity of sensor can be improved by increasing the specific surface area of the recognition materials. However, high sensitivity,

selectivity, ruggedness and low-cost disposable sensor fabrication is still a major challenge for scientists. Numerous methods have been designed to fabricate composite materials in order to achieve the required structures and properties.

6.2 Experimental

Chemicals

Diisocyanato-diphenylmethane (DPDI), bisphenol A (BPA), phloroglucinol and tetrahydrofuran (THF) were purchased from Merck and Fluka with highest purity available. Ag_2S nanoparticles were prepared as described in chapter 4.

Synthesis of Ag_2S-polyurethane nanocomposite material

Polyurethane was prepared according to an already published procedure [56]. We used diisocyanato-diphenylmethane (DPDI) containing about 30% of triisocyanates for this synthesis. 1.0 g of DPDI, 1.97 g of bisphenol A (BPA), 0.22 g of phloroglucinol and 2 ml of tetrahydrofuran (THF) were mixed together. After dissolution, 30 µl of pre-reacted solution was diluted with 970 µl of 1-butanol. We added 10 mg of Ag_2S nanoparticles in 500 µl of above oligomer solution and thus obtained a suspension of Ag_2S-polyeurethane composite material. This was further diluted 1+30 with the respective template solvent i.e. 1-butanol. We synthesized two types of composite material in order to see the difference in selectivity and sensitivity, one with imprinted polymer and other one with non-imprinted polymer.

Quartz Crystal Microbalance (QCM) design, preparation and measuring apparatus:

Dual electrodes quartz crystal microbalance were prepared according to already used method with same measuring set up as discussed in chapter 2. 5 µl

of nanocomposite suspension was coated on both sides of electrode by spin coating, dried overnight at 80°C and a layer of 2-3 kHz (1 kHz = 40 nm) was obtained.

6.3 Results and Discussion

Nanocomposite Characterization

First of all, the feasibility of synthesis of nanocomposite procedure has to be assured. For this purpose, nanocomposite was deposited on glass substrate

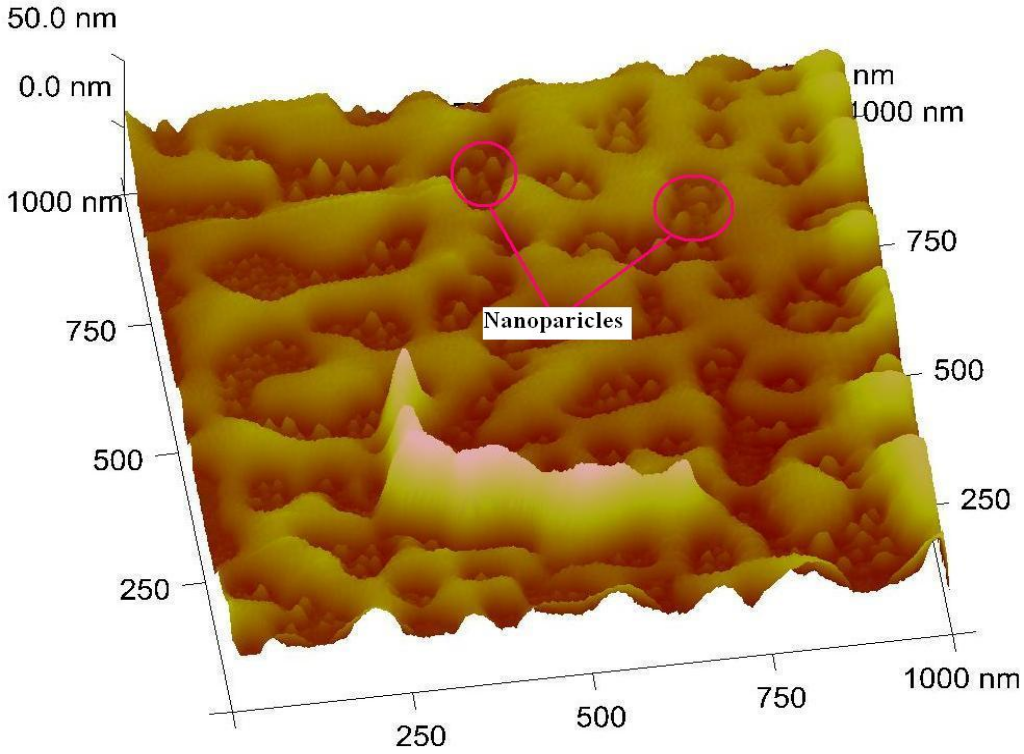

Figure 6.1 AFM image of composite material containing Ag_2S

to record the respective AFM images. Figure 6.1 shows typical result for the nanocomposite, in which one can clearly see the nanoparticles embedded in polyurethane thin film. The polyurethane is also well patterned and nanoparticles

of silver sulfide are evenly distributed throughout the whole surface. So, the feasibility of synthesis procedure of nanocomposite material has been assured.

Molecularly imprinted polyurethane without silver sulfide nanoparticles AFM image is shown in figure 6.2 below. One can see clearly see the difference between figures 6.1 and 6.2, as in first case particles are visible clearly indicating that the synthesis procedure to obtain nanocomposite has been successful. In the second case, no particles are visible.

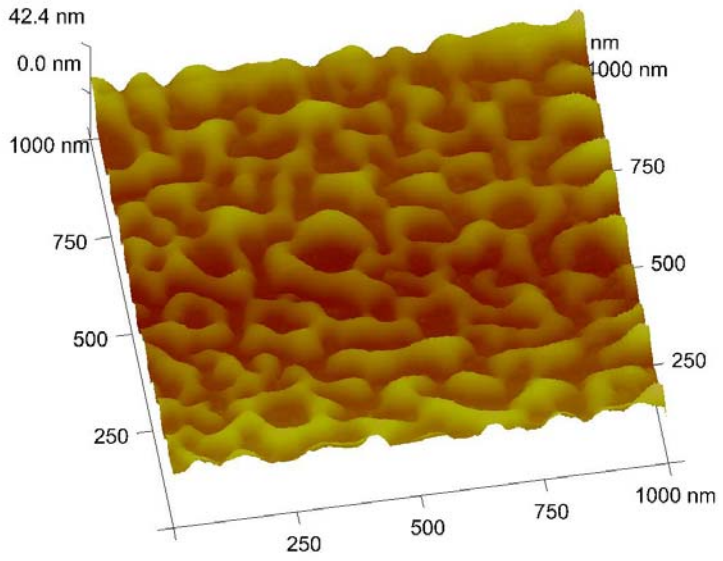

Figure 6.2 AFM image of MIP without particles

QCM Sensor Characteristics

Figure 6.3 shows the sensor response of nanocomposite and imprinted polyurethane towards different concentrations of 1-butanol ranging from 100 ppm to 400 ppm. One can clearly see that the sensor response of nanocomposite is higher by a factor of five as compared to imprinted polyurethane. At the concentration of 400 ppm of 1-butanol, the sensor response of imprinted polyurethane is 17 Hz with noise level of 0.14 Hz and with limit of detection 9.9

ppm. But nanocomposite yields a response of 70 Hz for 400 ppm of 1-butanol at 0.11 Hz noise level and limit of detection is 1.9 ppm. Therefore, the limit of detection of nanocomposite is substantially by the factor of 5 as compared to imprinted polymer. All sensor responses are fully reversible and reproducible.

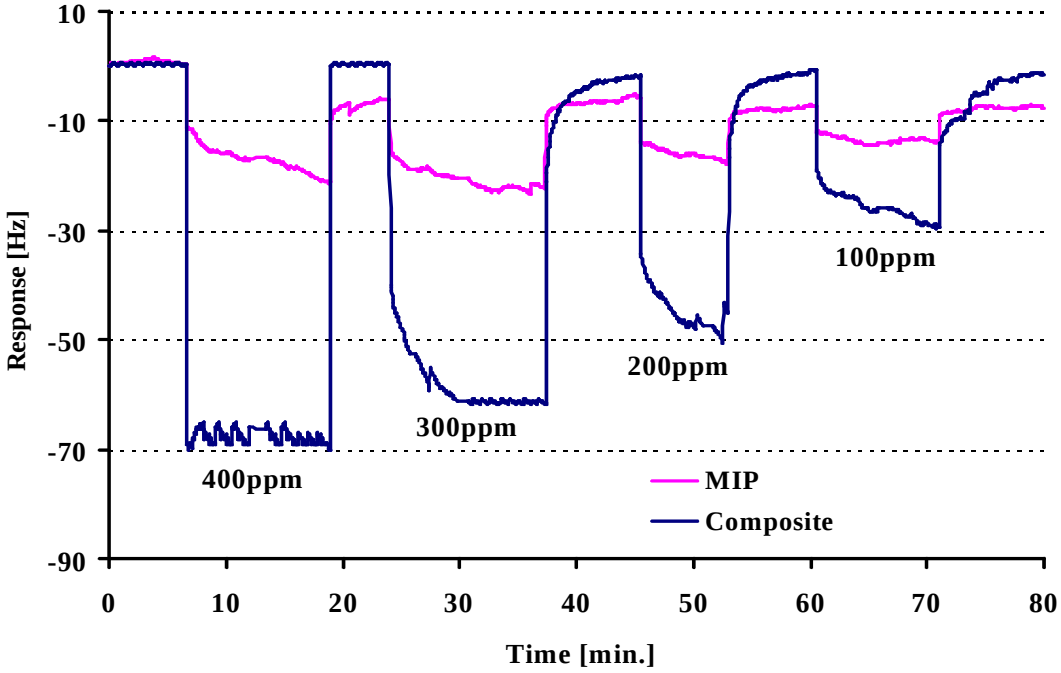

Figure 6.3 Sensor responses of MIP and nanocomposite towards 1-butanol

We believe that this substantial difference between the sensor responses of MIP and nanocomposite is because of the interactions between the silver sulfide nanoparticles and alcohol. Hence, merging molecularly imprinted polymers and materials having substantial interactions towards the analyte (in this case alcohol) can be utilized to improve sensitivity and selectivity of a sensor, probably even particularly for applications in complex mixture of analyte. The combination of material having affinity interactions with analyte and molecular imprinting should be favorable in view of robust layers and lower cross sensitivity towards other molecules. The diffusion pathway to embedded affinity material can be

seen as leading to a pre-equilibrium comparable to a pre-concentration of analytes in the imprinted polymer near the affinity material.

Regression analysis of the normalized response of nanocomposite is shown in figure 6.4. The value of correlation coefficient (R^2) is 0.999 which represents the complete linearity agreement of sensor signals with concentrations.

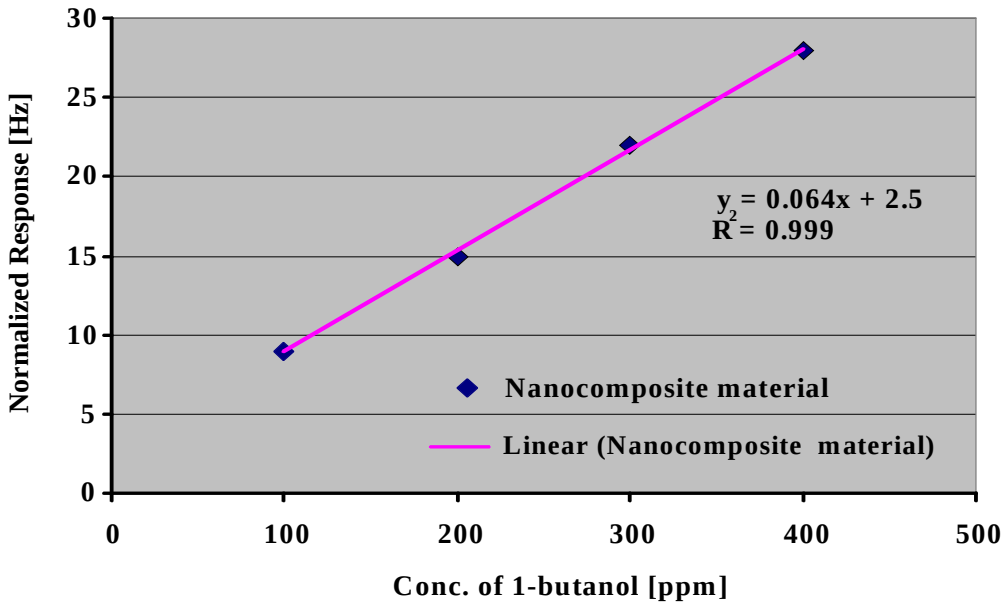

Figure 6.4 Normalized sensor response of nanocomposite along with regression analysis

Selectivity of Nanocomposite Material

Figure 6.6 shows the sensor response nanocomposite against n-octane at the concentration of 400 ppm and 500 ppm. It can be seen from figure that there is only 7.0 Hz response for 400 ppm and 7.5 Hz for 500 ppm of n-octane. On comparing the sensor signal of nanocomposite towards1-butanol at 400 ppm, with that of n-octane at 400 ppm, there is dramatic difference in the responses, even though the number of carbon atoms in n-octane is double than 1-butanol. This substantial difference in responses indicates the appreciable selectivity of nanocomposite material.

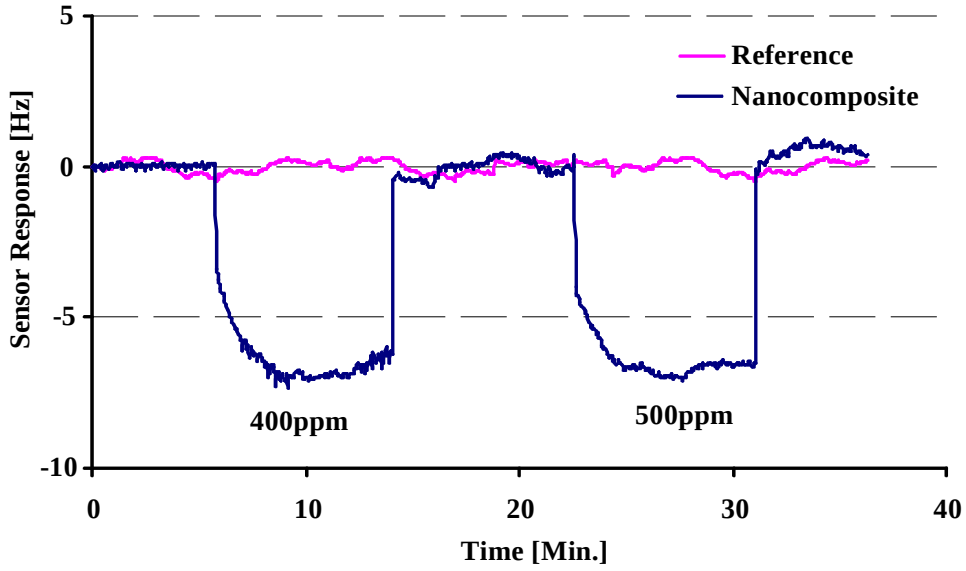

Figure 6.5 Sensor response of nanocomposite towards n-octane

Comparison of Nanocomposite Sensor Responses

Figure 6.6 summarizes the comparison of sensor responses of NIP, NIP+Ag_2S, MIP and nanocomposite towards different concentrations of 1-butanol ranging from 100 ppm to 400 ppm. As can be seen, the NIP yields lowest effects, thus indicating comparably low affinity between the polymer and the alcohol. The composite between the NIP (non-imprinted polymer) and NPs (nanoparticles) yields effects that are higher by a factor of 3 showing that particles exposed on the surface leads to increased interaction with alcohol due to affinity interactions. However, the pure MIP (molecularly imprinted polymer) gives sensor responses being a factor 4 higher than the NIP, showing the presence of a bulk phenomenon in this case: interaction sites for 1-butanol are distributed within the entire polymer bulk and lead to incorporation and therefore sensitive responses. Furthermore, the sensor response of pure NP is higher by the factor of 8 than that of NIP indicating that the affinity of Ag_2S towards alcohols is substantially higher than that of polymers. Of course, being present as

nanoparticles (NPs) means higher surface area and therefore also somewhat increased sensor responses.

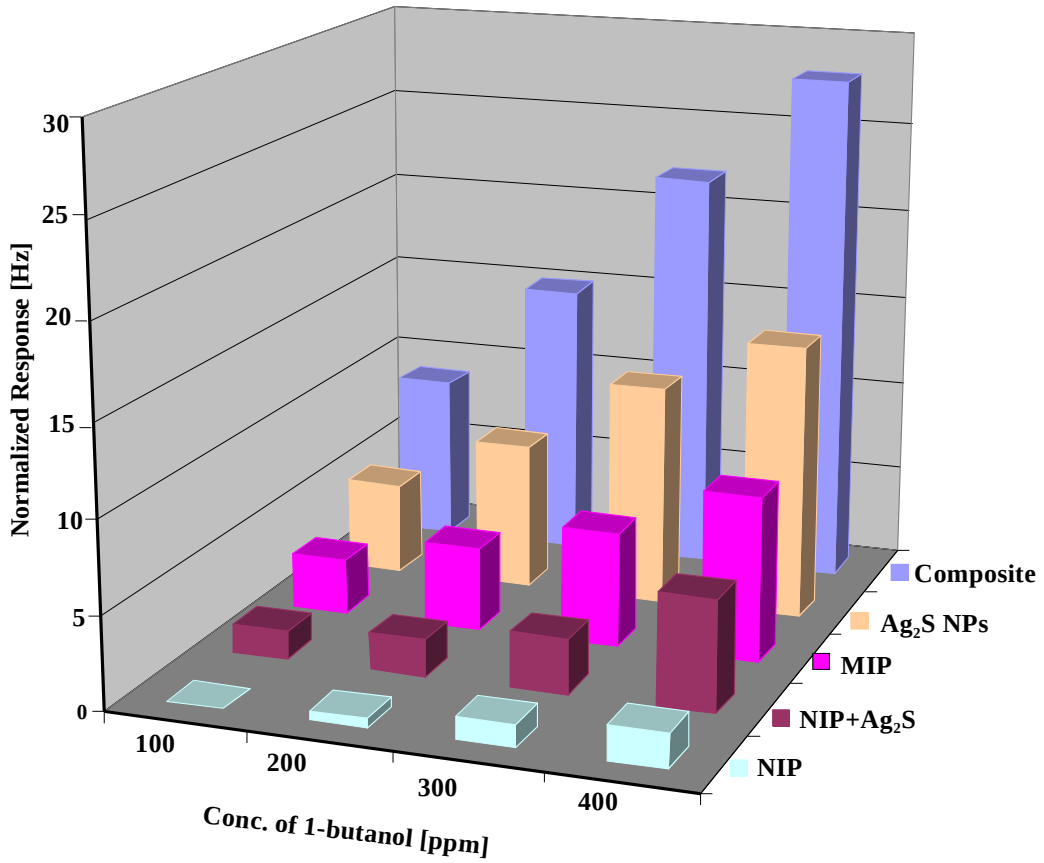

Figure 6.6 Comparison of sensor responses of different material towards 1-butanol.

Combining the Ag_2S NPs and MIP finally leads to another improvement factor of 15.5 over NIP, which is even two times larger than the response of the pure nanoparticles. This clearly indicates that the MIP functions as a "pre-concentrator" for alcohol around the Ag_2S nanoparticles. So the sensing capability of the silver sulfide-polyurethane composite material is high due to above mentioned two main factors.

Selectivity Comparison

Figure 6.7 shows the selectivity comparison between the normalized responses of NIP, NIP+NPs, MIP, NPs and nanocomposite material towards 400 ppm of 1-butanol and n-octane. Nanocomposite yields 28 Hz and 4 Hz towards 1-butanol and n-octane respectively, which leads to the selectivity factor of 7. Ag_2S NPs shows a sensor response of 15 Hz and 6 Hz for 1-butanol and n-octane

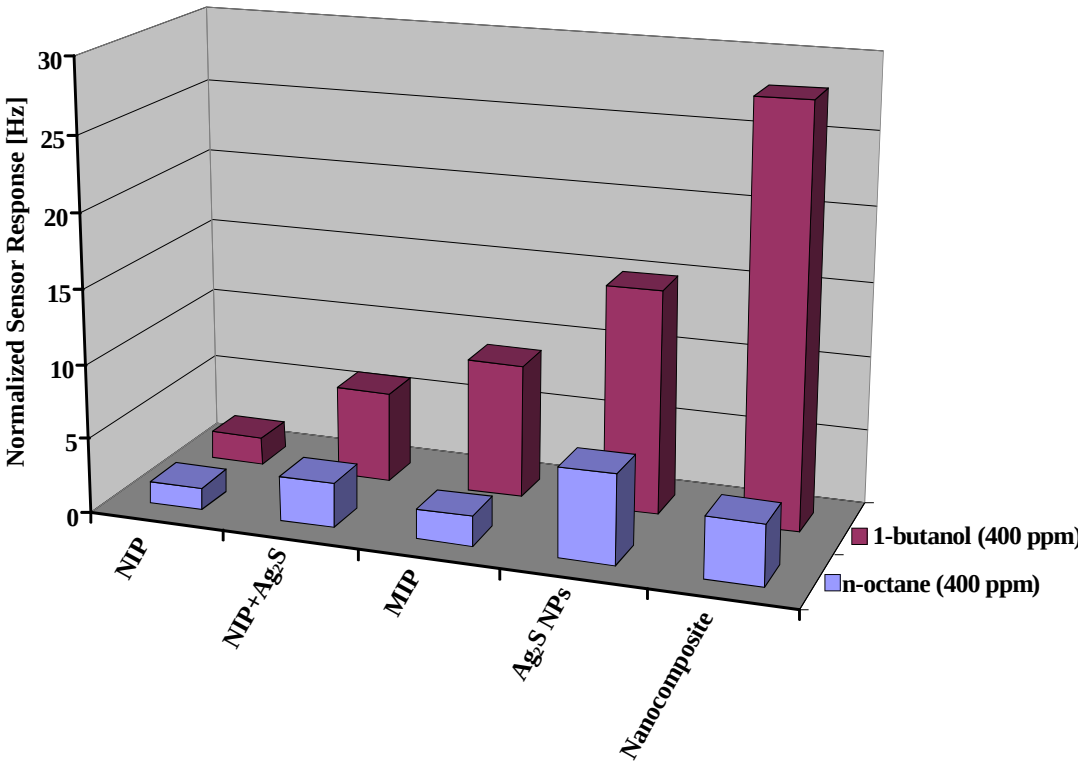

Figure 6.7 Selectivity comparison of nanocomposite

respectively, leading to a selectivity factor of 2.5. MIP gives a sensor response of 9 Hz for 400 ppm of 1-butanol and 2 Hz for n-octane, leading to a selectivity factor of 4.5. Composite with NIP yields a response of 6 Hz and 3 Hz for 400 ppm of 1-butanol and n-octane respectively, giving a selectivity factor of 2. Similarly, NIP gives a sensor response of 1.5 Hz and 1.8 Hz for 400 ppm of 1-butanol and n-octane respectively. But when we compare the sensor response of

Ag_2S NPs, MIP and nanocomposite towards same concentration of n-octane then we came to know that most selective is MIP and least one is Ag_2S NPs but we can see that by merging the both material we get pronounced sensitivity along with better selectivity by the factor of 7. So, it becomes clear from the above figure that the novel nanocomposite material have pronounced sensitivity and selectivity towards alcohols.

6.4 Conclusion

The combination of organic and inorganic nanosized materials is resulted into a nanocomposite material with novel collective properties. Nanocomposite materials approaches have proven to be highly suitable for generating recognition material for both environmental and process control applications. We have fabricated a new sensor material by merging the affinity interactions with imprinting technique and resultant nanocomposite sensor material bears novel collective recognition properties of affinity interactions and molecular imprinting. The high specific surface area of nanocomposite sensing material offers a substantially large surface area for affinity interaction and molecular imprinting contributes enough selectivity. Therefore composite material is highly sensitive, chemically selective enough and has proved itself, as a highly promising material for the detection of alcohols.

Abstract (English)

In recent years, the use of nanoparticles and nanocomposites in the fabrication of chemical sensor has become a focus of interest. The use of nanoparticles as a recognition layer material enhances the sensitivity and limit of detection of a sensor because availability of substantially increased surface area.

In preliminary studies it was found that molybdenum sulfide nanoparticles have substantial affinity towards gaseous thiols (RSH), based on Pearson hardness. The first part of this thesis consists of characterizing MoS_2 nanoparticles according to their sensing properties. This revealed that the sensitivity of sensor was increased by the factor of 5 by optimizing the particle size yielding direct relationship between particle diameter and sensor signal. The chemical background of MoS_2-thiol affinity interactions could be further clarified by selectivity studies with compounds with similar size but different functionality such as n-octane, limonene and ethyl methyl ketone. Resulting selectivity factors are round 80, 30 and 300 respectively as compared 1-octanethiol, which strongly suggest that interactions are based on thiol functionality.

In a further step, the effect of hardness has also been studied by extending this strategy to different metals with prominent hardness difference i.e. Cu_2S and Ag_2S systems. The sensor signal of Cu_2S is higher by the factor of 2.1 than MoS_2 and Ag_2S nanoparticles system has 21 times higher sensor signals than that of MoS_2 system. By comparing the sensor signals of metal sulfides between one another, it is observed that with decreasing hardness of metal sulfide, the affinity interaction towards thiol substantially increases further supporting the fundamental strategic approach for thiol sensing. Moreover, this lead to Ag_2S

being the optimal material with a quartz crystal microbalance (QCM) limit of detection of 18 ppb for 1-octanethiol in air.

Finally, the feasibility of composites combining Ag_2S nanoparticles with molecularly imprinted polymers (MIP) was assessed. AFM studies proved the feasibility of this approach, i.e. particles indeed were incorporated into the polymeric matrix. This nanocomposite, bearing novel collective recognition properties of affinity interactions and molecular imprinting, was found highly suitable as sensor material for alcohols with pronounced sensitivity and selectivity increased by the factor of 5 as compared to its nanoparticles and MIP separately. The reason may be that the MIP functions as a pre-concentrator for the analyte close to the affine surface.

Zusammenfassung (Deutsch)

Im Lauf der letzten Jahre geriet die Anwendung von Nanopartikeln und Nanokompositen zunehmend in den Brennpunkt wissenschaftlichen Interesses. Die Anwendung von Nanopartikeln als Erkennungsmaterialien erhöht aufgrund der stark erhöhten Oberfläche die Empfindlichkeit von Sensoren und verbessert daher das Detektionslimit.

Vorabstudien zeigten, daß MoS_2 Nanopartikel fundamentale Affinität zu organischen Thioldämpfen (RSH) zeigen, wahrscheinlich aufgrund passender Härte nach Pearson. Der erste Teil der vorliegenden Arbeit beschäftigt sich daher damit MoS_2 Nanopartikel hinsichtlich ihrer Sensoreigenschaften zu charakterisieren. Dabei stellte sich heraus, daß die Sensitivität der entsprechenden Sensoren durch Optimierung der Partikelgröße um bis zu einem Faktor 5 erhöht werden konnte. Daraus ließ sich auch der Zusammenhang zwischen dem Partikeldurchmesser und dem Sensorsignal erklären. Die chemische Ursache für die Erkennung konnte durch Selektivitätsstudien festgestellt werden, bei denen Verbindungen ähnlicher Masse, aber verschiedener Funktionalität getestet wurden, wie beispielsweise n-Oktan, Limonen und 2-Butanon. Die Selektivitätsfaktoren der Nanopartikel für n-Oktanthiol liegen bei 80 bzw. 30 bzw. 300 im Vergleich zu diesen Verbindungen. Die zur Erkennung führenden Wechselwirkungen basieren also tatsächlich auf der Thiolfunktion.

In einem weiteren Schritt wurde der Einfluß der Pearsonhärte durch Ausweiten der Studien auf witere Metallsulfide, wie beispielsweise Cu_2S und Ag_2S, ausgedehnt. Ersteres Material führt verglichen mit MoS_2 zu mehr als doppelt so großen Sensoreffekten, Ag_2S sogar zu 21-mal größeren. Aus dem direkten Vergleich der Sensorsignale der Sulfide untereinander ergibt sich, daß

diese bei abnehmender Pearsonhärte deutlich zunehmen. Dies stützt auch die grundlegende Annahme für die Strategie zur Sensorentwicklung für Thioldämpfe. Als optimal stellte sich dabei Ag_2S heraus, das auf der Quarzmikrowaage (quartz crystal microbalance QCM) Detektionslimits von 18 ppb Oktanoldampf in der Luft erreicht.

Der letzte Teil der Dissertation beschreibt erste Versuche zur Kombination dieser Nanopartikel mit Molekular Geprägten Polymeren (molecularly imprinted polymers, MIP). Mit Hilfe von AFM-Aufhahmen konnte gezeigt werden, daß Nanopartikel tatsächlich in der Polymermatrix verteilt werden können. Das dabei entstehende Nanokompositmaterial verbindet Affinität und die Erkennung mittels der MIP. Als Sensorschichte für Dämpfe aliphatischer Alkohole ermöglichen diese fünfmal höhere Meßeffekte, als die Partikel oder das MIP alleine. Ein Grund dafür ist, daß das MIP den Analyten in der Nähe der Affinitätspartikel vorkonzentriert.

List of Abbreviations

AFM	Atomic Force Microscopy
BAW	Bulk Acoustic Wave
BPA	Bisphenol A
DPDI	Diisocyanato-diphenylmethane
3D	Three Dimensional
EMF	Electro Motive Force
MIP	Molecularly Imprinted Polymer
NIP	Non-imprinted polymer
NPs	Nanoparticles
PANI	Polyaniline
PPM	Part Per Million
QCM	Quartz Crystal Microbalance
SAW	Surface Acoustics Wave
TSM	Thickness Shear Mode
THF	Tetrahydrofuran
UV/Vis	Ultraviolet/Visible
XRD	X-Ray Diffraction

References

1.A. Hulanicki, F. Ingman, Chemical Sensors: Definition and Classification, Pure and Applied Chemistry, 63 (1991) 1247.

2.W. GoPel, J. Hesse, J. N. Zemel, Sensors, Wiley-VCH, Weinheim, Vol. 2 (1989).

3.U. E. Spichiger-Keller, Chemical Sensors and Biosensors for Medical and Applications, Wiley-VCH, Weinheim, (1998).

4.U. Lehmann, H. Plehn, O. Krusemark, J. Muller, A Miniaturized Gas Chromatograph for Autonomous and Longtime Measurements, in Proc. Sensor, Nuremburg, AMA Service, Wunstorf, Vol. 1 (1999) 155-158.

5.S. Zimmermann, B. Riepenhusen, J. Muller, Micromachined Flame Analyzer: Flame Ionization Detector, Atomic Emission Spectrometer, in Proc. Sensor, Nuremburg, AMA Service, Wunstorf, Vol. 1 (1999) 409-413.

6.F. L. Dickert, P. A. Lieberzeit, Solid-State Sensors for Field Measurements of Gases and Vapours; in Encyclopaedia of Analytical Chemistry, R. A. Meyers (Ed.), John Wiley and Sons Ltd. Chichester, (2000) 3831-3855.

7.W. S. Hughes, Potential difference between glass and electrolytes in contact with the glass, Journal of the American Chemical Society, 44 (1922) 2860-7.

8.Rulfs, L. Charles, Elving, J. Philip, Oxidation levels of rhenium. II. Oxidation of rhenide at the dropping-mercury electrode. Nature of the rhenide species in hydrohalic acid media, Journal of the American Chemical Society, 73 (1951) 3287-92.

9.P.J. Elving, O.H. Muller, Stanley. Wawzonek, M.J. Astle, Louis, Polarographic behavior of organic compounds.Analytical chemistary, 22 (1950) 482–484II.

10.Elving, J. Philip, Tang and Ching-Siang, Polarographic behavior of organic compounds. III. The chloroacetic acids. Journal of the American Chemical Society, 72 (1950) 3244-6.

11.L. Clark, Measurement of oxygen in physiological fluids and tissues, Transactions of American society of artificial internal organs, 2 (1956) 41-47.

12.F. L. Dickert, A. Haunschild, Sensor materials for solvent vapor detection—donor–acceptor and host–guest interactions, Advanced Material, 5(1993) 887–889.

13.F. Dickert, U.P. A Baumler, G. K. Zwissler, Supramolecular structures and chemical sensing Synthetic Metals, 61 (1993) 47-51.

14.F. L. Dickert , P. A. Lieberzeit, Imprinted Polymers in Chemical Recognition forMass-Sensitive Devices, Springer Ser Chemical Sensor and Biosensor, 5 (2007) 173–210.

15.Z. Ali, Acoustic Wave Mass Sensors, Journal of Thermal Analysis and Calorimetry, 55 (1999) 397-412.

16.C.K. Ho, A. Robinson, D.R. Miller, M.J. Davis, Overview over sensors and needs for environmental monitoring, Sensors 5 (2005) 4–37.

17.Peter A. Lieberzeit, A. Afzal, A. Rehman, Franz L. Dickert, Nanoparticles for detecting pollutants and degradation processes with mass-sensitive sensors, Sensors and Actuators B 127 (2007) 132–136.

18.R.S. Niranjan, V.A. Chaudhary, I.S. Mulla, K. Vijayamohanan, A novel hydrogen sulfide room temperature sensor based on copper nanocluster functionalised tin oxide films, Sensors and Actuators B, Chem, 85 (2002) 26–32.

19. P.G. Datskos, I. Sauers, Detection of mercaptoethanol using gold-coated micromachined cantilevers, Sensors and Actuators B, Chem, 61 (1999) 75–82.
20. S.M. Briglin, T. Gao, N.S. Lewis, Detection of organic mercaptan vapours using thin films of alkylamine passivated gold nanocrystals, Langmuir, 20 (2004) 299–305.
21. M. Kikushi, S. Shiratori, Quartz crystal microbalance (QCM) sensor for CH_3SH gas by using polyelectrolyte-coated sol–gel film, Sensors and Actuators B, Chem, 108 (2005) 564–571.
22. T. Minamide, K. Mitsubayashi, H. Saito, Bioelectronic Sniffer with monoamine oxidase for methyl mercaptane vapour, Sensors and Actuators B, Chem, 108 (2005) 639–645.
23. T. Bartels, Lubricants and Lubrication, Ullmann's Encyclopedia of Industrial Chemistry. Weinheim: Wiley VCH. doi:10.1002/14356007.a15_423 (2002).
24. H. Topsøe, B.S. Clausen, F.E. Massoth, Hydrotreating Catalysis, Science and Technology. Berlin: Springer-Verlag (1996).
25. D. Dominique, B. Stephane, L.C. Claude, Chemical synthesis of molybdenum disulfide nanoparticles in an organic solution, Journal of Materials Chemistry, 12 (2002) 2430-2432.
26. J.C. Park and H. Song, Synthesis of Polycrystalline Mo/MoOx Nanoflakes and Their Transformation to MoO_3 and MoS_2 Nanoparticles, Chemistry of Materials, 19 (2007) 2706-2708.
27. C.R Hammond, The Elements, in Handbook of chemistry and physics, 81st Edition. CRC press, ISBN 0849304857, 2004.

28.Ni. Yonghong, F. Wang, L. Hongjiang, Y. Liang, G. Yin, J. Hong, X. Ma, Z. Xu, Fabrication and characterization of hollow cuprous sulfide ($Cu_{2x}S$) microspheres by a simple template-free route, Inorganic Chemistry Communications, 6 (2003) 1406–1408.

29.R.G. Parr, R.G. Pearson, Absolute hardness: companion parameter to absolute electronegativity, Journal of The American Chemical Society, 105(1983) 7512-7516.

30.S. K. Mathew, N.P. Rajesh, M. Ichimura, Udayalakshmi, Preparation and characterization of copper sulfide particles by photochemical method Materials Letters, 62 (2008) 591–593.

31.H. Fjellvag, F. Gronvold, S. Stolen, A.F. Andresen, R. Müller Käfer, A. Simon, Low-temperature structural distortion in CuS Zeitschrift für Kristallographie, 184 (1988) 111-121.

32.H.T. Evans, The crystal structures of low chalcocite and djurleite, Journal of Zeitschrift für Kristallographie, 150 (1979) 299-320.

33.J.G. DeWitt, Space-filling model of part of the crystal structure of silver sulfide, Ag2S. X-ray crystallographic data from Mineral J. 5 (1967) 124-143.

34.S. Shukla and S. Seal, Synthesis and characterization of silver sulfide nanoparticles containing sol-gel derived HPC-Silica film for ion-selective electrode application, Journal of Sol-Gel Science and Technology, 23 (2002) 151–164.

35.L.S. Ramsdell, The crystallography of acanthite, American Mineralogist, 28 (1943) 401-425.

36.M.M. Ayad, G. El-Hefnawey, N. L. Torad, A sensor of alcohol vapours based on thin polyaniline base film and quartz crystal microbalance, Journal of Hazardous Materials, 168 (2009) 85–88.

37.C.E. Collins, L.J. Buckley, Conductive polymer-coated fabrics for chemical sensing, Synthetic Metals, 78 (1996) 93–101.

38.M.S. Freund, N.S. Lewis, A chemically diverse conducting polymer-based electronic nose, Proceeding National Academy of Science, U.S.A. 92 (1995) 2652–2656.

39.M. Zinbo, Determination of one carbon to three-carbon alcohols and water in gasoline/alcohol blends by liquid chromatography, Analytical Chemistry, 56 (1994) 244–247.

40.M. Boujitita, J.P. Hart, and R. Pittson, Development of a disposable ethanol biosensor based on a chemically modified screen-printed electrode coated with alcohol oxidase for the analysis of beer. Biosensors and Bioelectronics, 15(2000) 257–263.

41.A.M. Azevedo, D.M.F. Prazeres, J.M.S. Cabral and L.P. Fonseca, Ethanol biosensors based on alcohol oxidase, Biosensors and Bioelectronics, 21 (2005) 235–247.

42.P. Aragón, J. Atienze, and M.D. Climent, Analysis of organic compounds in air: a review, Analytical Chemistry, 30 (2000) 121–151.

43.S. Bangalore, G.W. Small, R.J. Combs, R.B. Knapp, R.T. Kroutil, Automated detection of methanol vapor by open path Fourier transform infrared spectrometry, Analytical Chemistry Acta, 297 (1994) 387–403.

44.Q. Chang, J.R. Lakowicz, and G. Rao, Fluorescence lifetime-based sensing of methanol, Analyst, 122 (1997) 173–177.

45.G.J. Mohr, and U.E. Spichiger-Keller, Novel fluorescent sensor membranes for alcohol based on p-N,N-dioctylamino-4'-trifluoroacetylstilben, Analytica Chimica Acta, 351 (1997) 189–196.

46. G.J. Mohr, F. Lehmann, U.W. Grummt, and U.E. Spichiger-Keller, Fluorescent ligands for optical sensing of alcohols: Synthesis and characterization of p-N,N-dialkylamino-trifluoroacetylstilbenes, Analytica Chimica Acta, 344(1997) 215–225.
47. P. Blum, G.J. Mohr, K. Matern, J. Reichert, and U.E. Spichiger-Keller, Optical alcohol sensor using lipophilic Reichardt's dyes in polymer membranes, Analytica Chimica Acta,432 (2001) 269–275.
48. G. Orellana, A.M. Gomez-Carneros, C. de Dios, A.A. Garcia-Mertinez, and M.C. Moreno- Bondi, Reversible fiber-optic fluorescing of lower alcohols, Analytical Chemistry, 67(1995) 2231–2238.
49. S. Petrova, Y. Kostov, K. Jeffris, and G. Rao, Optical ratiometric sensor for alcohol measurements, Analytical Letters, 40 (2007) 715–727.
50. G.J. Price, A.A. Clifton, V.J. Burton, T.C. Hunter, Piezoelectric chemical sensors based on morpholine containing polymers, Sensors and Actuators B-Chemical, 84 (2002) 208–213.
51. P.N. Bartlett, S.K. Ling-chung, Conducting polymer gas sensors. Part III. Results for four different polymers and five different vapours, Sensors and Actuators B, 19 (1989) 287–292.
52. N.E. Agbor, M.C. Petty, A.P. Monkman, Polyaniline thin films for gas sensing, Sensors and Actuators B, 28 (1995) 173–179.
53. D. Nicolas-Debarnot, F. Poncin-Epaillard, Polyaniline as a new sensitive layer for gas sensors, Analytica Chimica Acta, 475 (2003) 1–15.
54. S.A.Q. Sukeerthi, Contractor, applications of conducting polymers as sensors, Indian Journal of Chemistry Sec A, 33 (1994) 565–571.

55.V. Hatfield, P. Neaves, P.J. Hicks, K. Persaud and P. Travers, Towards an integrated electronic nose using conducting polymer sensors, Sensors and Actuators B, 18/19 (1994) 221–228.

56.F.L. Dickert, P.A. Lieberzeit, P. Achatz, C. Palfinger, M. Fassnauer, E. Schmid, W. Werthera and G. Horner, QCM array for on-line-monitoring of composting procedures, Analyst,129 (2004) 432–437.

57.Y. Fang, C. Bai and Y. Zhang, Preparation of metal sulfide-polymer composites microspheres with patterned surface structures, Chemical Communications, (2001) 804-805.

58.Y. N. Chan, G. S. W. Craig, R. R. Schrock and R. E. Cohen, Synthesis of palladium and platinum nanoclusters within microphase-separated diblock copolymers, Chemistry of Materials,4 (1992) 885-894.

59.L. Han, A. Andrady, K. Guzan, and D. Ensor, Electrospun composite nanofibers for sensor applications, Materials Research Society Symposium Proceeding Volume 1240 (2010).

60.L. Han, D. R. Daniel, M. M. Maye, and C. J. Zhong, Core−shell nanostructured nanoparticle films as chemically sensitive interfaces, Analytical Chemistry, 73 (2001) 4441-4449.

61.H. Lei, W. G. Pitt, Resistivity measurements of carbon–polymer composites in chemical sensors: impact of carbon concentration and geometrySensors and Actuators B-Chemical, 101 (2004) 122-132.

62.F. Wang, H. W. Gu, and T. M. Swager, Carbon Nanotube/Polythiophene Chemiresistive Sensors for Chemical Warfare Agents, Journal of American Chemical Society, 130 (2008) 5392-5393.

Curriculum Vitae

Postal Address; Department of Chemical sensors and Molecular Spectroscopy, Institute Of Analytical and Food Chemistry, University Of Vienna, Wahringer Strasse 38,A-1090, Vienna ,Austria
Home Address : Room # 2039,Forsthausgasse 2-8 A-1200,Vienna ,Austria

Mobile Phone : +436506677164
Phone Office : +431427752342
E-mail gmustafa_uet@yahoo.com

Ghulam Mustafa

Education

- PhD (In progress)

Sep 2008 onwards University Of Vienna, Austria.

- M. Sc (Applied Chemistry)

2002-2004 UET, Lahore Pakistan..

- B. Sc (Chemistry, Physics, Mathematics)

2000-2002 University of Punjab Lahore, Pakistan.

- F. Sc (Pre-medical)

1997-2000 Punjab Board Lahore, Pakistan.

- Matriculation

1995-1997 Punjab Board Lahore, Pakistan.

Publication

QCM-Arrays for Sensing Terpenes in Fresh and Dried Herbs via Bio-Mimetic MIP Layers, Naseer Iqbal, **Ghulam Mustafa**, Abdul Rehman, Alexander Biedermann, Bita Najafi, Peter A. Lieberzeit and Franz L. Dickert, ***Sensors* 2010**, 10, 6361-6376.

Experience

- One year working experience as a researcher at Punjab University Lahore, Pakistan.
- Three years working experience as a chemist in Pak-china Chemicals, Lahore, Pakistan.